BIOMARKER BASED MULTI CLASS CLASSIFICATION OF ALZHEIMER DISEASE

A thesis submitted to

UPES

For the Award of

Doctor of Philosophy

in

Computer Science and Engineering

By

Amar Shukla

September 2023

SUPERVISOR(S)

Dr. Rajeev Tiwari

Dr. Shamik Tiwari

School of Computer Science

UPES, Dehradun, 248007: Uttarakhand, India.

BIOMARKER BASED MULTI CLASS CLASSIFICATION OF ALZHEIMER DISEASE

A thesis submitted to

UPES

For the Award of

Doctor of Philosophy

in

Computer Science and Engineering

By

Amar Shukla

SAP Id: 500064198

September 2023

Internal Supervisor

Dr. Shamik Tiwari

Professor, School of Computer Science, UPES

AND

External Supervisor

Dr. Rajeev Tiwari

Professor, School of Computer Science, IILM

UPES
UNIVERSITY OF TOMORROW

School of Computer Science

UPES, Dehradun, 248007: Uttarakhand, India.

DECLARATION

I hereby declare that the thesis entitled "**Biomarker based multiclass classification of Alzheimer Disease**" has been prepared by me, under the guidance of Dr. Shamik Tiwari, Professor, School of Computer Science, UPES, and Dr. Rajeev Tiwari, Professor, School of Computer Science IILM NOIDA. No part of this thesis has formed the basis for the award of any degree or fellowship previously.

AMAR SHUKLA

SAP Id: 500064198

School of Computer Science

UPES, Dehradun-248007, Uttarakhand

THESIS COMPLETION CERTIFICATE

(INTERNAL SUPERVISOR)

THESIS COMPLETION CERTIFICATE
(INTERNAL SUPERVISOR)

I certify that the thesis entitled **"Biomarker based multiclass classification of Alzheimer Disease"** by **Amar Shukla (SAP Id: 500064198)**, research scholar at UPES, Dehradun, submitted thesis in partial completion of the requirements for the award of the Degree of Doctor of Philosophy in School of Computer Science is an original work carried out by him under my supervision and guidance. It is certified that the work has not been submitted anywhere else for award of any other diploma or degree of this or any other University.

26-9-2023

Dr. Shamik Tiwari
Professor, School of Computer Science
UPES, Dehradun, India.

THESIS COMPLETION CERTIFICATE

(EXTERNAL SUPERVISOR)

IILM UNIVERSITY

16-18, Knowledge Park II,
Greater Noida
Uttar Pradesh 201306
www.iilm.edu

THESIS COMPLETION CERTIFICATE

(EXTERNAL SUPERVISOR)

I Dr. Rajeev Tiwari, certify that the thesis entitled " Biomarker based multiclass classification of Alzheimer Disease" by Amar Shukla (SAP Id: 500064198),research scholar at UPES, Dehradun, Submitted thesis in partial completion of the requirements for the award of the Degree of Doctor of Philosophy in School of Computer Science is an original work carried out by him under my supervision and guidance. It is certified that the work has not been submitted anywhere else for award of any other diploma or degree of this or any other University.

External Supervisor:

Signature

Name: Dr. Rajeev Tiwari

Post: Professor
Department: School of Computer Science and Engineering
University Name: IILM University, Greater Noida

ABSTRACT

Alzheimer Disease (AD), a degenerative neurological disorder, witnesses rising global prevalence, necessitating innovative diagnostic methods. This research emphasizes the significance of multimodality approaches for accurate AD detection and its various stages. We've combined two paramount imaging modalities, Positron Emission Tomography (PET) and Structural Magnetic Resonance Imaging (sMRI) in a fusion method, providing enhanced visualization and insight. Structural analyses of the brain, especially subcortical regions, are indispensable for a comprehensive diagnosis. The extracted features from fused and non-fused biomarkers undergo evaluation via an ensemble classifier coupled with a Random Forest-based feature selection strategy. Results, across binary and multiclass classifications, highlight remarkable accuracies: AD vs. Cognitively Normal (CN) and Mild Cognitive Impairment (MCI) vs. CN both achieve 99%, while AD vs. MCI reaches 91%, and the tri-classification of AD vs. MCI vs. CN accomplishes 96%. Further, employing traditional Machine Learning (ML) and Ensemble Learning (EL), we discern the impact of various cortical and subcortical brain regions in AD detection. Notably, regions like the hippocampus, amygdala, right hemisphere's parahippocampal, and entorhinal, alongside the left's inferior temporal and isthmus cingulate, emerged as highly influential. These findings underscore the promise of integrated modalities and machine learning techniques in diagnosing AD and its subtypes early and adequately.

ACKNOWLEDGEMENTS

CONTENTS

LIST OF FIGURES

xv

LIST OF TABLES

LIST OF ABBREVIATIONS

A_{cc} Accuracy. xii, xv, 16, 17, 21, 36, 37, 39–42, 50–52, 55, 56, 58–62, 65, 71, 73, 75–82, 85, 107, 109–115, 117–120, 126, 131, 135–157

AD Alzheimer Disease. iv, xvii, 1, 2, 4–9, 12–27, 29–42, 44, 47, 50, 52–56, 58–68, 70, 73, 78, 82–84, 90, 94, 99, 100, 102, 104, 107, 111, 120–122, 132–134, 138, 139, 141, 145, 147, 154–158

ADNI Alzheimer's Disease Neuroimaging Initiative. 12, 29

CN Cognitively Normal. iv, 21, 41, 65, 73, 78, 102, 132–134, 138, 139, 147

CNN Convolution Neural Network. 50, 57

DL Deep Learning. 15, 21, 22, 28, 41, 50, 51, 55, 60, 61, 64, 156, 157

DT Decision Tree. 64, 68, 70–72, 75, 78, 133

DTI Diffusion Tensor Imaging. 7, 8, 27, 43, 58, 156

EL Ensemble Learning. iv, 19, 68, 72, 73, 104

$F1_{score}$ F1-score. xii, xv, 76–78, 80, 81, 107, 109–113, 115, 135–153

CHAPTER 1

INTRODUCTION

1.1 Alzheimer Disease

AD is the most common form of dementia, a neurodegenerative disorder. This condition is characterized by the loss of neurons in the brain, resulting in the formation of plaques and tangles known as tangles[136]. Symptoms. People with AD may initially experience forgetfulness, apathy, and difficulty with daily tasks. Early diagnosis and treatment are essential to reduce symptoms and prevent disease progression [193]. As the condition worsens, the individual may have difficulty thinking, communicating, swallowing, speaking, and even moving [129]. In 1911, Auguste Deter was the first person diagnosed with AD. After her death, a histological examination of her brain revealed the presence of amyloid plaques and neurofibrillary tangles, which indicated that amyloid deposition is a major cause of AD. This finding was published in the Handbook of Psychiatry, and the American Psychiatric Association (APA) recognized memory loss, impaired judgment, decreased perceptual discrimination, and emotional instability as symptoms of AD classifications [170].

By 1975, the medical field had begun developing new patient evaluation methods. In 1992, diagnostic tests were developed to detect signs of dementia in the brain accurately. In 1976, AD had become one of the most common causes of death worldwide. In 1980, the National Alzheimer's Disease Research Center (NADRC) was established to investigate the origins of AD [134]. In the 1990s, cognitive psychology was employed to track the development of neurodegenerative diseases. Research showed various damage to brain structures, particularly in the medial temporal lobe, that influenced different areas of the cortical system. Visual impairment was also observed in cases of dementia. Proteins such as amyloid, chromosome 21, presenilin 1 gene, chromosome 14, presenilin 2 gene, and the apolipoprotein E (APOE) gene were discovered to affect brain function [36]. In 2000, individuals with MCI were identified, exhibiting signs such as memory problems, age-related memory impairment, and a general preserved condition. Recent Figure 1.1 suggests that around 6.5 million people live with AD. People 65 and older comprise the largest group affected by AD, with 2.41 million in the 75-84 age range and 2.31 million in the 85+ age bracket. However, AD can only be accurately identified if caught in its early stages, and there is currently no reliable test[9]. ML and other AI-based technologies can be used to detect diseases. PET, sMRI, clinical DTI, genetic (CSF) and biospecies (APOE) biomarkers can all be used to diagnose AD. These markers are beneficial for diagnosing AD patients and gaining more knowledge about the disease in general. The growth of AD disease in the world with data from 2022 is shown in Figure 1.1.

1.1.1 Symptoms of Alzheimer's disease

- In the early stages, the symptoms might not be detectable.

- Then, slowly the patient shows short-term memory loss.

- Loss of motor skills (eating without help) and language become affected.

- Long-term memory loss, spouse name.

- Risk of losing.

- Bedridden.

- Death from infection.

Distribution of Patients affected by Alzheimer's by Age Group (in millions)
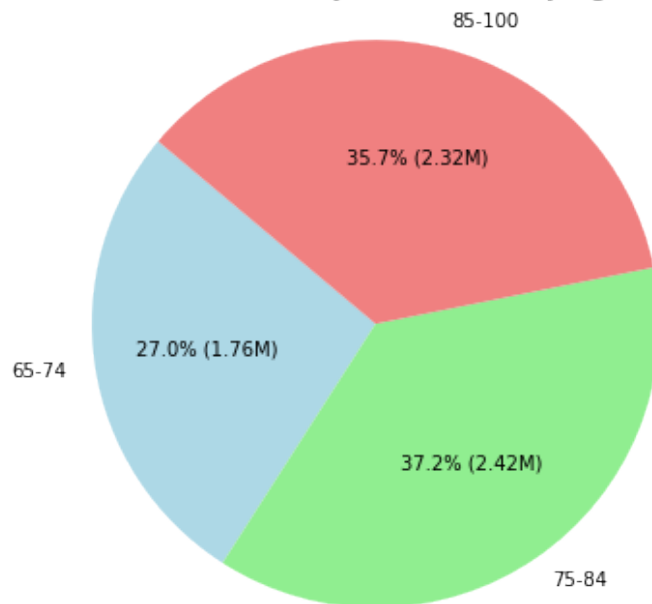
Figure 1.1: Age wise analysis of AD affected patients 2022[19]

.

1.2 Biological Constraints

The neuroregion of patients with AD is subject to various biological constraints. The primary causes of Alzheimer's are plaques and tangles. The Amyloid Precursor Protein (APP) is a small protein found in cell membranes, with one end inside the cell and the other outside. APP helps the neuron regenerate itself after injury and has the ability to break down and recycle. Alpha and gamma secretes are generated when APP is in the recycling process on both sides; the first side releases APP and the other gamma secretes. After decomposition, these alpha and gamma secretes dissolve. The region between Alpha and gamma secretes is used for the growth of different neuroregions [150]. If it is unable to achieve proper growth and dissolution of this tissue is not achieved, it can lead to the formation of a tissue called Amyloid Beta. These are sticky plaques that form outside the neuron, known as beta amyloid plaques. These plaques can be found between neurons, disrupting neuron-to-neuron communication. When one region of the brain cannot communicate with two other regions of the brain, it can result in serious signaling and memory loss. These bundles, which are formed in different sections of neurons, can transmit information to other neurons, leading to damage to other neuroregions. These amyloids can be bundled outside the blood vessel and cause various brain diseases such as dementia, Alzheimer's, and Parkinson's.

1.3 Modalities

AD is a debilitating disease that affects millions of lives around the world. It is a degenerative condition that destroys brain cells over time, making it difficult to care for oneself and one's possessions[202]. Bio marker-based research is one of the

most important strategies in the fight against AD. This is a revolutionary approach to studying AD, as it allows researchers to pinpoint specific individuals with the condition and follow their progression over time[92]. Biomarkers allow researchers to investigate possible links between this disease and other neurological problems. To better understand AD and develop more effective therapeutics, bio marker-based research has been a major advance in the battle against the disease. Biomarker preprocessing is essential for the diagnosis of AD and its subtypes[92]. sMRI in Figure 1.2 gives crucial information about the anatomy of the brain in Alzheimer's patients. It can identify changes in brain volume and thickness, as well as atrophy in particular structural regions [168]. Furthermore, sMRI can be used to detect changes in brain connections and network structure, which can aid in revealing the underlying causes of the disease.
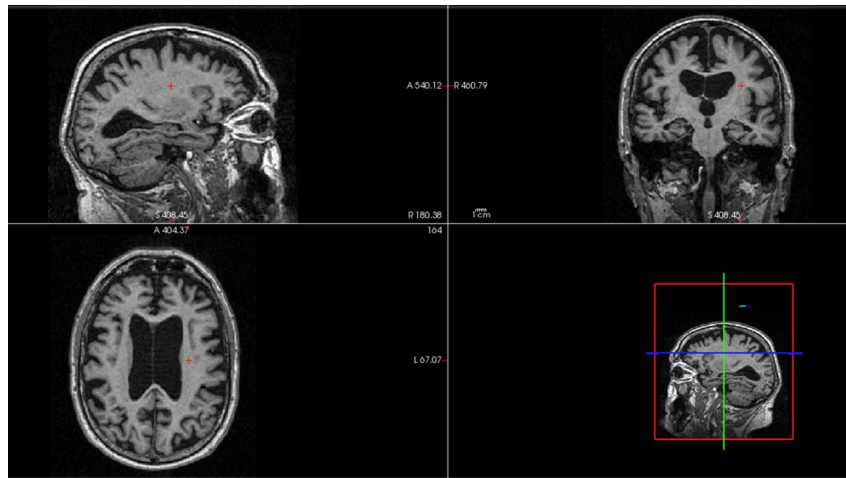
Figure 1.2: sMRI[84]

.

PET is a highly sensitive imaging method for detecting the presence of beta-amyloid plaques and neurofibrillary tangles in the brain. These are symptoms of AD and their accumulation is linked to cognitive loss. PET imaging can also be used to

assess cerebral blood flow and glucose metabolism, both of which are key indicators of brain function. Researchers can acquire a more complete picture of the anatomical and functional changes that occur in the brain during AD by combiningPET with other imaging modalities such as MRI and CT in Figure 1.3.
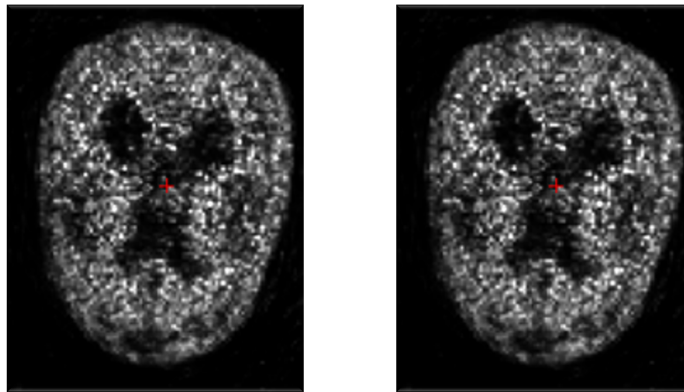
Figure 1.3: PET [84]

.

These research study continues with the three phases basically

- Bio markers Based Study

- Automated Pipelines

- ML Methods

Biomarkers are a key tool in the fight against AD. This new approach to the study of the disease enables researchers to identify people with AD and track their progression through various stages[92]. Additionally, biomarkers can be used to uncover other neurological issues associated with the condition. This type of research is a major breakthrough in the battle against Alzheimer's, allowing scientists to gain a

better understanding of the illness and develop more effective treatments. In this article, we will explore the use of biomarkers in the research of Alzheimer's. It is essential that the preprocessing of bio markers is done correctly in order to accurately identify Alzheimer's and its subtypes. [92]. The tract-based analysis of MCI patients, this stage is considered to be the middle part of normal cognition and the dementia[97].further proceeding in the analysis part, the author has gone with the classification of MCI with AD and control groups to understand the immediate effect of the MCI group. In the content, the author has gone with the generation of tractography and tract maps by measuring the mean fractional anisotropy (FA) and the apparent diffusion coefficient (ADC), uncinated fasciculus (UNC), posterior cingulate fasciculus (PCF), corticospinal tract (CST)[161].They used the study group of 17 people with probable AD, 16 people with mild control, and 16 with control. The authors used Diffusion Tensor Imaging (DTI) visualization for data processing and the Statistical Package for the Social Sciences for analysis. They applied sMRI and diffusion imaging-based studies to predict AD, using T1, T2-Flair and DTI, which included morphometry, structural connectome, and white matter hyperintensity [54]. 221 elderly people were tested, including 110 with Alzheimer's (ages 85-77), 77 with MCI (ages 77-76), and 78 with subjective MCI (ages 78-82). The authors first performed structural and anatomical analysis of the T1 and Flair images and then processed the diffusion images using ANT, SIFT, CSD, and various atlas formation procedures. After extracting features, they used ML classification models such as logistic regression (L1 regularization) and linear Support Vector Machine (SVM). Studies have shown that age-related reductions in certain age groups can be observed in white matter tractography. Investigations of the structural characteristics of various neural fibers were conducted, including interhemispheric fibers located in the corpus callosum, interhemispheric association fibers such as the cingulum,

uncinate, arcuate, inferior longitudinal, and inferior occipitofrontal fibers, as well as projection fibers such as corticospinal fibers. In addition, a variety of cognitive assessments were administered, including memory and executive function, vaso-motor dexterity, motor speed, attention and working memory, set-shift / flexibility, and visuospatial construction. to compare the differences between the AD and NC groups. The author highlights the substantial effect of diseases on the brain, particularly aging and AD. To investigate this, they employed whole-brain tractography with the FMRIB Software Library (FSL) tool "BET" and a Hough transform to identify fiber connections. 35 characteristics were evaluated using FreeSurfer[217], and comparisons were made between the eMCI, MCI, and AD groups. Global degree, efficiency, normalized characteristic path length, normalized clustering coefficient, and normalized small-world effect were the measurements used to illustrate the brain's response to these diseases[Pagani et al.].

To diagnose AD, a tract-based method was used to analyze the MCI and AD groups with probabilistic tractography and spatial statistics of DTI[153]. SVM was used for analysis and classification, taking into account measures such as the average FA value, the volume of the predefined fiber seed region and the volume of the thalamus being taken into account.

Diffusion-based diagnosis of AD was also performed using tractography in the hippocampus region. FDT, FSL, DTIFIT and PROBTRACKX were the tools used, and statistical analysis was performed after extracting characteristics and registering them with a weighted image T1[164].

The tract-based tractography technique was used to create a cortical network in the white matter region. The automatic anatomical labeling technique was used for 25 AD patients and 30 healthy control patients, and fiber assignment was carried out by continuous tracking and correlation approaches for various groups[109].

The impact of diseases on brain structure was studied using data from 202 people in the AD, MCI and NC groups. Nine tractography methods were compared to diagnose Alzheimer's patients, and regression and statistical analysis were performed after feature extraction and parcellation [217]. Multiple linear regression was used for prediction after feature collection in the MCI group with a tract-based approach and volumetric analysis [46]. Statistical analysis was performed after the FREE surfer with the tracula model was used to study the attention factor in patients with MCI with a tract-based approach[96].

Neuro imaging changes from normal to white matter affected by AD were examined using a data-driven estimation approach and probabilistic tractography on the population template[124]. A detailed biomarker-based analysis was performed in the Table 1.1 to compare the differences between the AD and NC groups.There are different preprocessing methods which are applied in the PET and sMRI modalities for AD detection in Table 1.1.

Table 1.1: Preprocessing techniques for enhancing the quality in sMRI and PET

S.No.	Method	Description
1	De-Oblique	The technique of rotating images to reduce perspective distortion reduces distortion and makes interpretation easier.
2	Field Inhomogeneity Correction	Artifacts are removed from the data by reducing the intensity of tissues that are not included in the mean intensity.

<div align="right">Continued on next page</div>

Table 1.1 Preprocessing techniques for enhancing the quality in sMRI and PET

S.No.	Preprocessing Method	Description
3	Bias Correction	Method used to correct nonuniform shading in an image by using a low-pass filter to remove the high frequency.
4	Non Brain Tissue Removal	Method used to remove non-brain tissue from captured images through a combination of techniques including segmentation, morphological operations, and filtering.
5	FSL and Eddy Current	Fourier Transformation is used to quantify the temporal dynamic of an image. During the recording of an image, Eddy Current flow preprocessing is used to identify small changes in the image.

1.3.1 Neuroimaging over EEG

Neuroimaging modalities such as sMRI, PET, and Computed Tomography (CT) scans provide a wealth of data and have several advantages over electroencephalography (EEG) for brain visualization and pathology detection. CT scans, also known as "CAT scans", use X-ray equipment to create images of the brain. They can provide detailed images of different types of tissue, including lungs, bones, soft tissues, and blood vessels. CT scans are often used in emergency situations because

they can provide images quickly and are excellent for detecting bleeds, fractures, or blood clots. In contrast, EEG measures the electrical activity of the brain. It can capture real-time information about brain activity, which makes it excellent for detecting abnormalities in brain function, such as seizures or sleep disorders. However, EEG cannot provide detailed sMRI of the brain or capture the in-depth information on brain metabolism and blood flow that imaging scans can. The advantages of neuroimaging over EEG include:

- Detailed Structural Information: Neuroimaging techniques provide detailed pictures of the structure of the brain, allowing for the identification of anatomical abnormalities such as tumors, blood clots, or damage from a stroke.

- Identifying Biochemical Changes PET scans can detect biochemical changes in the brain, which can help identify a variety of conditions before they cause anatomical changes big enough to be seen on CT or MRI scans.

- Less Vulnerable to User Errors: The quality of an EEG can greatly depend on the expertise of the technician who applied the electrodes. On the contrary, neuroimaging is less dependent on the operator's skill.

- Non-Invasive: Although EEG is also noninvasive, PET, MRI, and CT scans are often more comfortable for patients, as they do not require anything to be attached to the patient's head.

- Global and Regional Measurements: Neuroimaging allows for global and regional measurements of brain anatomy and activity, providing more comprehensive data on the brain.

Despite these advantages, EEG has its place in the diagnostic process, particularly when continuous or real-time brain activity data is required. However, when it

comes to obtaining detailed images of brain structure and detecting early stages of disease or small abnormalities, neuroimaging techniques such as MRI, PET, and CT scans have significant advantages.

1.4   Feature Extraction

The Automated Pipeline approach entails merging a number of algorithms into preprocessing and neuroregional activities. sMRI may identify abnormalities in brain tissue early and precisely. To examine the various brain areas, several pipelines, such as Free Surfer, SPM, AFNI, FSL, DIPY, NIPYPE, AAL, fMRIPrep, and Ants, are used. Various locations may be discovered using hand-crafted feature extraction approaches, enabling for more efficient identification and treatment of AD. Tactics are entirely dependent on image processing technology.

The Alzheimer's Disease Neuroimaging Initiative (ADNI) is a highly beneficial open source dataset for the detection of AD. The FREE Surfer feature extraction strategy appears to be effective, as Figure 1.4 demonstrates that it achieved more than 95% P_{rec} in recognizing AD and its subtypes. However, was not as good in multi class analyses when distinguishing AD at different stages, but it was more successful in binary classifications. Consequently, these automated pipelines contain strategies for recognizing various types of disease using multimodal approaches. To accurately detect AD, these techniques involve the combination of registered images and the combination of features.
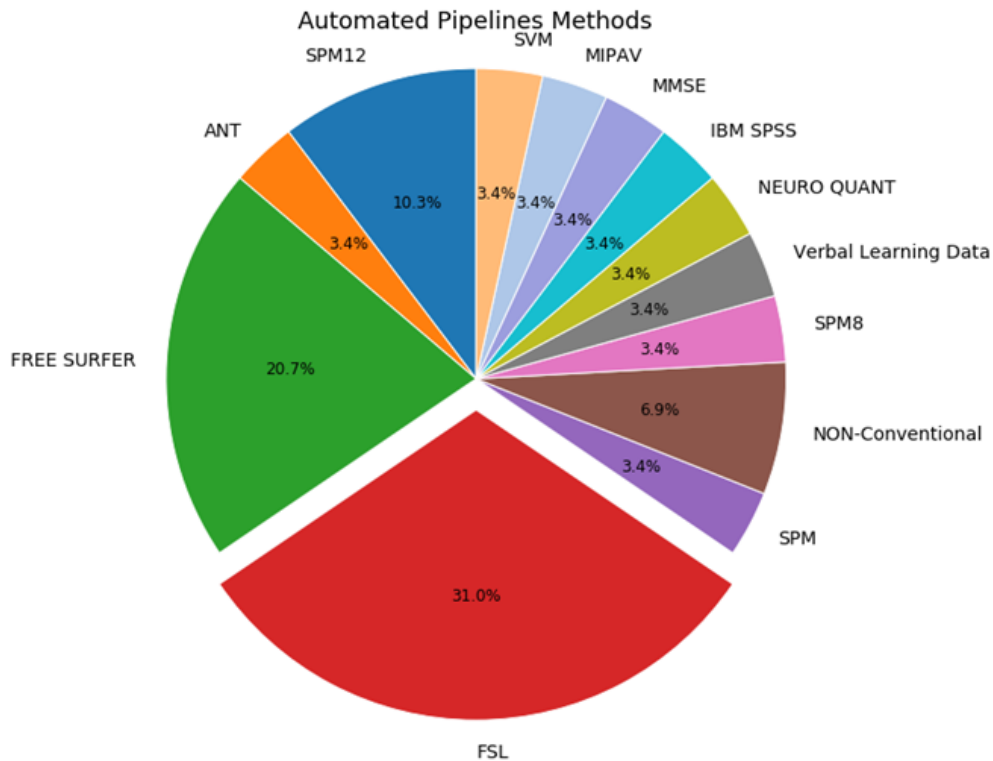
Figure 1.4: Automatic Pipelines Analysis for the Detection of AD and their subtypes

1.5   Registration Methods

Images captured with the same modality or of the same object can be registered with one another by utilising the same reference frame. The goal of image registration is to find the transformation that best fits the images so that they may be compared or combined for study. Image registration, as one of the initial steps in the fusion process, is critical for the correct diagnosis of AD and its subtypes using multimodality. Registration is the translation of data into a shared reference frame. The phrase "image fusion" refers to the process of integrating many images of the same item or modality into a single complete image. Picture registration is an important aspect of

the fusion process, since it ensures that the input images are properly aligned before being joined. Image registration reduces the impacts of misalignment and distortion caused by various views, camera placements, and other factors by matching the pictures. Some image fusion approaches that might be used to merge the photos in this arrangement include weighted averaging, maximum likelihood estimation, and multiresolution analysis.These detailed descriptions of the usability of registration methods in different modalities are described in the Table 1.2

Table 1.2: Detailed Summary of Registration Methods

S. No.	Registration Methods	Modalities	Usability
1	Mutual Information	A method that uses the statistical dependence between the image intensities of corresponding voxels in both images. It's often used in medical image registration.	Medical Imaging: Useful for aligning images from different medical imaging modalities.
2	Mutual Information	CT and MRI scans: Helps to identify pathological areas by combining information	Moderate usability in the method of CT and MRI
3	Mutual Information	The mutual information method allows the combination of functional and structural information.	Highly used in the AD detection

S. No.	Registration Methods	Modalities	Application
4	Rigid Registration:	A technique that assumes the transformation is a linear combination of translation, rotation, and scaling	3D Modeling: Commonly used to combine 3D models in one common space. Highly used in the multimodality approach

1.6   Machine Learning Methods

ML and Deep Learning (DL) are used to classify and evaluate patients, predict therapy outcomes, and identify risks. Researchers have used these algorithms to diagnose neurodegenerative diseases caused by AD and its stages using imaging-based detection. Automated pipelines make use of feature extraction techniques based on a variety of biomarker methodologies. DL enables preprocessing of biomarkers, extraction of characteristics, and construction of a model to diagnose AD and its stages. Common classification approaches for AD include SVM, ANN, and DNN, as summarized in the Table below. As a result, researchers and professionals in the field of medical image processing often use these approaches to diagnose AD at different stages. There are also many other classification methods that may provide further information about the area. Figure 1.5 illustrates the various classification methods used in the field of AD.
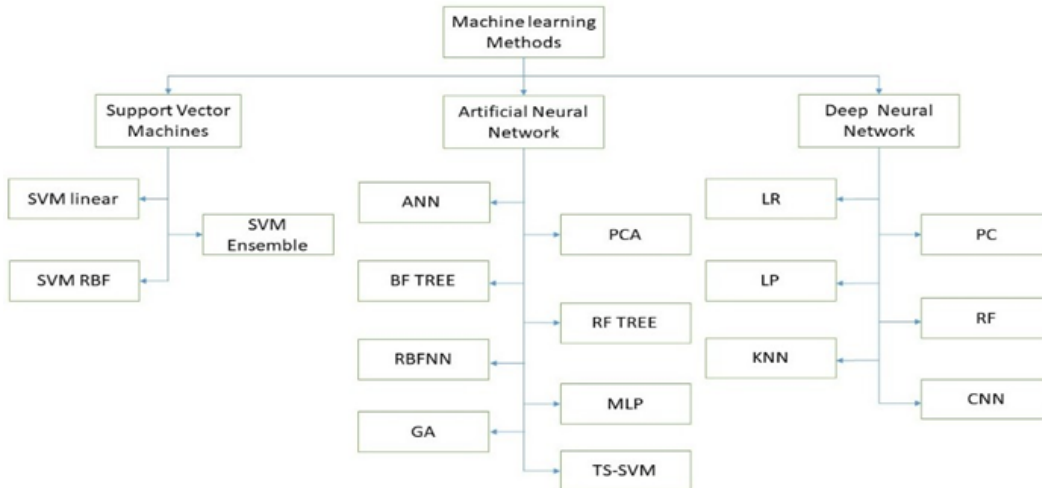
Figure 1.5: Different ML methods and there classification

1.7 Problem Statement

Brain structural difference in AD subjects as a binary classification has been well studied using the single set of Biomarker, but the multi-level classification of AD and the use of fused bio markers remains less developed.

The main challenge here lies first in the identification of fused biomarkers, which provides the most reliable features for Alzheimer's classification with a benchmark A_{cc}.

1.8 Gap Analysis

- While many research studies have primarily used binary biomarkers, the utilization and exploration of different types of biomarkers, especially in multimodal approaches, remain limited.

- Most studies focus on fusion at the feature level using identical structural

biomarkers. However, the full potential of multimodal fusion (PET+sMRI), such as image fusion, has not yet been explored to enhance the P_{rec} of classifying AD and its subtypes.

- Single-mode approaches have reached satisfactory A_{cc} levels for AD and its subtypes, but incorporating multiple biomarkers could potentially create a hybrid set of features to improve prediction A_{cc} in both binary and multiple classes.

- Previous research has marked the A_{cc} of the benchmark in binary classification. But still the multiclass A_{cc} is still the challenge.

1.9 Objective

Prediction of Alzheimer's disease using different biomarkers.

1.9.1 Sub objective

- Design image fusion of biomarkers.

- Develop the extraction of hybrid feature set from the fused and non-fused biomarkers.

- Design the multiclass classification model considering the various stages of Alzheimer with adequate A_{cc}.

1.10   Research Query

The research, prototyping and evaluation of this this work focused on the following research question

- How can a multiclass classifier be designed to differentiate between Alzheimer's patient and other diagnostic groups using different set of bio markers.

- What group of biomarkers are most suited for fusion for feature extraction.

- Which set of hybrid feature is most appropriate for the problem at hand.

- Which ML approach yields the best results by considering problem as the multiclass classification.

1.11   Contributions

- Fusion of biomarkers.

- Preperation of a hybrid set of features from the fused and Non-fused Modalities.

- Proposing the assembly of different ML models to remove the biasing of different classifiers.

- Subcortical regions analysis is done to find there effectiveness in the AD and there subtypes.

1.12   Thesis Layout

- **Chapter 2: Literature review:** Discusses the historical and recent studies made in the field of the detection of AD. The detailed study has been made in the field of biomarker-based studies, Fusion-based methods, which include the registration techniques, ML Methods. A detailed analysis is also provided in the chapter.

- **Chapter 3 : Alzheimer Disease Detection using Structural Magnetic Resonance Imaging:** In this chapter we have used sMRI using hand-crafted feature extraction methods for feature extraction and done binary and multi-class classification based on those features using the EL technique.

- **Chapter 4: AD detection using multimodality:** In this chapter we have not done the fusion of the two different modalities, which is PET and sMRI. Using EL, we have performed binary and multiclass classification.

- **Chapter 5: Cortical and Subcortical Structure Analysis using Single Modality and Multi-modality** In this chapter we have done the analysis of the different regions of the brain. We also understand which region has been more prominently affected in the detection of AD.

- **Chapter 6: Conclusion and Future Challenges:** In this chapter we have done a brief discussion and an analysis of the whole work. also discussed the future works and conclusions.

CHAPTER 2

LITRATURE REVIEW

2.1 Literature Review

AD has become prevalent in our society over a considerable period. It is recognized as a progressive neurological disorder [35]. Initial signs of AD can manifest as memory lapses, apathy, and despondency [11]. As the disease progresses, people affected by it may experience difficulties with cognition, speech, swallowing, mobility, and communication[71]. Globally, there are currently 6.5 million people 65 and older who have AD. Furthermore, there are 2.41 million people between the ages of 75-84 and another 2.31 million people 85 years or older who are grappling with this condition. Presently, there exists no singular dependable diagnostic test for AD instead early detection and diagnosis are crucial aspects to consider. The implementation of ML techniques along with other approaches based on artificial intelligence can significantly aid in the identification of this disease [180].

The identification of AD involves the use of various biomarkers, including sMRI, genetics, clinical data and biological samples[23]. However, there is still no definitive evidence regarding which biomarker has the highest degree of reliability

[70], which requires further exploration to find the most suitable one. Biomarkers serve as crucial information utilized in the detection of AD. To improve the diagnostic utility of computed tomography (CT) scans, it becomes essential to differentiate spatial parameters such as cortical thickness, brain volume, and brain surface area through post-processing techniques [77]. The extraction of features from biomarkers is achieved by employing a combination of handcrafted methods and DL approaches. When it comes to manually processing biomarkers using widely-used Automatic Pipeline Methods like FSL, Free Surfer SPM12,and ANT are commonly employed [7], whereas DL techniques such as CNN and Transfer Learning Methods are often used for detecting AD.

Alzheimer's Disease encompasses various subtypes and stages, ranging from CN to MCI, and from MCI to AD. The P_{rec} of identifying AD is quite high when comparing it with CN, MCI, or distinguishing between CN and MCI [128]. However, there is still room for improvement in multiclass detection, especially when dealing with three or four classes and subclasses of MCI. The current binary and multiple class detection methods for the subtypes of MCI are not yet satisfactory. Therefore, numerous research approaches have been employed to find an effective methodology for detecting these stages. Some pipelines have demonstrated acceptable A_{cc} in recognizing AD in different classes. This review focuses on screening and extensively investigating the most significant research studies in this area.IN this study, we have reviewed the three modes of study, biomarker-based, fusion-based, and automatic pipline-based approach and machine and DL methods.

- In this study, the efficacy of biomarkers in detecting AD and its subclasses is examined through a comprehensive analysis. This article covers a wide range of types of biomarkers, highlighting their potential as effective tools for the detection of AD in different classes.

21

- Additionally, the study explores various handcrafted methods, specifically Automatic Pipelines, to determine which offer superior preprocessing capabilities for structural biomarker scans and yield optimal statistical features. Moreover, it investigates pipelines that exhibit favorable approaches to fusion and registration in order to access multimodal features.

- An in-depth examination of ML and DL based methods is conducted with the aim of identifying those that facilitate the creation of appropriate models for AD detection across all subclasses.

2.2 Biomarker Based Study

A diverse range of biomarkers has been shown to be valuable in the diagnosis of many neurological disorders. Research has revealed that the erratic behavior displayed by individuals with AD is a direct consequence of a brain condition that arises due to these abnormalities[11]. In particular, the amyloid precursor protein (APP), which is present in various regions of the brain, serves as an effective tool for precise biological localization [70]. Under specific pathological conditions, APP plays an important role in facilitating processes such as neuronal regeneration, degradation, and recycling. In particular, reduced levels of APP have been associated with elevated levels of protease within synapses. This increase in protease activity has been associated with deficiencies and disruptions within neuroregions caused by said deficiencies. Synapses act as crucial intermediaries between neurons by transmitting messages throughout the brain. Neurons utilize membranes containing APP molecules as protective barriers against harmful stimuli, since protease enzymes are predominantly located outside of blood vessels, a phenomenon known to induce

inflammation.

2.2.1 Clinical Research

Within the realm of healthcare research, a clinical trial serves as an extensive examination of data, encompassing both the microcosm of patient care and the macroscopic nature of clinical trials. The primary motivation behind gathering this information is to evaluate patient outcomes, achieved through rigorous clinical studies[187]. The fundamental objective driving these trials lies in subjecting novel medical innovations, therapeutic approaches, and technological advances to real-world testing scenarios. In doing so, the researchers aim to validate their efficacy in practical healthcare settings[141].

2.2.2 Genetic Biomarker

Due to the wealth of information they reveal regarding an individual's physical condition and state of being, DNA samples are inherently private. When DNA and RNA sequencing is analyzed, it becomes possible to determine whether the observable characteristics of a person were inherited from their parents[86]. Genetic samples have increased sensitivity due to their ability to convey personal health-related data and overall well-being.Thorough examination of genetic elements within the human body necessitates meticulous scrutiny of neurological, pulmonary, and cardiovascular domains. These crucial attributes in the brain play a pivotal role in accurately diagnosing individuals afflicted with AD. The APOE4 allele, specifically the Apo lipoprotein E (APOE) 4 allele, stands out as the most substantial genetic predisposition to develop this neurodegenerative disorder. Despite extensive research efforts dedicated to unraveling the underlying mechanism responsible for this increased

23

susceptibility, uncertainties persist regarding how apoE4 precisely triggers the onset of AD[203].

2.2.3 Positron Emission Tomography

PET imaging utilizes a scanner that not only detects Gamma rays, but also performs three-dimensional picture reconstruction. This technology can be used to measure the proportion of amyloid in the brain, which is a key factor in diagnosing AD. Additionally, PET imaging allows the quantification of glucose levels in various areas of the brain, distinguishing between different groups of subjects, and tracking glucose movement among individuals[135]. This biomarker helps explain the functional alterations observed in the brain structure of AD patients and can be used to monitor glucose content within different regions of the brain. Using PET imaging, researchers gain valuable information on both structural changes and metabolic processes that occur within affected brains. This information is essential to better understand the progression of AD and to develop more effective diagnostic techniques and treatment strategies[139].

2.2.4 Biospecimen Biomarker

The collection of patient biological samples during the sequencing analysis is of utmost importance in the context of AD. The emergence of biomarkers has revolutionized the field by introducing a revolutionary way of diagnosing diseases, representing a major change in the way diseases are identified[75]. This has enabled the use of a novel approach that has altered the way diseases are identified. By measuring the mobile structural components of the brain, researchers can perform structural brain quantification, which is an effective way to track and monitor

neurological function in people aging. These markers allow for a comprehensive evaluation and assessment of neurological functioning in this particular group.

2.2.5   Structural Magnetic Resonance Imaging

The use of sMRI has been found to be a beneficial tool in studying the intricate anatomy of certain regions of the brain[6]. This technology takes advantage of the preservation qualities of hydrogen atoms and resonance within static and magnetic fields, allowing for the detection and recording of signals through a radio receiver. It has been especially useful in distinguishing Alzheimer's patients based on anatomical differences between various parts of the brain. To detect morphological changes, several imaging techniques have been used, such as structure analysis, volumetric analysis, cortical thickness measurement, voxel-based analysis, longitudinal analysis, and structural morphology. Of these, sMRI stands out due to its ability to generate unique attenuation patterns that show different types of gray matter composition. Additionally, it provides information on the various dimensions of brain regions and subregions, which helps to accurately pinpoint areas affected by AD. Using sMRI techniques in combination with other diagnostic tools and evaluations, researchers can better understand how this debilitating disease affects particular areas of the brain[220].

2.2.6   Cerbro Spinal Fluid

Cerebrospinal fluid (CSF) is a key element in the investigation of AD. A protein levels between healthy people and those with Alzheimer's. The diagnosis is based on whether there is an increase or decrease in the protein[31]. Other important brain biomarkers include A40, A42, phosphorylated tau (p-tau), and total tau protein (t-

tau). These proteins in the CSF provide useful information on the various factors that affect certain areas. In particular, individuals with Alzheimer's have significantly lower levels of active A42 protein than healthy people. CSF concentration can be affected by physical conditions through its relationship to A40. In addition, it should be noted that increased cognitive awareness leads to better information retention in the body than during periods of rest. All of these diagnostic markers are essential to identify and diagnose AD [195].

2.2.7 Fluid Attenuated Inversion Recovery

The FLAIR image, also known as the flare image, is a significant MRI biomarker that can be used to identify brain lesions that hinder the proper functioning of the cerebrospinal fluid (CSF). To ensure that image quality is not affected by CSF, certain measures must be taken [127]. The FLAIR MRI sequence is designed to suppress fluid signals, thus improving visibility of periventricular hyperintense lesions, such as those associated with multiple sclerosis (MS) plaques. Furthermore, the weighted percentage of T2 is often used in Flair Modality to detect potential disorders within distinct class clusters and to detect the presence of white matter in affected brain regions. These areas can also lead to differences between different age groups. In general, understanding and interpreting flare images can help medical professionals diagnose conditions related to brain abnormalities and lesions that affect the CSF in the brain. Using advanced imaging techniques, such as FLAIR sequences and T2 weighting analysis, researchers can gain valuable information on the structural and functional aspects of these complex neurological phenomena [162].

2.2.8 Diffusion Tensor Imaging

DTI is a type of magnetic resonance imaging that uses isotropic diffusion to measure the structural integrity of brain white matter pathways [137]. Data from DTI can be used to create three-dimensional reconstructions of neural pathways through fiber tractography (FT). DTI is a well-known technology that is often used to analyze the diffusivity of water molecules in tissue [13]. When water molecules do not move consistently throughout the brain, it can lead to a gradual decline in memory and eventually loss of memory. AD is characterized by changes in the movement of water molecules in the brain, which is important for identifying structural differences and diagnosing symptoms. This study supports the idea that the use of a single modality is the most practical approach to diagnosis[119].

2.2.9 Electroencephalography

Electroencephalography (EEG) is a widely used neurophysiological technique to document and assess brain electrical activity, particularly brain waves. It is a valuable tool for identifying neurological processes and conditions[88]. A typical EEG examination typically displays consistent frequency and waveform characteristics. People with epilepsy tend to have an increased prevalence of electrical activity in the brain, which is characterized by a higher number of active brain waves. The electrical conductivity of different tissues varies between individuals and over time.For diagnostic purposes, EEGs are usually done for less than an hour. On the other hand, ambulatory EEGs are longer procedures that involve continuous monitoring for one hour or more. Electroencephalography (EEG) combined with video monitoring is commonly used during long-term procedures that can take an entire day or up to a week to collect data.The term "long-term monitoring" refers to the practice of contin-

uously observing and recording data over an extended period to gain comprehensive insight into brain activity patterns and potential abnormalities associated with certain conditions or disorders such as epilepsy. Electroencephalography (EEG) is essential to objectively capture the intricate electrical dynamics within the human brain through the measurement of distinct wave forms known as brain waves. Its various applications provide valuable information on neurological processes and are highly beneficial for diagnostics, treatment planning, and understanding complex conditions such as epilepsy both on short- and long-term bases[87].

The Figure 2.1 presented below illustrates the comprehensive processing of the biomarker using both Handcrafted Feature Extraction techniques and DL methods.
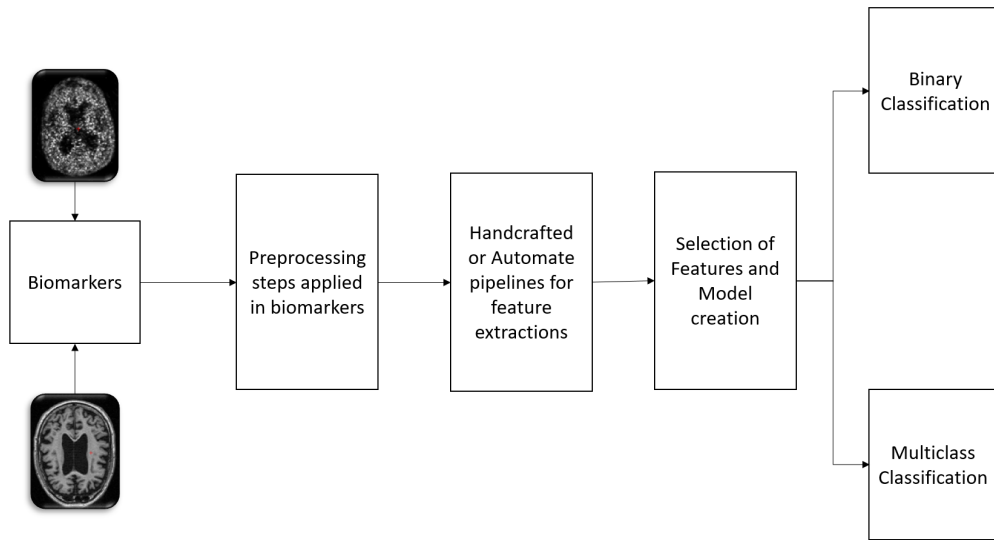
Figure 2.1: Biomarker based AD detection approach

Additionally, it covers the validation procedure for each category. After delving into recent studies on biomarker levels, our objective is to identify shortcomings in disease diagnosis methodology in the following Table 2.1.

Table 2.1: Biomarker based study for AD detection

S.No	Author	Modalities	Observations
1	[209]	sMRI, T1-Weighted	In the study, 221 older adults were included, 110 with AD (85 to 77), MCI (77 to 76) and subjective MCI (78 to 82). T1 and Flair images were taken first to assess the structure and anatomical relationship. They then used ML classification with logistic regression (L1 regularization) and linear SVM models.
2	[217]	MRI, DTI, T1-Weighted	The author explains AD and aging. The FSL tool "BET" was used on 111 ADNI patients, 15 of whom had AD, 68 MCI. The results were compared with 35 features in the Hough transforms. MCI and AD were examined. Take advantage of the normalized characteristic path length, clustering coefficients, and small-world effects.
3	[182]	MRI,DTI	Based on tracts (20 MCI, 20NC, 38 DTI). Probabilistic tractography was applied to 84 patients with MCI and AD. Analysis and classification were based on SVM and average FA values, fiber predefined seed region volume, and thalamus volume.

Table 2.1 Biomarker based study for AD detection

S.No	Author	Modalities	Observations
4	[142]	MRI,DTI	A total of 202 people were tested for AD, MCI, and NC.In this study, two ODF-based deterministic and probabilistic tractography methods (Probtrackx) were tested and analyzed.The results are similar for MCI and the regular groups.
5	[142]	T1-Weighted MRI	Using basic data processing, the author performed tract analysis with a FSL and cortical surface analysis with a free surfer to produce a t1 weighted image. After collecting the data, the author used multiple linear regression to predict the MCI group.
6	[137]	DTI,T2 Weighted	The author used the FREE surfer with tracula model for tract-based analysis and the statistical package for social sciences for a group analysis to determine the attention factor in MCI patients.
7	[212]	DTI,T2 Weighted	This cingulum tractography was developed based on the volume of left hippocampal tissue affected in 20 subjects. Volumes of the right and left hippocampi (mm3): RHV, LHV, RHV, F A of the left cingulum, FA of the right cingulum.

Table 2.1 Biomarker based study for AD detection

S.No	Author	Modalities	Observations
8	[124]	DTI	AD causes normal white matter to become abnormal. The study included 49 people with cognitive impairment and 33 healthy individuals. Consolidation of spherically confined free tissue. Using the population template, this can be easily done.
9	[109]	DTI,T2 Weighted	In the white matter, it forms a cortical network. Twenty-five Alzheimer's patients and thirty healthy controls were analyzed based on cortical resorption with anatomical labels. There are several diffusion magnetic resonance tractography groups that use orbital path, medial, orbital, middle temporal gyrus, and dorsolateral correlations.
10	[215]	DTI,T2 Weighted	Scanners with DTI and cross-lag ALD DA cross-lag detect early AD. It was all DTI. A K-S test. ABSURD VALUES It counted. A dementia biomarker study 135 A test for ADs. Psych anisotropy Structured connectivity data helps model predict progression. Dementia brain damage.

Table 2.1 Biomarker based study for AD detection

S.No	Author	Modalities	Observations
11	[138]	sMRI	A total of 871 elderly ASPS participants and 347 family members participated in our study. In this study, we used a simple SVD score derived from MRI scans to predict the future risk of dementia. This score is calculated based on cognitive tests.
12	[64]	DTI	A Graph-based Lobar Network Analysis was performed on the global brain and AD. Patients with AD have a decreased amount of functional connectivity in the hippocampus, temporal, parietal, frontal, and occipital ganglia nodes.
13	[210]	TI,T2-Weighted	There were 43 to 89 affected by DTI, DSEG-A, cognitive and statistical analysis SVD. EF and GC decreased faster in patients with more SVD disease. The findings suggest that DSEG- can be used to predict disease flow and impact. DSEG predicts cognitive decline in healthy individuals.
14	[98]	MRI	In this study, voxel morphometry is used. White matter degeneration in the elderly can be accurately detected using LIMM and image analysis. Using this model, the classification P_{rec} is greater than 90.

Table 2.1 Biomarker based study for AD detection

S.No	Author	Modalities	Observations
15	[108]	MRI	A CNN genomics study MRI and A is being carried out in 151 people, 51 of whom have AD and 100 of them do not. The image prediction algorithm eliminates transgender subjects with high heterozygosity after normalizing and processing the image.
16	[199]	DTI	Cognitive function is determined by statistical analysis of gray matter, tractography, and white matter. Memory is reduced in patients with AD according to MMSE scores. WM is also affected in AD.
17	[99]	Genetics Data	A four-year clinical trial administered RAVLT to 51 older people with FH dementia and Apo lipoprotein E4 (52%). These factors were associated with genetic and metabolic risk factors for AD.
18	[192]	DTI	The study included 31 patients with AD, MCI and spinal cord injury aged 51 to 89 years. According to the researchers, the diffusivity of the fibers and the projection were inversely related. The researchers found that the perivascular spaces had less water diffusivity than the severity of AD.

Table 2.1 Biomarker based study for AD detection

S.No	Author	Modalities	Observations
19	[171]	GENETICS	This article's data is based on ADNI. The study also includes elderly people with and without dementia. The metabolism of FDG PET decreases in the hippocampus region.

Thus, these are the various analyses of the biomarker-focused studies found in recent research articles. Different observations have been made in these studies. We have also performed the analysis using various parameters for AD detection using modalities, data source, result achieved and multiclass and binary class classification in Table 2.2.

Table 2.2: Detail analysis of different modalities, data source for the AD detection

S.No	Author	Data Source	Modalities	Result	Multi class	Binary Class
1	[85]	OASIS	MRI	AD 73.25	✓	X
2	[190]	HAVARD	MRI	-	✓	X
3	[62]	ADNI	MRI	95.23 AD	X	✓
4	[122]	OASIS	MRI	98.88% A_{cc}	X	✓
5	[116]	OASIS	MRI	92.85% AD	✓	✓
6	[165]	ADNI	MRI	99% AD	✓	✓
7	[113]	OASIS	MRI	90%AD	✓	X

Table 2.2 Detail analysis of different modalities, data source for the AD detection

S.No	Author	Data Source	Modalities	Result	Multi class	Binary Class
8	[55]	ADNI	MRI	92% AD	✓	X
9	[69]	ADNI	BIO	99.67% AD	✓	X
10	[58]	GERAD1	GENETIC	90%AD	X	X
11	[90]	AIBL	MRI	86% MCI for AD	✓	X
12	[66]	ADNI,	CSF	ABeta-42 neuronal pentraxin decreased	✓	✓
13	[151]	DIAN	CSF	Neuronal Pentraxin decreased NLF rate	X	X
14	[52]	ADNI	PET	changed to AD 98%	X	X
15	[52]	ADNI	CSF,MRI,PET	MCI to AD 41.3% to 28.4%	✓	✓
16	[131]	ADNI	PET,CSF	94% AD	X	X
17	[39]	ADNI	FDG, PET	AD detection	✓	X
18	[50]	ADNI	MRI	AD 86.8	✓	X
19	[110]	ADNI	MRI	91.74% MCI from CN	✓	✓
20	[47]	NICDS	MRI	88.6% AD	✓	X
21	[188]	PRIVATE	MRI	86% MCI to AD	X	X

Table 2.2 Detail analysis of different modalities, data source for the AD detection

S.No	Author	Data Source	Modalities	Result	Multi class	Binary Class
22	[103]	PRIVATE	CT,MR,CSF	91% AD	X	X
23	[159]	PRIVATE	GENETIC	28 score AD	✓	X
24	[123]	PRIVATE	CLINICAL	-	X	X
25	[121]	HIPAA	MRI	AD 93%	✓	✓
26	[184]	NINCDS	MR CLINICAL	95% AD	X	X
27	[196]	PRIVATE	CLINICAL	-	X	X
28	[152]	ADNI	PET	Group 1 to 5 4% to 27%,64% and 100% MCI	✓	X

The results of the previous study, presented in Table 2.1 and Table 2.2, indicate that sMRImethods, such as T1 and T2, are highly precise when it comes to detecting AD in binary or single class scenarios. However, this technique does not provide the same level of A_{cc} when used for binary, unary, or multilayer classifications. Although the AD class shows a high degree of prediction A_{cc}, it requires extensive observation to make predictions in multiple classes. Therefore, further research and potential improvements are needed.The categorization of various groupings of classes attains a high degree of A_{cc} at both binary and unary levels. Thus, it is essential to augment these findings in order to attain a more precise identification of individuals with AD.

2.2.10 Fusion and Registeration Methods

Image fusion combines the information from multiple images into a single, updated view from the MRI for AD classes. Image fusion aims to reduce data while simultaneously producing more understandable images for people and robots. Hybrid feature extraction requires the registration process in order to fuse images. Registration is the process of transforming data into a single coordinate system. Image registration, in which images are overlaid to integrate numerous images, plays an important role in image analysis. It is possible to capture them at different times using different vantage points and using different sensors. Medical imaging uses registration to combine data from several modalities such as CT, sMRI, SPECT, and PET to obtain complete patient information. It is important to take into account the type of data, the collection technique, as well as the level of A_{cc} and sensitivity required when choosing an appropriate registration method. Since image registration tasks are so varied, there is no universal method that works in all cases.The detail analysis of the different Fusion and registration method is used for the anlaysis is decribed in the Table 2.3.

Steps for Registeration

Using the Fusion method, detailed and informative information can be extracted from an image for AD detection. The preprocessing process is integral to the image fusion phase to achieve the desired result, enhancing the registration process through alignment using both geometric and alignment terminologies.

- This Block Diagram illustrates the first process component of the set of pre-processed images. These images underwent processes such as skull stripping, bias correction, and normalization.

- The images are grouped and collated together. A pre-processed image serves the purpose of alignment, determining the intensity. Variations in MRI structure intensities are key parameters for the analysis of this study.

- Evaluating the region of interest stands out as one of the most vital parts in determining the different subjects that make up the various studies.

- On the basis of vectors of intensity, the direction in which a subject is identified can be determined, signaling the occurrence of multivalued intensity.

- The registered image gets a label according to the decision parameters. In decision labeling, symmetric equivalence is essential as the alignment matrix of the images might not always be accessible.

- For a more detailed and precise depiction, the preprocessed images are amalgamated. A meticulous description is the result of this amalgamation of pre-processed images.

Table 2.3: Registeration and fusion method for the detection of AD

S.No	Author	Data Source	Methods	Results	Multi class	Binary class
1	[105]	ADNI	fusion of classifiers	AD vs. NC = 92%	×	✓
2	[225]	ADNI	fusion of classifiers	AD vs. NC = 93.35%	×	✓

Table 2.3 Registration and fusion method for the detection of AD

S.No	Author	Data source	Methods	Results	Multi class	Binary class
3	[102]	ADNI	Multimodal fusion MRI-PET	AD vs.NC, MCI vs NC 96.93% and 82.75%	×	✓
4	[28]	ADNI	Multispectral Fusion for CT and PET Modalities	Multispectral Fusion shows the promising result	×	✓
5	[149]	ADNI	Label Fusion	Automatic Segmentations	×	✓
6	[198]	ADNI	Multi-Modality Fusion	AD vs NC 98%	×	✓
7	[191]	PRIVATE	Multifusion	ITL effectiveness were more	×	✓
8	[156]	ADNI	Fusion of features	Fusion approach of NCST and NSst provides better	×	✓
9	[154]	ADNI	Fusion of Imaging Modifications	MRI + PET Modality Acceptable A_{cc}	×	✓

Table 2.3 Registration and fusion method for the detection of AD

S.No	Author	Data source	Methods	Results	Multi class	Binary class
10	[51]	ADNI	Fusion of Features	Modalities Based Fusion	✗	✓
11	[4]	ADNI	Multispectral Fusion	AD 70.2% A_{cc}	✗	✓
12	[57]	ADNI	Decision Fusion	84.73% A_{cc}	✗	✓
13	[49]	ADNI	Decision Level Fusion	92.6% A_{cc}	✗	✓
14	[15]	ADNI	Decision Level Fusion	80.9% A_{cc}	✗	✓
15	[221]	ADNI	Multimodal Fusion	MRI + PET = 0.97% A_{cc}	✗	✓
16	[160]	Private	Gating Mechanism	0.792% A_{cc}	✗	✓
17	[223]	ADNI	Adverse hypergraph Fusion	93.0% A_{cc}	✗	✓
18	[204]	ADNI	Image Fusion	94.11% A_{cc}	✗	✓
19	[32]		Acrostic Fusion	84–90% A_{cc}	✗	✓
20	[224]	Private Data	Attribute Level Fusion	94% HC vs. MCI	✗	✓

From the Table 2.3 above, the following analysis shows the potential impact of fusion

techniques and summarizes what sort of improvements in the diagnostic process are necessary.Hybrid level of features are mostly taken in to the account from the multi-modality imaging techniques for the AD Detection.Promising A_{cc} is achieved using the Hybrid level of features in the Binary, Unary and multiclass analysis of ADIn terms of detection of AD, the hybrid set of procedures provides the maximum level of A_{cc}.

2.3   Feature Extraction

In conventional methodologies, automated systems are often used that include functionalities to rectify picture irregularities and identify prominent characteristics. The tools are used to discern and juxtapose different cerebral regions in various participants, taking into account their respective limits. This is accomplished via the use of graphical representations that delineate the segregated cortical sections. The use of ML and DL techniques is employed to utilize diverse learning algorithms in the diagnosis of AD development. It is feasible to categorize distinct cohorts into three categories: individuals diagnosed with AD, individuals with MCI and those with normal CN. Additionally, subcategories can be established within the MCI category. Advancements in the diagnosis and treatment of age-related cognitive decline have led to improved efficacy in the detection and management of symptoms associated with AD To quickly and precisely determine a diagnosis, medical professionals often use sMRI techniques to examine both the structural and functional aspects of brain tissue.

2.3.1 Significance of Feature Extraction

The Handcrafted Feature Extraction approach in the field of medical research has proven to be a valuable tool for predicting AD. By utilizing image processing techniques, researchers can extract key features from biomarkers through a fusion process. These extracted features play a vital role in the subsequent steps of the analysis, such as selection and validation of features. The handcrafted process ensures that only relevant and significant features are considered in the classification of classes with AD symptoms.When compared to traditional methods, which often employ a multi-mode approach for feature extraction, the Handcrafted Feature Extraction approach offers several advantages. The use of image processing techniques allows for more precise identification of important disease markers. Additionally, the fusion process improves the A_{cc} of feature extraction by combining information from multiple biomarkers.An important aspect of this approach is optimal feature selection. By carefully selecting the most informative features, researchers can improve the A_{cc} and efficiency of their predictive models. This step is crucial in ensuring that only relevant information is used in the classification process.Moreover, validation techniques play a key role in confirming the effectiveness and reliability of the selected characteristics. Through rigorous testing and evaluation, researchers can determine whether the extracted features truly contribute to accurate predictions of AD. the Handcrafted Feature Extraction approach represents a sophisticated and effective method for predicting AD. Its reliance on image-processing techniques and fusion processes ensures that only relevant features are considered, leading to more accurate classifications. With further advancements in this field, we can hope to see even greater progress in our understanding and detection of this debilitating disease.

2.3.2 Automated Pipelines

The structural and functional connectivity of the brain, as well as to identify abnormalities and patterns in the data. These tools employ various algorithms and methodologies to extract features from MRI data, such as cortical thickness, gray matter volume, DTI metrics, and functional connectivity networks. Free Surfer is one of the most widely used software packages for automated feature extraction from MRI data. It offers a variety of capabilities, including brain segmentation, cortical surface reconstruction, and volumetric analysis. SPM (Statistical Parametric Mapping) is another popular tool that allows the extraction of features from neuroimaging data. Provides a comprehensive suite of functions for preprocessing, statistical analysis, and visualization of brain imaging data. AFNI (Analysis of Functional NeuroImages) is a powerful tool for analyzing functional MRI data. It offers a wide range of preprocessing steps and statistical analysis methods to study brain function. FSL (FMRIB Software Library) is a comprehensive library of image analysis tools specifically designed for functional and structural brain imaging. DIPY (Diffusion Imaging in Python) is an open source software library that focuses on the processing and analysis of diffusion MRI. NIPYPE (NeuroImaging in Python: Pipelines and Interfaces) provides a unified interface to many neuroimaging software packages, allowing for seamless integration and workflow automation. AUTOMATIC ANALYSIS is an open source software tool that aims to provide fully automated processing pipelines for sMRI data analysis. fMRIPrep is a robust preprocessing pipeline specifically tailored for functional MRI data. Ants (Advanced Normalization Tools) offers tools for image registration, segmentation, template building, and more. In conclusion, these tools play a crucial role in the field of neuroimaging research by enabling researchers to extract meaningful features from

MRI data in an efficient and standardized manner.

2.3.3 Feature Extraction Methods

These handcrafted feature extraction models have been used in various studies for various diseases. They are highly confirmed in setting out the characteristics in Table reftab:6 with different parameters that justify the prediction characteristics for the Neuroimaging Disease Organization.The different Automated and handcrafted methods are used for the AD detection in Table 2.4

Table 2.4: Analysis on the automated piplines and feature extraction methods.

S.No	Author	Method	Description
1	[146]	SPM	Statistical Parametric Mapping refers to the creation and analysis of spatially extended statistical processes to evaluate hypothesis concerning functional imaging data. It is a piece of software that puts these principles into action and studies brain imaging data. Sequences might be made up of photos from a single cohort or a collection spanning a time period. A current version is optimized for fMRI analysis, PET analysis, SPECT analysis, EEG analysis, and MEG analysis.

Table 2.4 automated piplines and feature extraction methods

S.No	Author	Method	Description
2	[42]	AFNI	AFNI (Analysis of Functional Neuro Images) is a well-known software package that includes scripts written in C, Python, R, and shell specifically designed to analyze and visualize MRI data from multiple modalities, including anatomical FMRI and DW. It is open to the public for research purposes (both open source code and precompiled binaries).
3	[1]	FreeSurferI	based on tracts (20 MCI, 20NC, 38 DTI). Probabilistic tractography was applied to 84 patients with MCI and AD. Analysis and classification were based on SVM and average FA values, predefined fiber seed region volume, and thalamus volume.
4	[211]	FSL	FSL is a complete tool library to analyze brain imaging data from FMRI, MRI, and DTI. It is straightforward to install and work on both Apple and PCs (Linux and Windows through a Virtual Machine). The majority of tools can be launched from the command line and through graphical user interfaces ("point-and-click" graphical user interfaces).

Table 2.4 automated piplines and feature extraction methods

S.No	Author	Method	Description
5	[67]	DIPY	The Python 3D/4D+ imaging library is what it is called. It encompasses methods for spatial normalization, signal processing, ML, statistical analysis, and medical image visualization, in general. I [82] also incorporates computational anatomy methodologies such as diffusion, perfusion, and sMRI.
6	[72]	Nipype	Nipype is part of the NiPy open source community effort. This Python project provides a uniform interface to current neuroimaging technologies and promotes interactions between different packages within a single workflow.
7	[44]	Automatic analysis	The Matlab-based pipeline system, known as Automatic Analysis (AA), is designed for neuroimaging analysis. It is compatible with SPM 5/8 and specific FSL functions.

Table 2.4 automated piplines and feature extraction methods

S.No	Author	Method	Description
8	[59]	fMRIPrep	A robust interface for scanning protocols with minimal user input, fMRIPrep offers a variety of methods, including co-registration, normalization and unwarping, extraction of noise components, segmentation, and skull stripping. The processed data can be further analyzed using graph theory metrics, surface- or volume-based statistics, and fMRI task or resting state measurements.
9	[201]	ANTs	Advanced Normalization Tools (ANT) allow the extraction of brain anatomy statistics from complex datasets, especially high-resolution images.
10	[91]	Brain Suite	Brain Suite comprises a collection of open source software tools to analyze brain scans from MRI, with a primary focus on automation.

Following the approach of recent research conducted in the field of AD detection, a more in-depth analysis was performed within the framework of particular automated pipelines and handcrafted feature extraction methods in various studies. An analysis of the results obtained through binary and multiclass classification is presented in the table. 2.5.

Table 2.5: Recent study of FE method using automated and non automated pipelines

S.No	Author	Data Source	FE Method	Result	Multi class	Binary class
1	[24]	ADNI	SPM 12 and VBM	AD VS HC 99.93	×	✓
2	[33]	NCRD	SPM12	AD vs CN 93.33%	×	✓
3	[101]	ADNI	SPM12 and FSL	HC vs mAD, p<0.001,p<0.001	×	✓
4	[100]	ADNI	ANT Tool and SPM12	AD vs HC 98.33%	×	✓
5	[104]	ADNI	FREE SURFER	MCnc vs MCic = 73.91%	×	✓
6	[120]	ADNI	FSL	CN vs AD = 0.82%	×	✓
7	[145]	Private	SPM	CSF parameter,AD (p=0.03)	×	×
8	[26]	ADNI	SPM8	AD vs NC = 88% , AD vs MCI=75	×	✓
9	[61]	ADNI	FREE SURFER	MCI to AD p= 1.07e-5	×	✓
10	[76]	ADNI	Verbal Learning Data	AD vs MCI=R= 0.43,R=0.050	×	✓

Table 2.5 FE method using automated and non automated pipelines

S.No	Author	Data Source	FE Method	Result	Multi class	Binary class
11	[172]	ADNI	FREE SURFER	NA	×	×
12	[93]	ADNI	NON Conventional	NC to EMCI= 0.45%	×	×
13	[219]	ADNI	NEURO QUANT,NEURO READER	AD vs. MCI = 0.69%	×	✓
14	[8]	ADNI	FSL	AD VS NC =90.2%	×	×
15	[125]	ADNI	FSL	NC vs AD= 95%	×	✓
16	[133]	ADNI	FSL	CN VS AD = 90%	×	✓
17	[130]	Klinikum Rechts-deisar	FSL	AD vs MCI 95	×	✓
18	[218]	ADNI	SPM	AD (R = 0.51, p = 2.2 * 10 1)	×	✓
19	[38]	ADNI	Free Surfer	mAD vs. HC = 96.51%	×	✓
20	[179]	ADNI	MMSE	NA	×	×

Table 2.5 FE method using automated and non automated pipelines

S.No	Author	Data Source	FE Method	Result	Multi class	Binary class
21	[163]	ADNI	FSL	Changes in Hippocampus observed in EMCI	×	×
22	[111]	Private	Free Surfer	AD(P<.05)	×	✓
23	[169]	ADNI	FSL	AD = 0.98%	×	×
24	[144]	ADNI	MIPAV,SPSS	AD=0.001, p<0.005	×	×

The results of Table 2.5 demonstrate that Free Surfer is the most successful approach to extracting characteristics and has the highest A_{cc} for the detection of AD compared to other techniques. Handcrafted feature extraction techniques, which involve binary and unary classes processed through image processing methods, have been found to be more effective in detecting AD classes. It is obvious that medical imaging techniques are the most reliable way to detect AD classes, although there is still room for improvement. Fusion and registration approaches are being explored and evaluated to detect AD classes.

2.3.4   Machine Learning

Medical imaging has shown great promise in the application of DL, a type of ML based on Convolution Neural Network (CNN). Artificial intelligence (AI) is predicted to become commonplace in all professions due to its ability to improve efficiency, A_{cc}, value, and quality. DL is one of the techniques that does not require

Handcrafted Feature Extraction. Radiology uses ML and DL to classify patients, assess risk, segment them, diagnose, anticipate results, and even predict treatment outcomes. Imaging-based diagnosis, ML, and DL methods were used to classify neurodegenerative disorders, epilepsy, and desalinating diseases. The traditional ML method used in the identification for AD detection 2.6.

Table 2.6: ML models for AD detection

S.No	Author	Model	Description
1	[73]	SVM	The purpose of this article is to create and evaluate classifiers that can differentiate between Alzheimer's patients and healthy controls based on their FA or MD volume. We constructed an SVM classifier using FA/MD data and achieved excellent A_{cc}, sensitivity, and specificity with a linear SVM classifier.
2	[126]	SVM	personalized medical care that meets the needs of the patient and his environment can improve the quality of life of both the patient and his environment. Computer-generated FDG PET scans may be beneficial in early detection of the condition. The temporal and parietal lobes were affected. An SVM was used to categorize these lobes.

Table 2.6 – ML models for AD detection

S.No	Author	Model	Description
3	[155]	SVM	People living withAD often experience memory loss. Medical image analysis is increasingly being used to help diagnose and track the effectiveness of treatment. SVM are being employed in this process. The suggested technique has been found to accurately diagnose AD in 90% of cases.
4	[10]	SVM	AD and MCI may be simpler to identify. This technique could furnish information on the volume of the brain. SVM are utilized to recognize cancer cells. In human choriocarcinoma cells, Alzheimer's was detected with 93.85% specificity (Free Surfer). These features differentiate MCI from Healthy Controls (HC) and AD (AD.
5	[37]	SVM	A statistical learning theory classifier has been developed to detect early AD. The dimensionality curse is overcome by using feature correlation weighting in the t-test. A temporoparietal SVM built from the 20 most discriminative features achieves a maximum A_{cc} of 98. 3%.

Table 2.6 – ML models for AD detection

S.No	Author	Model	Description
6	[27]	ANN	In AD, prodromal clinical variation makes diagnosis and prognosis more difficult. Some studies have used sMRI data instead of case-control research to predict clinical assessment scores (such as the AD Assessment Scale or the Mini-Mental State Examination).
7	[143]	ANN	Multiomics data and the small sample size make AD modeling difficult. Too many differentially expressed genes and methylation sites. This model outperforms standard ML. They outperform previous ML techniques in feature selection and prediction. DNA methylation data can be used to estimate gene expression.
8	[40]	ANN	and hippocampus images from brain sMRI were used to detect AD, moderate cognitive impairment, and normal controls (MRI). ADNI (ADNI) supplied the data sets for the study. The patient's sMRI images were automatically segmented using 3D-Slicer software. Artificial neural networks (ANN) are utilized in clinical diagnosis.

Table 2.6 – ML models for AD detection

S.No	Author	Model	Description
9	[147]	ANN	ANN may outperform linear regression in this scenario. Chemicals were discovered in both people living with early AD and healthy controls. The radial and polynomial SVM models outperformed each other wonderfully. Contour extraction from convolutional layers, The AUC of each test fold was outstanding.
10	[95]	DNN	No more memory or prototyping. Therefore, the system may offer reliable clinical predictions, allowing for the categorization of new patients and the eventual bespoke use of pharmaceuticals. The use of EEG waves to detect AD early has attracted the attention of researchers as an alternative to more Handcrafted Feature Extraction methods. Data have an impact on inverse spectral ranges. In diagnosis, deep neural networks (DNNs) outperform short neural networks (SNNs). We investigate how deep neural networks might be utilized to identifyAD (DNN).

Table 2.6 – ML models for AD detection

S.No	Author	Model	Description
11	[74]	DNN	It is essential to detect AD early on. DL may be helpful in this situation. Data for this research were segmented and selected using nondementia longitudinal magnetic resonance imaging data. DNN also divides AD into many groups. DNN has the potential to improve computer-assisted MRI diagnosis.
12	[114]	DNN	Malocclusions and crooked teeth are common today. AD impairs oral and vocal dental records sifted by robot STATISTIQUES DENTAL They chose the best. DNNs examine AD traits analyze an ideal dental characteristic for oral difficulties.
13	[222]	DNN	To find CMB voxels, we used susceptibility-weighted imaging. To address the A_{cc} issue induced by the CMB/non-CMB voxel mismatch, we adopted undersampling. DNN is made up of an input layer, four sparse auto-encoder layers, a softmax layer, and an output layer. The simulation has a sensitivity of 95.13, a specificity of 93.33, and an A_{cc} of 94.23. Outperforms three contemporary techniques.

Table 2.6 – ML models for AD detection

S.No	Author	Model	Description
14	[34]	DNN	DNN are used in Alzheimer's sMRI. DNN drag-nets exist in LRP. A final picture for categorization. Contributions to negative network classification take time. AD has minimal impact on healthy people.

After examining recent research in the area of AD detection using traditional ML methods, it was observed that SVM is the primary ML model used for AD detection and its classes for identification and its subtypes. Therefore, a complete analysis of the classes, modalities, FE methods, and A_{cc} achieved in the binary class and the multiclass for AD detection is presented in Table 2.7.

Table 2.7: FE methods analysis on the basis of subjects,modalities   .

S.No	Article	Subjects	Modality	F E Methods	A_{cc}	Multi Class	Binary Class
1	[205]	AD, CN	fMRI	ROI	81%	X	✓
2	[48]	CN, FTD	MRI, PET	VBM	93%	X	✓
3	[121]	CN, AD	sMRI	Morphometry	89%	X	✓
4	[158]	CN, AD	SPECT	ROI	89%	X	✓
5	[194]	CN, AD	sMRI	VBM	82%	X	✓

Table 2.7– FE methods analysis on the basis of subjects,modalities

S.No	Article	Subjects	Modality	F E Methods	A_{cc}	Multi Class	Binary Class
6	[186]	CN, MCI	sMRI	SAE	89	X	✓
7	[79]	CN, AD	sMRI	Voxel	87%	X	✓
8	[106]	CN, MCI	sMRI	ROI	91%	X	✓
9	[17]	AD	sMRI	SVM	74%	X	✓
10	[20]	MCI,CN	sMRI	CNN	98%	X	✓
11	[213]	AD,CN	sMRI	CNN	97.52%	X	✓
12	[173]	AD ADNI	MRI	SVM	97.13%	X	✓
13	[200]	ADNI	MRI, PET	PCA	91.4%	X	✓
14	[167]	ADNI	FMRI	Google Net	100%	X	✓
15	[185]	ADNI	MRI	SVM	98.8%	X	✓
16	[89]	ADNI	MRI	CNN, RNN	98%	X	✓
17	[56]	ADNI	MRI	2D Convolution Network	98%	X	✓
18	[63]	ADNI	MRI	3D CNN	94%	X	✓
19	[29]	EEG, ADNI	MRI	CNN 96% Deep Boltzmann Machine	96%	X	✓
20	[65]	ADNI	sMRI	ADNet-DA	52.3%	X	✓

Table 2.7– FE methods analysis on the basis of subjects,modalities

S.No	Article	Subjects	Modality	F E Methods	A_{cc}	Multi Class	Binary Class
21	[12]	OASIS	sMRI	12-Layer CNN	97.75%	X	✓
22	[81]	ADNI	sMRI	Hog-CNN	98%	X	✓
23	[115]	ADNI	sMRI	Res-NET, DenseNET	97%	X	✓
24	[2]	ADNI	sMRI	JD-CNN	94.20%	X	✓
25	[117]	ADNI	sMRI	RNN, Neural Network	90%	X	✓

2.4 Discussion

Neuroimaging is the most effective way to identify anatomical differences between the brains of people with neurological disorders and healthy individuals. Biomarker analysis, which provides two-dimensional (2D) and three-dimensional (3D) structural data, is especially useful for understanding the spatial characteristics of cortical areas affected by AD. DTI is a valuable biomarker for evaluating brain disorders, particularly in different stages of AD. DTI quantifies water molecules and fibers in specific brain regions, providing valuable information on the pathophysiological changes that occur in the brain. Other biomarkers, such as PET, CSF analysis, and genetic biomarkers, can accurately distinguish between healthy brains and those with AD. MRI and PET biomarkers are often used to detect AD due to their widespread use and relatively accurate results. Data classification is usually done using a binary or multiclass framework. The A_{cc} of the binary class is usually above 95%, while

58

the A_{cc} of the multiclass is below 85%. Although the A_{cc} of connections from the anterior cingulate cortex (ACC) to the caudate nucleus (CN) and from the medial prefrontal cortex (mPFC) to the CN is satisfactory, a more detailed examination of the stages reveals unsatisfactory A_{cc} in connections between the mPFC and the ACC, as well as between the ACC and the CN. After analyzing biomarker levels, we performed a systematic review using automated pipelines to diagnose AD and its various stages. Several studies have used automated processes to differentiate AD individuals from healthy controls (HC) or MCI. The investigations used different data sets, software applications, and classification systems, and have demonstrated a notable level of A_{cc} in binary classification tasks. However, further progress in multiclass classification is needed. Studies have revealed significant differences in brain areas or biomarkers when comparing AD-positive individuals with those classified as HC or MCI. Some research used unconventional methodologies or proprietary software, which may impede the ability to replicate their findings. In general, the research mentioned above highlights the potential of automated pipelines in categorizing AD and discovering biomarkers. However, it also brings to light the issues and limitations of this approach. Automated pipeline approaches such as Free Surfer and FSL (FMRIB SOFTWARE LIBRARY) are renowned for detecting AD and its stages. These approaches are more effective when used with smaller data samples. Generally, the data set on AD has a limited scope concerning a particular population. These tactics employ various sequential preprocessing approaches to categorize topics. The three or four classes of categorization, or subgroups, of MCI need more improvement than the other categories. Several research studies have investigated fusion approaches to improve the A_{cc} ofAD diagnosis. Data sets such as ADNI and privately sourced data were used, and diverse modalities such as MRI, PET, CT, and SPECT were employed. The decision-level fusion approach was

used, which involved combining the results of different classifiers. Additionally, feature-level fusion was used, which involved combining different features from various modalities. Other reviews combined feature-level and decision-level fusion techniques. The findings showed promising levels of P_{rec}, ranging from 80.9% to 98%, depending on the fusion approach used. Combining multiple diagnostic characteristics has significantly increased diagnostic P_{rec}. Advanced DL algorithms are expected to improve diagnostic A_{cc} further. More research is needed to confirm the results of these studies and determine their usefulness in clinical practice. The success of fusion and registration validation depends on the use of ML and DL techniques. Several imaging modalities, such as MRI, PET, SPECT, and fMRI, have been studied to detect AD using ML methods. This review covers a variety of feature extraction and classification approaches, including ROI, VBM, SVM, CNN, PCA, and dDL networks. The A_{cc} of classification varies between different methods, with some achieving A_{cc} rates above 90%, while others have lower A_{cc} rates. The combination of multiple modalities and the use of DL networks, such as Convolutions Neural Networks (CNN) and Recurrent Neural Networks (RNN), have shown promising results in achieving higher A_{cc} levels. Most research has also used classification models for binary and multiclass classification problems. This paper examines the potential of using ML methods for the early and accurate diagnosis of AD.

2.4.1 Future Direction and Challenges

AD is a major global problem that deeply affects many people and their families. Identifying the illness as soon as possible is essential to implement treatment and control strategies effectively. However, current diagnostic methods can be costly and

intrusive. Fortunately, a comprehensive study has revealed promising findings that could revolutionize the diagnosis of AD and its various stages. The review proposes using Handcrafted Feature Extraction, Fusion, and ML techniques to detect AD. This approach combines multiple techniques to create a diagnostic tool with improved A_{cc} and dependability.

Biomarker approaches provide a notable P_{rec} in binary classification to identify AD. However, their effectiveness decreases when used in multi-group classification, highlighting the need for further improvements. Handcrafted feature extraction and categorization using ML approaches are recommended to address this issue. To address unique challenges, multimodal techniques require accurate registration and prepossessing of the biomarker.

For identifying AD and its many classes, include using several methodologies, including handcrafted feature extraction, fusion and ML methods. Previous studies have investigated the efficacy of handcrafted feature extraction techniques in binary or single modes to detect AD. However, the study and use of multimodality fusion techniques and various degrees of inquiry for detecting AD have not been as effective. To enhance the fusion methodologies, several picture modalities might be used. In addition, significant progress has been made in traditional and alternative feature extraction and classification techniques methodologies.

There are two distinct methodologies in ML. One of them, DL, can be used to develop a computational model for diagnosing AD. The first approach involves the construction of a model using predetermined characteristics. In contrast, the subsequent approach requires extracting features to construct a model to identify AD and its corresponding classes. These methodologies have been used in several research investigations to detect AD. Correct identification of binary classes has been achieved; nevertheless, to improve A_{cc} for classifications involving more than

61

two classes, it is essential to use non-conventional methodologies. Hand-made feature extraction techniques have shown encouraging results in identifying structural biomarkers. However, an opportunity exists to improve classification A_{cc} in patients with AD by incorporating multimodal approaches. ML methodologies, including SVM, have significantly improved classification P_{rec} and are widely used for the automated detection of AD and its many subtypes.

From perusing the literature review, we have examined the singular modality-based method deployed for identifying AD. In the subsequent chapter, we will delve into the multiple results derived from this singular modality in AD detection. Chapter 3 will also encompass an analysis of multiclass and binary class categorizations. Binary class categorization achieves remarkable precision. However, multiclass categorization shows a degree of flexibility in accuracy when identifying AD and its various subtypes.

CHAPTER 3

ALZHEIMER DISEASE DETECTION USING STRUCTURAL MAGNETIC RESONANCE IMAGING

3.1 Introduction

AD is a neurological disorder affecting millions of people worldwide. It is characterized by the accumulation of amyloid plaques and neurofibrillary tangles in the brain, leading to the death of brain cells [41]. This results in memory loss, cognitive decline, and behavioral changes [60]. Early diagnosis of AD is essential for prompt intervention and therapy, which can slow the progression of the disease and improve cognitive performance [30]. The diagnosis is based on medical history, physical examination, cognitive tests, and brain imaging [14]. sMRI and PET are methods used to detect amyloid plaques and neurofibrillary tangles. SMRI can identify structural differences in the brain. This involves preprocessing, segmentation, and statistical analysis to compare measurements between healthy individuals and those with AD. This helps to understand the progression of AD and provides information

for early diagnosis and treatment evaluation. Data preprocessing and enhancement techniques are used to filter sMRI and stat features to improve results.

In recent studies to detect AD and its subtypes, numerous ML modules have been used, including supervised learning, unsupervised learning, and reinforcement learning methodologies. In recent years, medical research has significantly shifted towards using artificial intelligence (AI) and ML techniques to improve diagnostic capabilities in various healthcare domains. Supervised learning approaches, such as SVM and Decision Tree (DT), have been extensively utilized for the diagnosis of AD by training models on labeled data with known output [132]. Furthermore, DL techniques, which encompass robust neural networks, have shown remarkable potential to recognize complex patterns in large datasets, helping to identify AD-related biomarkers. In medical research, various structural and feature-level analyses are required, so research shows that ML models have shown the most significant impact in detecting AD and its subtypes [177]. The inherent ability of ML algorithms to analyze large amounts of data presents an opportunity to rapidly and accurately detect AD early, which can lead to improved patient outcomes. Additionally, ML algorithms can uncover intricate patterns and trends in data that may not be readily discernible to human observers. Using these capabilities, personalized treatment strategies can be developed based on an individual's cognitive performance and disease progression [174].

Using ML techniques for AD detection presents several challenges, such as ensuring data quality, addressing model interpretability issues, and guaranteeing generalizability across different populations. This article examines the significance of ML algorithms in diagnosing and detecting AD, demonstrating their potential to revolutionize early disease identification and personalized treatment approaches while highlighting the obstacles that must be overcome for successful implementa-

tion. The main challenge lies in accurately identifying the various regions of the brain where AD and its subtypes are affected and detecting AD and subtypes with sufficient A_{cc}. Furthermore, there is a challenge in the multiclass and binary classification for the detection of AD as well as in understanding the impact of different cortical regions in the brain. To address these challenges, we explore various ML algorithms to detect individuals with AD, MCI, and CN. Also, to understand the impact of different regions with different feature sets. In this article, our primary focus is to enhance the $A_{cc}$of classifying multiple categories. AD, MCI, and CN. We conducted a binary classification of AD vs. CN, AD vs. MCI, and MCI vs. CN. Subsequently, we performed preprocessing of the extracted features to classify different subtypes of AD. The contributions proposed through this research work in the AD field are as follows.

- This work used a multiple data preprocessing approach, i.e., the N4 Bias correction and feature extraction technique using an Automatic Pipeline (Free Surfer) from sMRI.

- This work emphasizes the importance of proper data enhancement and preprocessing of raw MRI data to achieve adequate classification results, followed by preprocessing the extracted features to classify different subtypes of AD using trending ML and EL techniques.

- The study involves the classification of multiclass and binary class to detect AD and its subtypes. It also shows the impact of the subjects' different cortical and subcortical regions.

3.2 Data Set

These images were taken at the Laboratory of Neuro Imaging University of Southern California in Los Angeles (ADNI ACCESS DATA (usc.edu)). They are in their original state in Table 3.1 and have not been altered. The database can be accessed at adni.loni.usc.edu.

Table 3.1: Data set of different stages of AD

S. No	Stages	Modality	Age	Gender	Quantity	Properties
1	AD	T1-Weighted MRI	80-85	M/F	200	Raw and Non Filtered
2	CN	T1-Weighted MRI	82-85	M/F	200	Raw and Non Filtered
3	MCI	T1-Weighted MRI	74-87	M/F	200	Raw and Non Filtered

The data set consists of 600 T1-weighted MRI scans of people in three cognitive stages: AD, CN, and MCI. Each stage includes 200 participants of both genders from different age groups. sMRI is unprocessed and unfiltered, providing a broad and detailed data set to investigate AD and related cognitive impairments.

3.3 Method

To identify and recognize AD, ML and Expert Learning (EL) approaches were employed. Our process included various essential stages, beginning with data enhancement and eliminating unnecessary interference from the originalsMRI using the N4-biased correction technique. Subsequently, features were extracted from the preprocessed data utilizing ML and EL, which enabled us to detect AD based on the statistical information obtained. The approach was divided into three sections: The first focused on analyzing multiple classes, the second involved researching single

classes to identify AD and its different types, and the third involved analyzing cortical and subcortical structures to understand their impact on the neuroregions of these individuals. However, both experiments used the same data-processing method. Figure 3.1 presents a comprehensive explanation of the preprocessing process, including calculating statistical characteristics and classifying AD subtypes.
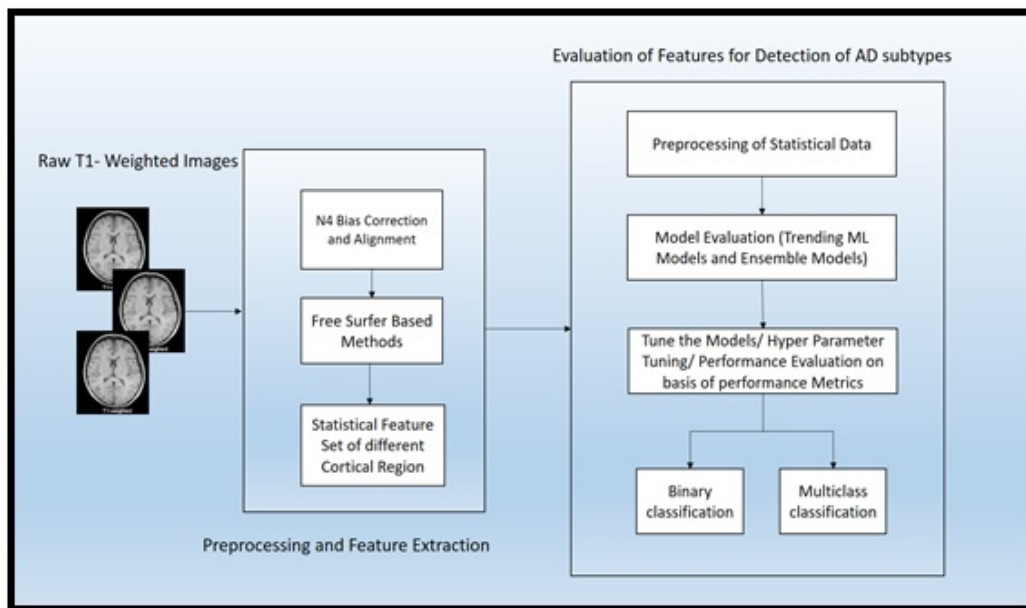
Figure 3.1: Illustrates the complete architecture of the experimental approach employed in Single modality approach

3.3.1 Data Processing

The detection of AD and its subtypes heavily depends on data preprocessing. We obtained sMRI data from the ADNI data set repository, which has essential characteristics. We used the N4 bias correction method to remove any artifacts from the raw data. After that, we used the free surfer method for feature extraction. The resulting stat file, which focused on features, was normalized using techniques such as handling NaN and infinity, data type conversion, and normalization. These steps

are essential for accurate data processing in Figure 3.2.
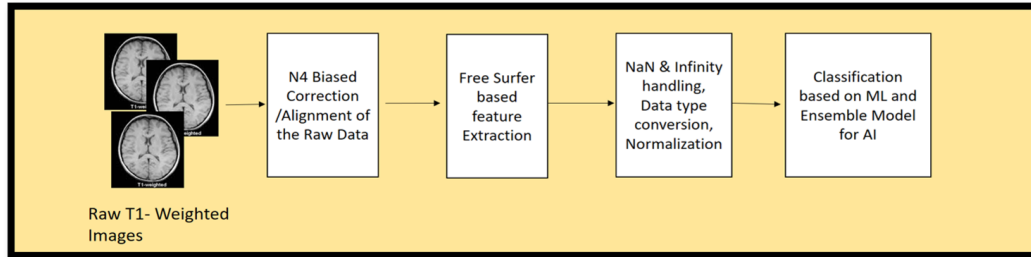
Figure 3.2: Data preprocessing for single modality

3.3.2 Feature Selection

We employed the Select K-Best technique in our feature selection process to detect AD disease in both multiclass and binary class classification. This method helps to reduce the dimensionality of the data set and can improve the performance of ML algorithms. Select K-Best ranks features based on their correlation with the target variable using statistical tests. The value of K determines the number of selected top features, representing its depth. The steps for implementing Select K-Best include choosing an appropriate scoring function based on the problem and data type, ranking features according to their scores calculated by this scoring function, and selecting the top K features with the highest scores for further analysis.

3.4 Machine Learning Methods

The utilization of feature selection techniques has caused the adoption of various ML models such as Logistic Regression (LR), DT, SVM, RF, Gradient Boosting (GB), and Ensemble (LR+SVM) with the Voting classifier for disease classification. ML and EL are heavily relied upon for AD classification. EL, a popular ML technique,

combines multiple models to generate more accurate predictions. This approach has considerably affected AD classification by providing reliable and robust predictions for different types and stages of AD as shown in Figure 3.4.
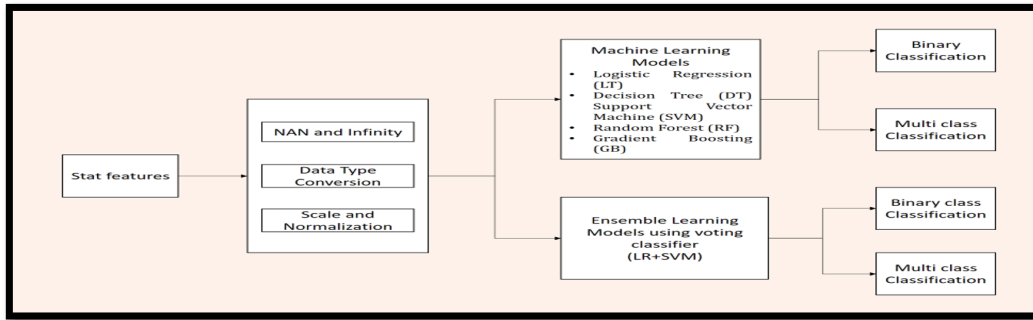
Figure 3.3: Stat data preprocessing, model creation and execution for binary and multi-class classification

3.4.1 Logistic Regression

LR is a statistical technique that examines and models the relationship between one or more independent variables and a binary dependent variable. It is commonly used in healthcare, marketing, and credit scoring to predict outcomes. The technique utilizes a logistic function to transform the linear combination of independent variables into a probability value ranging from 0 to 1. The model estimates the coefficients that maximize the probability of the observed data. The probability of the dependent variable taking value 1 is represented by P(Y=1), which is calculated using the equation 3.1.

The probability is given by:

$$P(Y = 1) = \frac{1}{1 + e^{-(b_0 + b_1 x_1 + b_2 x_2 + \ldots + b_n x_n)}} \tag{3.1}$$

The intercept or constant term is represented by b0, while the coefficients or weights

of the independent variables X1, X2, ..., Xn are represented by b1, b2, bn. The mathematical constant e is also used in the equation. A statistical model employs maximum likelihood estimation (MLE) to obtain the optimal coefficients in the context of diagnosing AD, MCI, and CN subject. These coefficients maximize the probability of the observed data. Based on predictor factors, the model employs a logistic function to estimate the chance, P(Y=1), that a particular individual falls into a specific group (AD, MCI or CN). This function converts any input to a number between 0 and 1, which may be considered as the likelihood of a specific categorization.

3.4.2 Decision Tree

A DT is useful for classifying or predicting outcomes. This ML algorithm creates a tree-like structure, with each branch representing a decision rule based on a feature or attribute and each leaf node representing a possible outcome or class label. To construct the tree, we calculate each attribute's information gain or Gini impurity and select the one with the highest value as the root node. This recursively occurs until all the data is correctly classified or a stopping point is reached. The following are the formulas for information gain in equation 3.2 and Gini impurity 3.3 .

The Information gain is :

$$I_{g(s,a)} = H(s) - \sum (P_t * H_t) \tag{3.2}$$

The Gini Impurity is defined as:

$$\text{Gini}(S) = 1 - \sum [P(i)]^2 \tag{3.3}$$

3.4.3 Support Vector Machine

The SVM is a supervised ML algorithm used for both classification and regression tasks. The primary objective of SVM is to determine the optimal hyperplane that distinguishes data points of different classes with the largest possible margin. For linearly separable data, SVM finds a hyperplane described by the following equation 3.4.

The defined equation for SVM :

$$\mathbf{W}^T \cdot \mathbf{x} + b = 0 \tag{3.4}$$

The Support Vector Machine (SVM) aims to maximize the margin between the two classes. The margin is defined as:

$$\text{Margin} = \frac{2}{\|w\|} \tag{3.5}$$

In SVM optimization, the objective is to minimize $\|w\|$ while satisfying certain constraints. If the data isn't linearly separable, SVM employs the kernel trick. This trick maps the data points to a higher-dimensional space, where a linear separator might be found. For nonlinear SVMs, the optimization problem aims to minimize $\|w\|_2$ along with a regularization term. Misclassifications are addressed using slack variables. The decision boundary, termed the "hyperplane," is determined to maximize the distance, or "margin," from the samples in each category.

3.4.4 Random Forest

Random Forest (RF) is a technique that combines multiple DT to make predictions. This method improves the A_{cc} of the model and prevents overfitting by averaging

the results of the trees. The algorithmic process involves drawing random bootstrap samples from the dataset, growing trees using a random subset of features, and aggregating predictions from all trees. In this case, a linear separator, such as a straight line or a plane, divides classes. Depending on the complexity of the data, a linear, polynomial, or radial basis function (RBF) kernel is chosen. A linear kernel is used if a straight line can separate the classes, a polynomial kernel for slightly complex data, and an RBF kernel for highly complex, non-linear data. The selection of the kernel has a significant impact on the effectiveness of the classification process.

3.4.5   Gradient Boosting

GB is an ML technique that builds a strong predictive model by combining weak learners, usually DT. It focuses on minimizing a loss function by iteratively adding new DT that corrects the errors made by the previous trees.

3.4.6   Ensemble Learning

EL is a ML technique that combines multiple models, or "base classifiers," to make a final prediction. This concept is based on the idea that collective decisions are usually more accurate than those made by individuals. In this research, an EL was used that combined a Logistic Regression (LR) model and a SVM model. These two models were chosen due to their complementary nature; LR is a linear model that is good at estimating probabilities, while SVM with appropriate kernels can handle non-linearity in the data. The LR and SVM models were trained independently on the same dataset, and then their separate predictions were combined to form the ensemble's final decision. This combination is usually done using a method called "voting," which can be either "hard" or "soft." In hard voting, the class label

predicted most frequently is chosen as the final prediction, while in soft voting, the class with the highest average probability across models is chosen. EL like the LR+SVM can improve A_{cc} and reliability, particularly in challenging tasks with complex or high-dimensional data, by leveraging the strengths of different models and mitigating their weaknesses. This is mainly due to diversity and error reduction, as well as the mitigation of overfitting, which can boost the ensemble's overall A_{cc}.

3.5   Result Analysis and Discussion

This research focused on recognizing different subtypes of AD, MCI, and CN To do this, a three-dimensional analysis was performed to process and present data that could differentiate between subtypes. Initially, a data set of the characteristics of the sMRI scan and a target variable that indicated the specific subtype was examined. Preprocessing steps were then taken to address missing and extreme values and standardize the data for consistency. The Select KBest method with ANOVA F value was used to determine the 10 most influential features that distinguished AD subtypes. A new data frame was created for further analysis using these chosen features and the target variables. A pair plot was generated in Figure 3.4 to explore the relationships among these selected characteristics. This pair plot showed how different variables were related to each other in the context of AD subtypes.
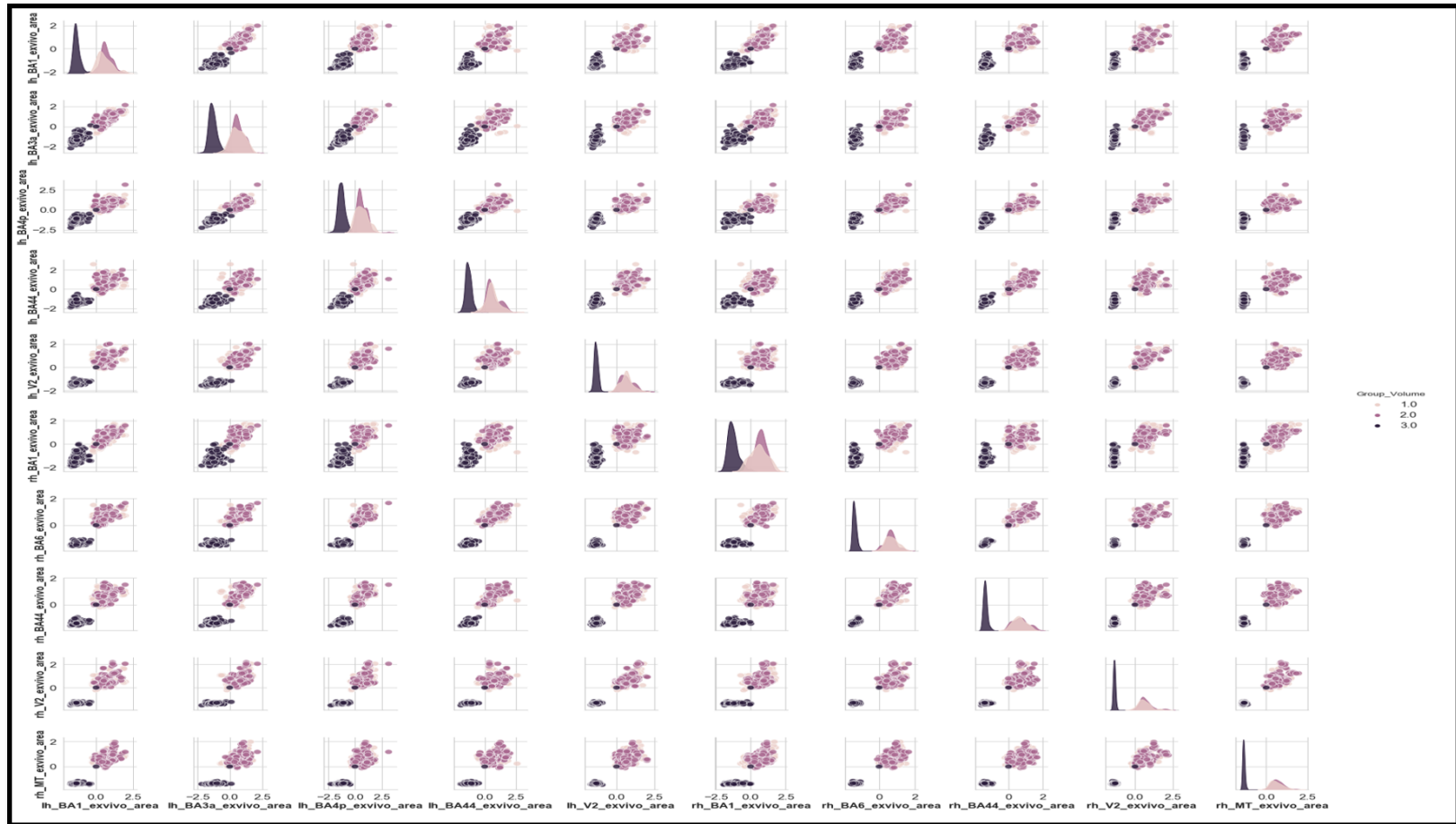
Figure 3.4: Pair plot of the selected features set by using the feature selection method.

3.6 Binary Class classification

In the binary class evaluation, we have performed the three classes analysis which provides more validation of the study, AD vs. MCI, AD vs. CN, and MCI vs. CN. This experiment classifies instances into three stages of Alzheimer's conditions: AD, MCI, and CN. Binary classification tasks involve sorting cases into two categories: AD vs. MCI, AD vs. CN, and MCI vs. CN. Various ML algorithms determine the most effective classifier for this problem. We utilize a five-fold cross-validation to measure how well the model performs. Before then, the data set was separated into training and testing sets, with 60% allocated to training and 40% to testing. A list of classifiers created includes well-established ML models such as logistic regression, DT, SVMs with linear and RBF kernels, RF, gradient boosting, and an ensemble of LR and SVM. The class labels are stratified to ensure that both sets have a balanced distribution of classes. This method objectively assesses the A_{cc} of the model and its standard deviation. The model is trained on the entire training dataset and used to predict labels for the test dataset. The model learns from the complete training data and assesses its generalizability on unseen data in figure 3.5.

A confusion matrix is generated to represent the model's performance visually. The matrix shows the number of true positives, true negatives, false positives, and false negatives for each class, giving insight into the model's strengths and weaknesses in classifying instances. A classification report is also generated, which provides a detailed breakdown of P_{rec}, R_{rec}, score, and support for each class and the overall A_{cc}. Comparison of model performance across various evaluation metrics is now simple. These metrics comprehensively evaluate the model performance, considering multiple aspects such as the proportion of correct predictions and the balance between sensitivity and specificity. The ROC curve shows how the actual

positive rate (sensitivity) and the false positive rate (1 specificity) change at different threshold settings. To evaluate the performance of a model, with a higher AUC indicating better results. In MCI vs. CN, the DT model performs the best across all metrics, with an A_{cc}, P_{rec}, R_{rec}, and $F1_{score}$ of 0.99. The GB model has shown impressive performance, achieving values around 0.98. Meanwhile, the LR, SVM, and Ensemble_LR_SVM models display similar performance across all metrics, with values hovering around 0.96
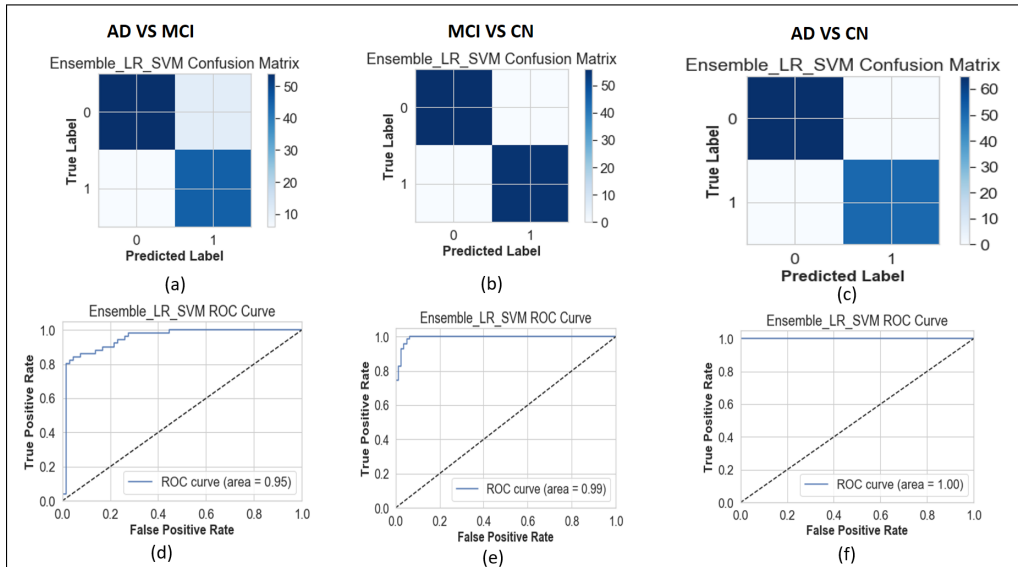
Figure 3.5: (a) Plotting the confusion matrix for, AD. Vs MCI. (b) Plotting the confusion matrix for, MCI vs CN. (c) Plotting the confusion matrix for, AD vs CN. (d) Plotting the roc curve for the AD. vs MCI. (e) Plotting the roc curve for the MCI vs CN.(f) Plotting the roc curve for the AD vs CN.

After analyzing the confusion matrices of the various models, which showed the normal distribution of the data set for both classes, Table 3.2 provides information on detecting these classes in a binary comparison with different performance metrics.

Table 3.2: Peroformance obtained for the binary class in a single modality of AD, MCI, and CN

Model	AD vs MCI				AD vs CN				MCI vs CN			
	A_{cc}	P_{rec}	R_{rec}	$F1_{score}$	A_{cc}	P_{rec}	R_{rec}	$F1_{score}$	A_{cc}	P_{rec}	R_{rec}	$F1_{score}$
LR	0.84%	0.84%	0.82%	0.83%	0.98%	0.75%	98%	0.83%	0.95%	0.96%	0.96%	0.96%
DT	0.76%	0.77%	0.77%	0.76%	0.98%	0.6%	0.99%	0.66%	0.94%	0.99%	0.99%	0.99%
SVM	0.85%	0.85%	0.85%	0.85%	0.99%	0.75%	98%	0.83%	0.95%	0.97%	0.97%	0.97%
GB	0.82%	0.82%	0.82%	0.82%	0.97%	0.6%	0.99%	0.66%	0.95%	0.98%	0.98%	0.98%
Ensemble_LR_SVM	0.85%	0.85%	0.86%	0.85%	0.99%	0.99%	0.98%	0.99%	0.96%	0.96%	0.96%	0.96%

In AD vs MCI, LR, SVM, and Ensemble_LR_SVM models have similar performance across all metrics, with A_{cc}, P_{rec}, R_{rec}, and $F1_{score}$ around 0.85%. The GB model performs slightly worse than the previously mentioned models, with values around 0.82%. The DT model has the lowest performance among all models, with an A_{cc} and $F1_{score}$ of 0.76% and P_{rec} and R_{rec} of 0.77%. In AD vs. CN, the Ensemble_LR_SVM model performs exceptionally well across all metrics, with an A_{cc} of 0.99%, P_{rec} of 0.99%, R_{rec} of 0.98%, and an $F1_{score}$ of 0.99%. The LR and SVM models have similar performance, with an A_{cc} of 0.99%, P_{rec} of 0.75%, R_{rec} of 1, and an $F1_{score}$ of 0.83%. The DT and GB models have a lower performance compared to the other models, with an A_{cc} of 0.97%, P_{rec} of 0.6%, R_{rec} of 0.99, and an $F1_{score}$ of 0.66%. In MCI vs CN, the DT model performs the best across all metrics, with an A_{cc}, P_{rec}, R_{rec}, and $F1_{score}$ of 0.99. The GB model has demonstrated impressive performance, achieving values around 0.98%. Meanwhile, the LR, SVM, and Ensemble_LR_SVM models display similar performance across all metrics, with values hovering around 0.96% in Figure 3.5 and Figure 3.6) by analysis.
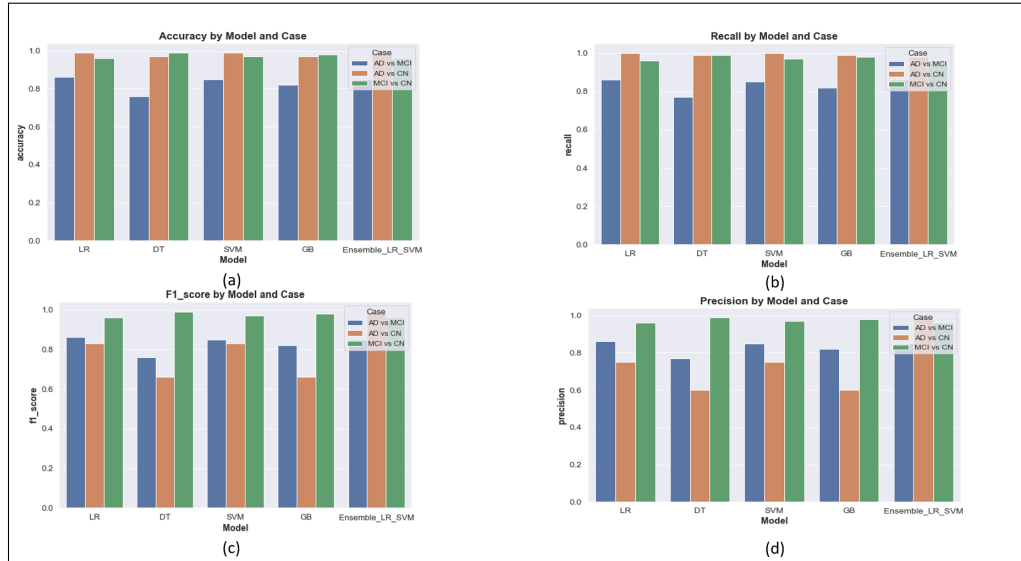
Figure 3.6: Plotting of the performance metrics of the different models applied in single modality approach (a).A_{cc}, (b).R_{rec}, (c).$F1_{score}$, (d).P_{rec}

.

3.7 Multiclass Classification

This research aims to create models that can accurately distinguish between AD, MCI, and CN subtypes based on input features. The data set was divided into training and testing sets in a 70-30 proportion to ensure proper distribution for model training and evaluation. Five classifiers were initialized: Logistic Regression (LR), DT, SVM, RF, and an Ensemble Model (EM) combining LR and SVM. These classifiers were used to detect different AD, MCI, and CN subtypes. Training and validation curves were plotted to visualize the model learning progress and to identify any overfitting or underfitting. After evaluating individual classifiers, the two main models were combined using a soft voting classifier to improve overall performance by taking advantage of the strengths of the main models in figure 3.7.
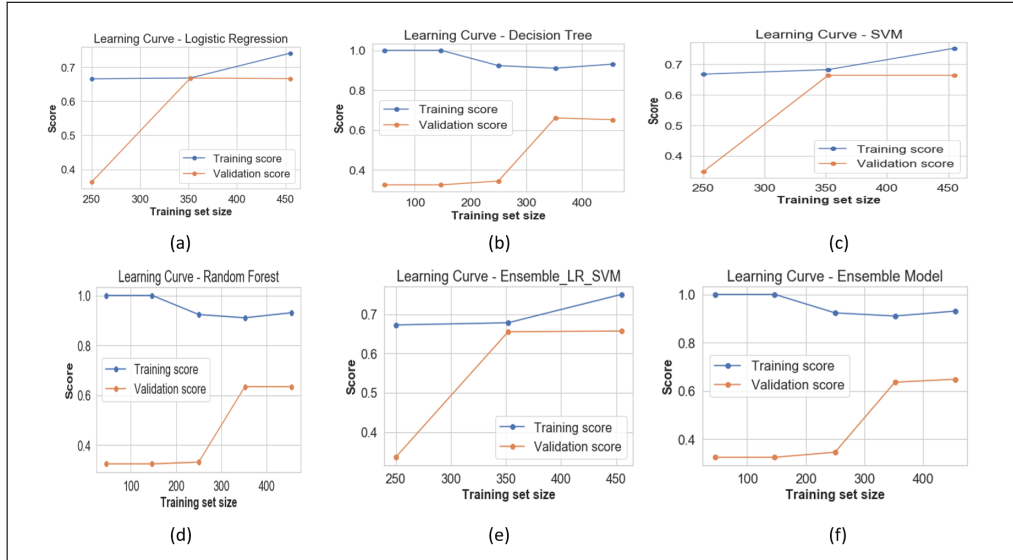
Figure 3.7: Training and validation curve for the multiclass classification of AD vs. MCI vs CN : (a) logistic regression, (b) decision tree, (c) SVM,(d) random forest, (e) ensemble LR_SVM,(f) ensemble model

We assess the performance of our classifiers through various methods. First, we calculate and store confusion matrices to provide a general overview of the A_{cc} classification. To better understand how well the classifiers perform, we create plots called Receiver Operating Characteristic (ROC) curves for each model. These plots show the balance between how often the classifier correctly identifies a positive result and how often it incorrectly identifies a negative impact. This helps us understand more thoroughly how effective the classifiers are in figure 3.8.
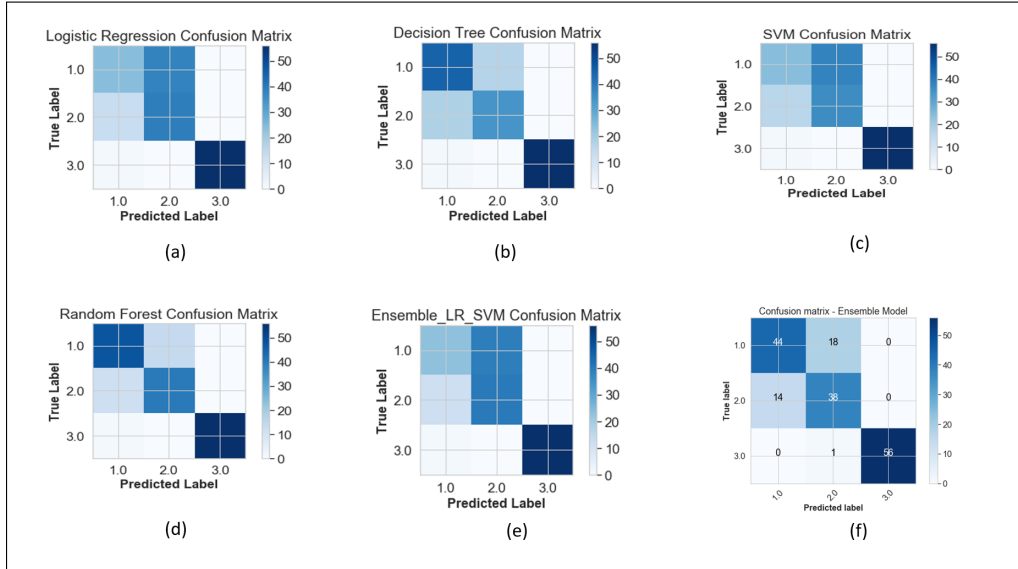
Figure 3.8: Confusion matrix for the different ml models : (a) logistic regression, (b) Decision Tree, (c) SVM Confusion Matrix, (d) Random Forest (e) Ensemble LR_SVM (f) Ensemble model

We conducted a multiclass classification analysis on the ADNI data set with single modality using six classifiers: `LogisticRegression`, `DecisionTree`, `SVM`, `RF`, `Ensemble_LR_SVM`, and `EM`. The data set included features extracted from brain sMRI scans of individuals with AD, MCI and healthy individuals. The `RF` classifier outperformed all other classifiers with an A_{cc} of 82.5. The `DT+RF EM` was the second-best classifier, with an A_{cc} of 80. The `LogisticRegression`, `SVM`, and `Ensemble_LR_SVM` classifiers had the lowest A_{cc} of 69.6, 67.8, and 69.6, respectively. We also analyzed each classifier and the class's P_{rec}, R_{rec}, and $F1_{score}$ metrics. The `RF` classifier achieved the highest P_{rec}, R_{rec}, and $F1_{score}$ for all three categories. In conclusion, the `RF` classifier was the most effective. Finally, the classifiers are trained using the training data and evaluated to determine their effectiveness in detecting the subtypes in Figure 6. We also generate performance evaluations that include the P_{rec}, R_{rec}, and $F1_{score}$ for each class. This provides a

detailed analysis of the classifiers used in Table3.3.

Table 3.3: Performance obtained for multiclass classification of AD, MCI, and CN

Model	A_{cc}	P_{rec} (AD)	P_{rec} (MCI)	P_{rec}(CN)	R_{rec} (AD)	R_{rec} (MCI)	R_{rec} (CN)	$F1_{score}$ (AD)	$F1_{score}$ (MCI)	$F1_{score}$ (CN)
LR	70%	63%	51%	99%	39%	75%	95%	48%	60%	99%
DT	79%	72%	65%	97%	74%	65%	93%	73%	65%	97%
SVM	68%	59%	49%	96%	39%	69%	94%	47%	57%	96%
RF	79%	76%	72%	95%	76%	73%	96%	76%	72%	99%
LR+SVM	70%	64%	51%	97%	37%	77%	95%	47%	61%	94%
DT+RF	80%	74%	66%	95%	68%	73%	98%	71%	69%	99%

Table 3.4 presents the evaluation metrics of six classifiers trained on a dataset for AD classification. These classifiers are LR, DT, SVM, and RF, an ensemble of LR and SVM (LR + SVM) and an ensemble of (DT+RF). The metrics include A_{cc}, P_{rec}, Rrec, and $F1_{score}$ for three classes: AD, MCI, and CN. RF has the highest A_{cc} of 82% , followed by DT+RF with 80% , and the highest $F1_{score}$ for all three classes. On the other hand, SVM has an A_{cc} of only 62% and the lowest $F1_{score}$ for the AD and MCI classes. The results suggest that ensemble classifiers such as DT+RF and LR+SVM are more effective than single classifiers like LR, DT, and SVM. We compared our proposed method with current state-of-the-art multiclass and binary classification techniques to further validate this. The results indicate that our method outperforms or is at least on par with existing techniques in terms of A_{cc}, P_{rec}, Rrec, and other performance metrics in multiclass and binary classification tasks in Table 3.4.

Table 3.4: Validation of Bianry and multiclass classification

Author	Methods	Features	Result	Binary class	Multi Class
[13]	SCNN	sMRI from OASIS	98.72%	✓	×
[94]	ML	MRI measures: entorhinal cortex, banks of superior temporal sulcus, anterior cingulate	93%	✓	×
[25]	Feature Ranking	sMRI from ADNI (130 AD, 130 HC)	92.48%	✓	×
[216]	CNN	T1 weighted MR images (2D projections)	80%	✓	×
[167]	CNN	LeNet-5 for sMRI classification	98.84%	✓	×
	Proposed EL & RF	sMRI from ADNI	AD vs MCI vs CN = 82 AD vs CN = 99 MCI vs CN = 99	✓	✓

From the analysis, the above Table 3.4 demonstrates the effectiveness of various methods used to diagnose AD. The bar graphs indicate that the SCNN and CNN methods and the Proposed Ensemble and Traditional Methods have the highest A_{cc} rates, with values close to or above 98%. On the other hand, the ML and DBN methods have lower A_{cc} rates, ranging from 80-93%. The pie chart provides an alternative view of each method's contribution to the overall A_{cc} as a percentage of the total. These results suggest that SCNN, CNN, and EL methods are the most promising for AD diagnosis. This research investigated three levels of analysis: binary, multiclass, and region-wise. The Ensemble_LR_SVM model was the most successful in binary classification, achieving an A_{cc} of 85.5% in the AD vs. MCI comparison, 99% in the AD vs. CN comparison and 96% in the MCI vs. CN comparison. The RF model was the most effective in multiclass categorization, with an overall A_{cc} rate of 82%. Furthermore, subcortical structures were found to significantly affect different types of AD in both the left and right hemispheres. Specifically, the Para hippocampal and entorhinal regions in the right hemisphere and the inferior temporal and isthmus cingulate regions in the left hemisphere substantially influenced AD. However, challenges must be addressed to improve the performance and clinical applicability of ML models in diagnosing AD. These include incorporating a more comprehensive range of biomarkers or utilizing various imaging techniques, which can be difficult

due to their complexity or cost implications. If these challenges are addressed, it could lead to better early detection methods for AD patients and ultimately better treatment outcomes.

Consequently, contemplating the challenges associated with multimodality, we utilized a multimodal approach for detecting AD. The forthcoming Chapter 4 incorporates this multimodal strategy, employing the fusion of sMRI and PET modalities for the recognition of AD including its various subtypes. This method also integrated an Ensemble learning model to eliminate biases, a feat successfully achieved in the results section, to aid in accurately identifying AD and its subtypes. Therefore, the Ensemble learning model significantly contributes to achieving consistent precision in detecting AD and its subtypes. Subsequently, we conducted multi-class and single modality class evaluations in the next chapter for further identification of AD and its subtypes..

CHAPTER 4

ALZHEIMER DISEASE DETECTION USING MULTI-MODALITY

4.1 Introduction

AD is a debilitating neurological disorder affecting millions worldwide. AD is now one of the leading causes of death in old age [3], and, through trends, the number of cases will increase in the coming years. The biological reason for this condition is the accumulation of a protein called beta-amyloid in the brain, leading to the loss of nerve cells[16]. Around 55 million people are affected by the severe neurological disorder known as dementia, with more than 60% cases occurring in middle- and low-income countries. Economic, social, and mental stress are among the main factors contributing to AD onset. As a result, there is a growing need to understand the disease better and identify effective treatments. In the modern era, using artificial intelligence (AI) techniques to detect AD and its substages is common practice [18]. These techniques include both single- and multimodality methods. However, though contributions from researchers have been made in this field, the most appropriate and effective methods have yet to be identified. AD

has various biological and other causes, and the primary reasons cannot be placed through a single-modal approach [21]. In addition, there are other methods, such as clinical evaluations, demographic conditions, and MMSE scores, but none have been proven to be a sustainable approach for AD detection [45]. In their search for a reliable method to detect AD, many experts are exploring using a multimodal approach. This technique combines biomarkers, such as sMRI and PET, to diagnose more accurately. Therefore, various performance metrics are compared for these classes to validate the study. The significant contribution which is made in the article is described here.

- This work proposed the Image Fusion technique for the fusion of (PET+T1-Weighted MRI) scans and feature fusion from the fused and non-fused Imaging modalities for detecting AD.

- This work proposed the ensemble classification method (GB+SVM_RBF) for the multiclass classification and (SVM_RBF+ADA+GB+RF) methods for the binary class classification of AD.

- This work also reached adequate A_{cc} in the multiclass and the binary class. Classification of AD and its subtypes, i.e., from (AD to MCI), which is 91%, and for other classes (AD to CN) and (MCI to CN) it is 99%. In multiclass, the A_{cc} achieved (AD vs. MCI vs. CN) is 96%.

In this portion, we employ various pre-processing methods on T1-weighted images derived from both statistical and volume-generated images. This section provides an in-depth description of the preprocessing procedure for PET scans. It also details the PET and sMRI fusion process performed using the registration technique. The section then explains the combination of features from both fused and non-fused

85

modalities. The detailed flow for the proposed work is shown in figure 4.6. MRI scans are taken of these different classes: AD, MCI, and CN. These are raw scans. These scans come with high-rated features with unwanted features for disease diagnosis. So, to reduce the unwanted and noise-oriented elements, here, the different preprocessing steps were applied, which it contain the Normalization N4-Bias correction. Then, preprocessed MRI scans are processed for the feature extraction using automatic pipeline methods and different statistical, volume- generated features from the feature extraction method.
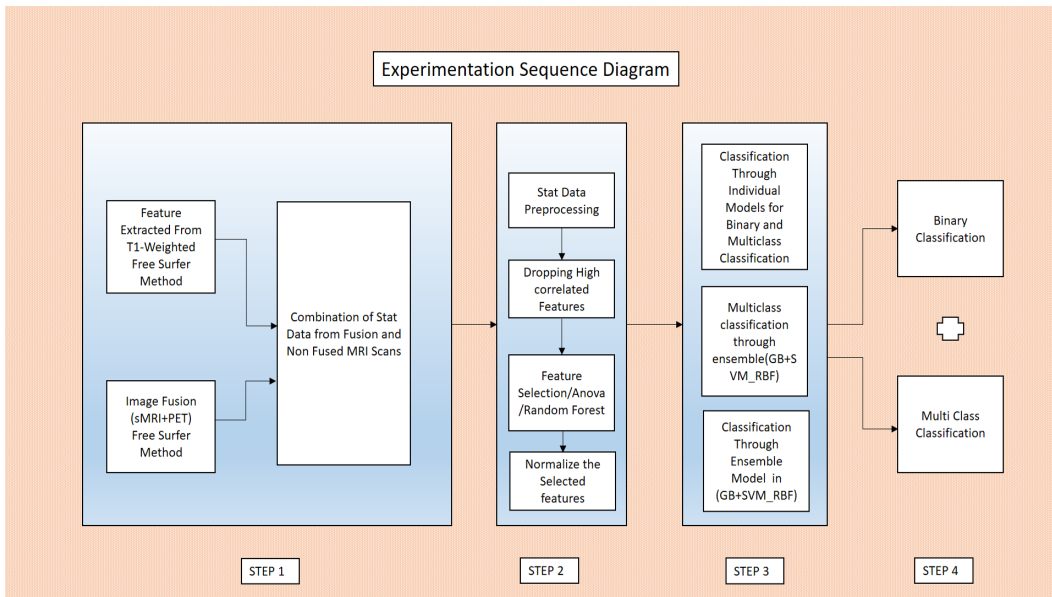
Figure 4.1: Entire Architecture of the Proposed Work

4.2 Data Set

This data set has been taken from the Alzheimer's Disease Neuroimaging Initiative (ADNI). All the images taken here are raw; they are not preprocessed. The database link is (adni.loni.usc.edu). Los Angeles, CA: Laboratory of Neuro Imaging, Univer-

86

sity of Southern California Table 4.1 . The PET images were acquired in December, with the data set comprising various subjects from 2010 to 2022. The data were downloaded in November 2022 for preprocessing and feature extraction purposes, specifically for the PET modality of all AD, MCI, and CN subjects. Similarly, the sMRI data for AD, MCI, and CN subjects spanned from 2006 to 2014 and were downloaded in April 2022 in Table 4.1.

Table 4.1: Data Set used in the Work

S. No	Stages	Modality	Age	Gender	Quantity
1	AD	T1-Weighted MRI	80-85	M/F	200
2	CN	T1-Weighted MRI	82-85	M/F	200
3	MCI	T1-Weighted MRI	74-87	M/F	200
4	AD	PET	85-86	M/F	200
5	CN	PET	70-84	M/F	200
6	MCI	PET	85-89	M/F	200

This Table 2.5 describes using two different modalities (T1-Weighted MRI) and PET. These data sets are a combination of male and female. Their ages generally range from 70 to 90, and the average age is 80. A total strength of 1200 images was used in this research work, and each stage, such as AD, MCI, and CN, is individually 200 in strength. The quality of these images is raw and unfiltered and is not processed anywhere. Figure 4.2 describes more detailed information about the relationship between various attributes using different graphs.
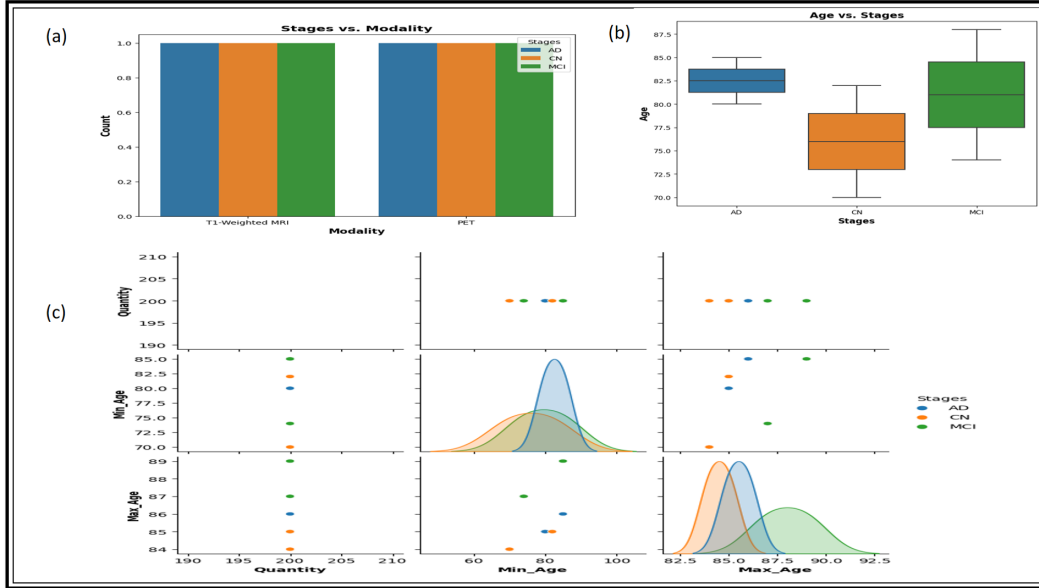
Figure 4.2: Multimodality dataset used for the AD detection

In Figure 4.3 (a), the bar plot represents the plot of Stages vs. Modality, which represents the distribution of different stages (AD, CN, and MCI) across the two imaging modalities, T1-Weighted MRI and PET. Figure 4.3 (b), the age versus stage box plot, illustrates the age range distribution for each stage, highlighting the differences and similarities in age ranges between the AD, CN and MCI groups. Lastly, the Figure 4.3 (c) pair plot presented pairwise relationships between columns in the data set.

4.3   Method

4.3.1   MRI SCANS

MRI scans of these different classes, AD, MCI, and CN are taken. These are raw scans. These scans come with high-rated features with unwanted features for

disease diagnosis. So to reduce the unwanted and noise-oriented elements, here the different preprocessing steps were applied, which contain the Normalization N4-Bias correction. Then, preprocessed MRI scans are processed for feature extraction using automatic pipeline methods and different statistical features generated by volume from the feature extraction method in figure 4.3.
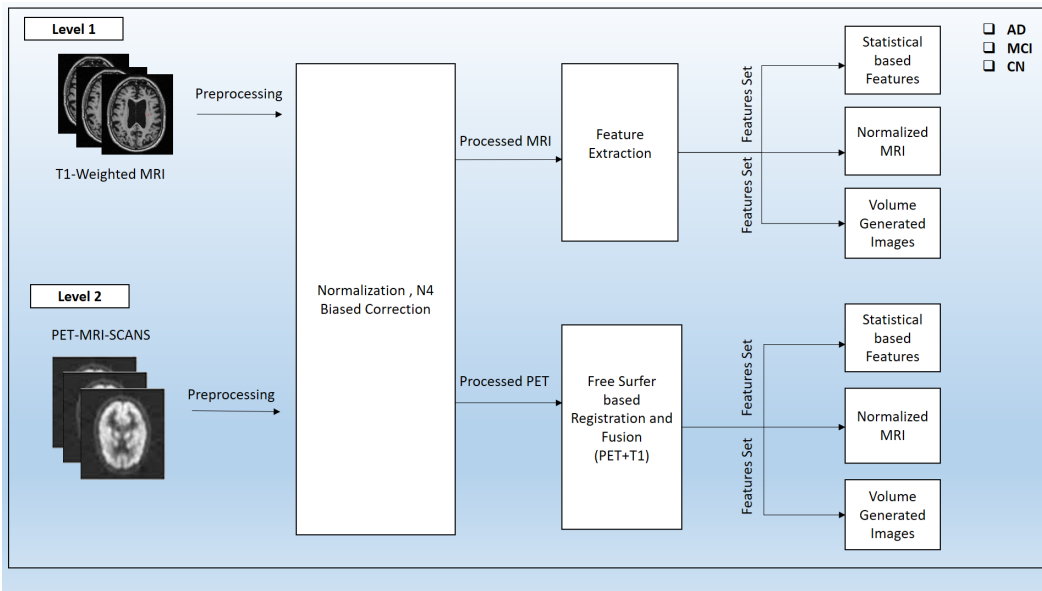
Figure 4.3: Propsed architecture for dual modality approach for fusion PET and sMRI

Normalization is necessary to identify the anatomical features from the cortical area correctly. This formula involves the calculation of each pixel in the percentage range from 0 to 100 and mapping this range with the other pixel, which normalizes the different intensities also. The desired formulae for the calculation of the normal image intensity are described in Equation 4.1.

Normalization is defined :

$$N_{pv} = \frac{P_v - M_v}{M_{av} - M_v} \qquad (4.1)$$

In equation 4.1, N_{pv} defines the normal pixel intensity value, M_v stands for the minimum pixel intensity and M_{av} describes the maximum pixel intensity. This preprocessing technique is an essential technique that includes the removal of various artifacts from the MRI scanners of the other version. This pre-processing is applied in the MRI, PET, and DTI scans for better visualization. These corrections can be achieved through the formulae in Equation 4.2.

Correction achieved in the desired modality:

$$N_{pv} = \frac{1}{1 + \exp(-k(p_v - c))} \tag{4.2}$$

In equation 4.2, the normal pixel intensity value N_{pv} is calculated with respect to the exponential constant and the pixel value obtained from the different AD modalities. After preprocessing, the processed T1-weighted sMRI of the MCI, AD, and CN stages are fed as input to the feature extraction method, which utilizes the Automatic Pipelines method for the feature extraction in figure 4.4.
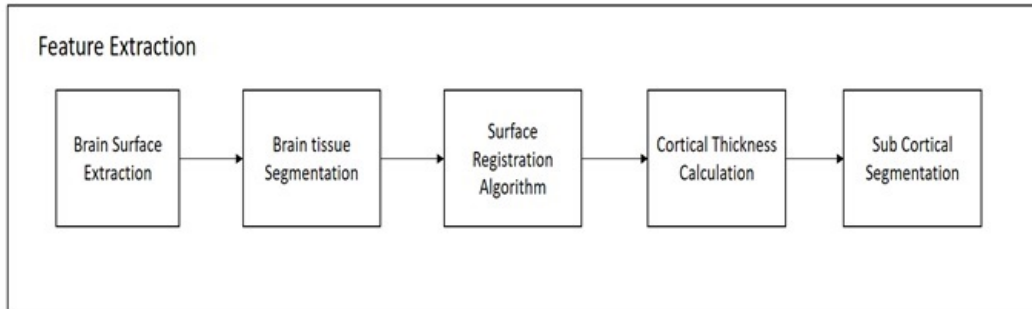
Figure 4.4: Free Surfer Based Feature Extraction from T1-Weighted MRI Scans of AD, MCI, CN.

In the proposed approach, feature extraction from the single modality, specifically T1-weighted MRI scans, plays a crucial role in the detection of AD. T1-weighted sMRI provides detailed anatomical information about brain structure,

making them a valuable source for extracting discriminative features. The feature extraction process involves analyzing T1-weighted sMRI scans to identify relevant patterns and characteristics that are indicative of AD. Various techniques can be applied to extract meaningful features from these scans, such as intensity-based measures, texture analysis, shape analysis, and volumetric measurements, as shown in Algorithm 1.

Algorithm 1 Feature Extraction from Single Modality (T1-Weighted MRI Scans)

1: **Step 1:** Start with a set of raw T1-weighted MRI scans: $T1wMRIs_1$ to $T1wMRIs_n$

2: **for** each MRI scan in the set **do**

3:     **Step 2:** Normalize the image, denoted as $T1_wMRIs_{N4}$

    $\{N_{pv} = (P_v - M_v)/(M_{av} - M_v)\}$

4:     **Step 3:** Perform N4 Bias Correction on $T1_wMRIs$

    $\{N_{4v} = (1/(1 + \exp(-k * (p_v - c))))\}$

5:     **Step 4:** Obtain the corrected $T1_{wMRI}$

6:     **Step 5:** Process the corrected $T1_wMRI$ for feature Extraction, which includes:

    {

        Step 5.1: Extract the brain surface: $T1_{WMRIBSE}$

        Step 5.2: Perform brain tissue segmentation: $T1_{BTS}$

        Step 5.3: Register the surface: $T1_{SR}$

        Step 5.4: Measure cortical thickness: $T1_{CT}$

        Step 5.5: Register the sub-cortical regions: $T1_{SR}$

    }

7: **end for**

8: **Step 6:** End

Algorithm 1 describes the transformation of raw T1 weighted data into processed

$T1_{wMRIs}$ using the bias N4 correction approach, which removes artifacts and normalizes images for uniformity. Feature extraction techniques such as Brain Surface Extraction $T1_{wMRIs}$ and Brain Tissue Segmentation $T1_{BSE}$ are applied to compare different brain regions, followed by surface registration $T1_{BTS}$ to identify other parts of the T1 weighted image. Then the thickness of the cortical $T1_{SR}$ is calculated, and the subcortical registration (T_{CT}) is implemented to produce volumetric shapes, constructed regions, and various regions of the cortical and subcortical brain in the stat files. After completing level 1 experiments, similar preparation steps are taken to prepare the PET modality for the fusion process.

4.3.2 PET-SCANS

Before fusion, the Preprocessing of the PET scans is one of the most important features. The Preprocessing in the PET scans removes noise, reduces artifacts, and improves the signal-to-noise ratio from the scans. PET scans' most common preprocessing techniques include N4 Bias Correction, normalization, and registration. Artifact reduction such as median filtering, helps to remove artifacts by keeping the originality of the image. These artifacts are generally removed from the PET scans using the Adaptive noise filtering technique. In this technique, the noise-oriented input signal and then subtracted from the template signal by preserving the signal's original form, as shown in equation 4.3 and Figure 4.3.

$$PET_{tscans} = (1 - \alpha) * PET_{tscans_{old}} + \alpha * x \qquad (4.3)$$

In equation (4.3), PET_{tscans} is the new noise level, $PET_{tscans_{old}}$ is the old noise level, α is the adaption rate, and x is the current noise sample. These preprocessing techniques are followed using the Free Surfer method. Filtering involves using a low-

pass or high-pass filter to remove high-frequency noise and artifacts. Calibration ensures that the intensities of the pixels are consistent across images. Normalization is used to adjust the intensities of pixels so they are within a certain range. Finally, registration is used to align the images in multiple PET scans. It is done by using an adaptive noise reduction technique, which helps reduce noise without affecting the original image. Then these preprocessed PET scans are further supplied to the Free Surfer-Based Registration method in Algorithm 2.

Algorithm 2 Preprocessing of Single Modality (PET Scans)

1: **Step 1:** Start with a set of raw PET scans: $PETscans_1$ to $PETscans_n$

2: **for** each PET scan in the set **do**

3:     **Step 2:** Apply N4 Bias Correction on the scan: PET_{scans1}
$$\{N_{4v} = (1/(1 + \exp(-k * (p_v - c))))\}$$

4:     **Step 3:** Normalize the scan: $PETscans2$
$$\{N_{pv} = (P_v - M_v)/(M_{av} - M_v)\}$$

5:     **Step 4:** Perform adaptive noise filtering on the scan
$$\{PET_{tscans} = (1 - \alpha) * PET_{tscans_{old}} + \alpha * x\}$$

6:     **Step 5:** End =0

PET scans are highly integrated in the features, but the vigilance of these features cannot be integrated through this individual modality. This Modality requires a certain fusion approach with the T1 Weighted image to obtain a clear vision of the amyloid protein and suffered cortical region in the brain. These Pet scans undergo the N4 Bias Correction methods, Normalization and Adaptive Noise Filtering methods. These methods help to make PET scans undergo further in the fusion approach for feature extraction.

4.3.3 Fusion

Image Fusion is the technique in which the different modalities of Images fuse to provide a hybrid set of features. Pixel-level, feature-level, and decision-level fusion are the practices' basic types of image-fusion approaches. In this process, we have chosen the pixel-level fusion approach to see the actual difference in the cortical region of AD and their different stages through these fused modalities. This helps reduce the noise level and provides a better resolution of the affected area of the brain region. In which the T1-weighted scans are processed through free surfer by the recon-all methods, which contains the pipeline of the different preprocessing steps and helps to evaluate the significant features of volume, area, mean, and other from the different cortical regions of the brain. T1 and PET scans are taken by a register method where a global affine transformation is implemented for alignment. This transformation method produces a better comparison and study of these modalities. This can be enriched with different GM, WM, cortical thickness, and presence in the neuroregion. This is carried out through three aligned translation and adaptation approaches. After the registration method, the mutual characteristics of these modalities are required to determine the similarity between the two scans. After the fusion of these two scans, the volume registration approach wraps the PET and MRI images by translating the source volume into the target volume space in Figure 4.5.
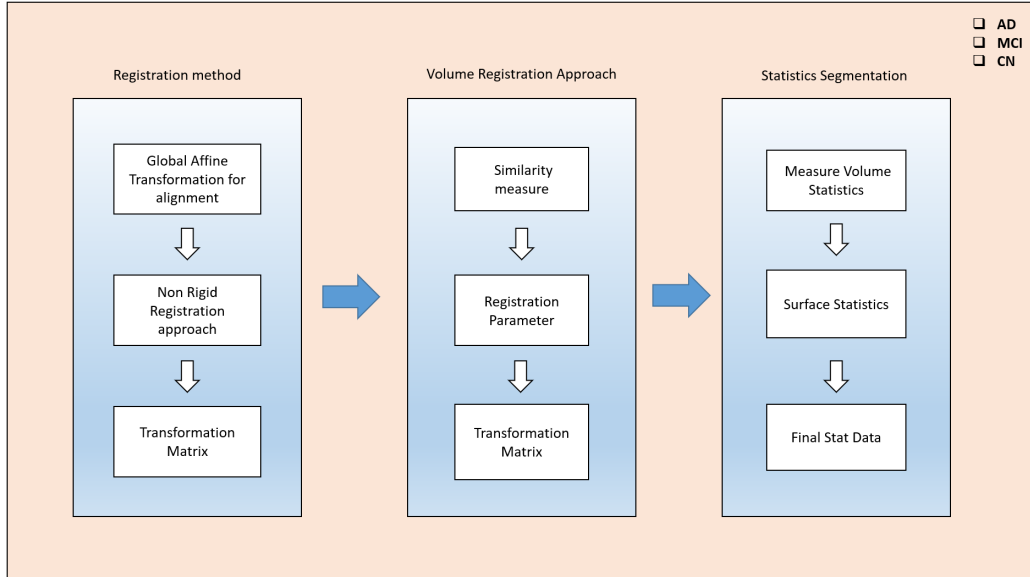
Figure 4.5: Feature extraction approach applied on T1-Weighted MRI scans of AD, MCI, CN.

The fused (PET and MRI) image's similarity measures were optimized through the different registered parameters. They also have been fine-tuned through this approach. These recorded parameters are taken into account when creating the transformation matrix. This matrix calculates the segmented features via the stat segmentation approach from the Free Surfer method. Hence, the volume statistics are measured in the different regions, and the additional stat data for those calculations are performed from this approach. This stat data is calculated on the specific ROI in the brain, such as the frontal lobes, temporal lobes, occipital lobes, and cerebellum, and sub-cortical structures, such as the Hp, amygdala, thalamus, and basal ganglia. Hence these generations of the different stat contain cortical thickness, surface area, folding index, curvature, mean curvature, and cortical volume in Algorithm 3. Mutual Information (MI) is a measure from information theory that quantifies the statistical dependence between two variables. In the context of

image registration, MI quantifies the dependence between the pixel intensities in two images. It is particularly suitable for multi-modal image registration where the images are acquired using different imaging modalities in equation(4.4).

MI for two discrete random variables X and Y is given by:

$$MI(X;Y) = \sum_x \sum_y p(x,y) \log \left[\frac{p(x,y)}{p(x)p(y)} \right] \tag{4.4}$$

where:

- $p(x,y)$ is the joint probability mass function of X and Y,

- $p(x)$ is the marginal probability mass function of X,

- $p(y)$ is the marginal probability mass function of Y.

In the context of image registration, X and Y represent the pixel intensities in the two images, and the probability mass functions are estimated from the intensity histograms of the images. The alignment of edges in the two images, specifically, the white/gray matter boundary. It is computed by summing the squared differences in intensities along the white/gray matter boundary. Thus, the 'similarity measure' here is not based on the overall intensity of the image, but rather on the alignment of anatomical boundaries. A lower cost indicates better alignment.

4.3.4 Mean Squared Error

The Mean Squared Error (MSE) measures the average squared differences between estimates and actual values in equation 4.5.

$$MSE = \frac{1}{n} \sum_{i=1}^{n} (Y_i - \hat{Y}_i)^2 \tag{4.5}$$

Here, Y_i is the actual value, $\hat{Y}_i$ is the estimated value, and n is the number of data points.

4.3.5 Normalized Cross-Correlation

The Normalized Cross-Correlation (NCC) measures the similarity between two signals as a function of the displacement of one relative to the other in equation4.6.

$$NCC = \frac{\sum_{i=1}^{n}(X_i - \bar{X})(Y_i - \bar{Y})}{\sqrt{\sum_{i=1}^{n}(X_i - \bar{X})^2(Y_i - \bar{Y})^2}} \tag{4.6}$$

Here, X_i and Y_i are the two data points These represent two signals or sequences of data points that you are comparing. The index i runs from 1 to n, which means considering n data points in each sequence, and $\bar{X}$ and $\bar{Y}$ are their means.

4.3.6 Normalized Mutual Information

Normalized Mutual Information (NMI) is a normalization of the Mutual Information (MI) score to scale the results between 0 (no mutual information) and 1 (perfect correlation) in equation 4.7.

$$NMI(A, B) = \frac{2 * I(A, B)}{H(A) + H(B)} \tag{4.7}$$

Here, $I(A, B)$ is the mutual information between A and B, and $H(A)$ and $H(B)$ are the entropies of A and B respectively. The entropies measure the amount of information or uncertainty in A and B.A and B represent two random variables or datasets for which you want to measure the mutual information. Algorithm 3 describes the fusion of the T1 Scans and PET Modality. Here in this first we applied the bb-registration methods where we perform the registration.

Algorithm 3 Fusion Dual Modality (PETscans + T1scans)

Require: Preprocessed PETscans and T1scans

Ensure: Stat_data_neuroregion

1: **for** $I = 1$ to n **do**
2:     **Step 1:** Register_method
3:         **Step 1.1:** Apply Global affine transformation to PETscans and T1scans
4:         **Step 1.2:** Perform Non-Rigid Registration on PT1rscans
5:         **Step 1.3:** Return Matrix (NRPETscans + NRT1scans)
6:     **Step 2:** Volume to Volume Mapping
7:         **Step 2.1:** Measure Similarity between NRPETscans and NRT1scans
8:         **Step 2.2:** Generate Correlation Matrix for NRPETscans and NRT1scans
9:         **Step 2.3:** Return Matrix (NRPETscans + NRT1scans)
10:     **Step 3:** Stats Extraction From Output of v to v Mapping
11:         **Step 3.1:** Calculate Volume Statistics for NRPETscans and NRT1scans
12:         **Step 3.2:** Compute Surface Statistics for NRPETscans and NRT1scans
13:         **Step 3.3:** Return Stat Data (NRPETscans + NRT1scans)

In which the Global Affine transformation, Non rigid transformation, and then we return the registered Modality. Then these fused modality went to the volume to volume mapping, where it is altered in the similarity measurement, Correlation Matrix and return the Matrix. From those correlations Matrix the Stat features are extracted in which the Volume statistics and surface statistics for the variation in the classification of AD, MCI and CN classes.

4.4   Feature Level Fusion

For our Feature Level Fusion, we have extracted the relevant features from T1-MRI scans, which include calculation of the volume, area, white matter, curvind, folding, Gaussian curv, thickness, and foldind from the different cortical region of

the brain. In the same way, after fusion (T1+PET), we extracted the features from the combined modality and compiled them into one stat file for further classification. Before applying these combined features we have used the, correlation and drop out techniques for the removal of unwanted features before the selection of features. We have applied binary and multi class level classification for the intended classes AD, MCI, CN .The concept of a fused feature refers to the integration or combination of multiple distinct features into a single entity. The procedure known as "non-rigid registration" is utilized to obtain this combination. Within the field of medical imaging, the term "registration" pertains to the process of aligning two or more photographs that depict the identical anatomical region of the human body. The term "non-rigid" denotes the characteristic of the alignment process that permits a certain degree of adaptability in the matching of pictures, thereby allowing minor deformations or variances in anatomical structures between scans. Ensuring precise alignment of pictures prior to fusion is of utmost importance. After aligning and combining the pictures, the fused image is subjected to feature extraction. The incorporation of these qualities allows for a holistic understanding of the region of interest as they encompass data from multiple modalities. The non-fused modality feature refers to a linguistic phenomenon when the expression of modality, or the speaker's attitude or degree of certainty towards a proposition, is not.In addition to the fused features, the paragraph also references "non-fused" features, which are only derived from sMRI. sMRI is a neuroimaging technique that offers high-resolution visual representations of the anatomical features present in the brain.The sMRI modality is capable of capturing and analyzing various structural characteristics found in distinct regions of the brain that have been linked to AD and its subtypes. The provided information is of significant importance, as alterations in the structural composition of the brain, such as the atrophy of specific regions, might serve as

potential indicators of the progression or existence of AD.The identification and diagnosis of AD).The primary objective of extracting and analyzing these variables, encompassing both fused and non-fused characteristics, is to identify and diagnose AD. AD is a neurodegenerative disorder, and obtaining a thorough understanding through the utilization of diverse imaging techniques can contribute to its precise diagnosis. Through the examination of alterations in metabolic activity as observed in positron emission tomography (PET) scans, as well as changes in structural anatomy as depicted in sMRI, a comprehensive comprehension of the presence and advancement of the disease can be attained. The proposed methodology involves the integration of T1-weighted MRI and PET images to create a fused feature set. Additionally, the analysis of structural changes in the brain will be conducted using non-fused sMRI features. Both methodologies offer supplementary perspectives on the condition and advancement of AD. The whole process is represented in the equation 4.7 and 4.8 and the figure 4.6 .

$$CSR = [F_{T1}, F_{FNFR}] \tag{4.8}$$

Let n_{t1} be the number of features extracted from the $T1$ modality (F_{T1}) and n_{fnfr} be the number of features extracted from the $FNFR$ modality (F_{FNFR}). If we have m samples, then the matrix representation of the CSR will be an $m \times (n_{t1} + n_{fnfr})$ matrix, denoted as CSR_{mat}:

$$CSR_{mat} = \begin{bmatrix} F_{T1_1} & F_{FNFR_1} \\ F_{T1_2} & F_{FNFR_2} \\ \vdots & \vdots \\ F_{T1_m} & F_{FNFR_m} \end{bmatrix} \tag{4.9}$$

100
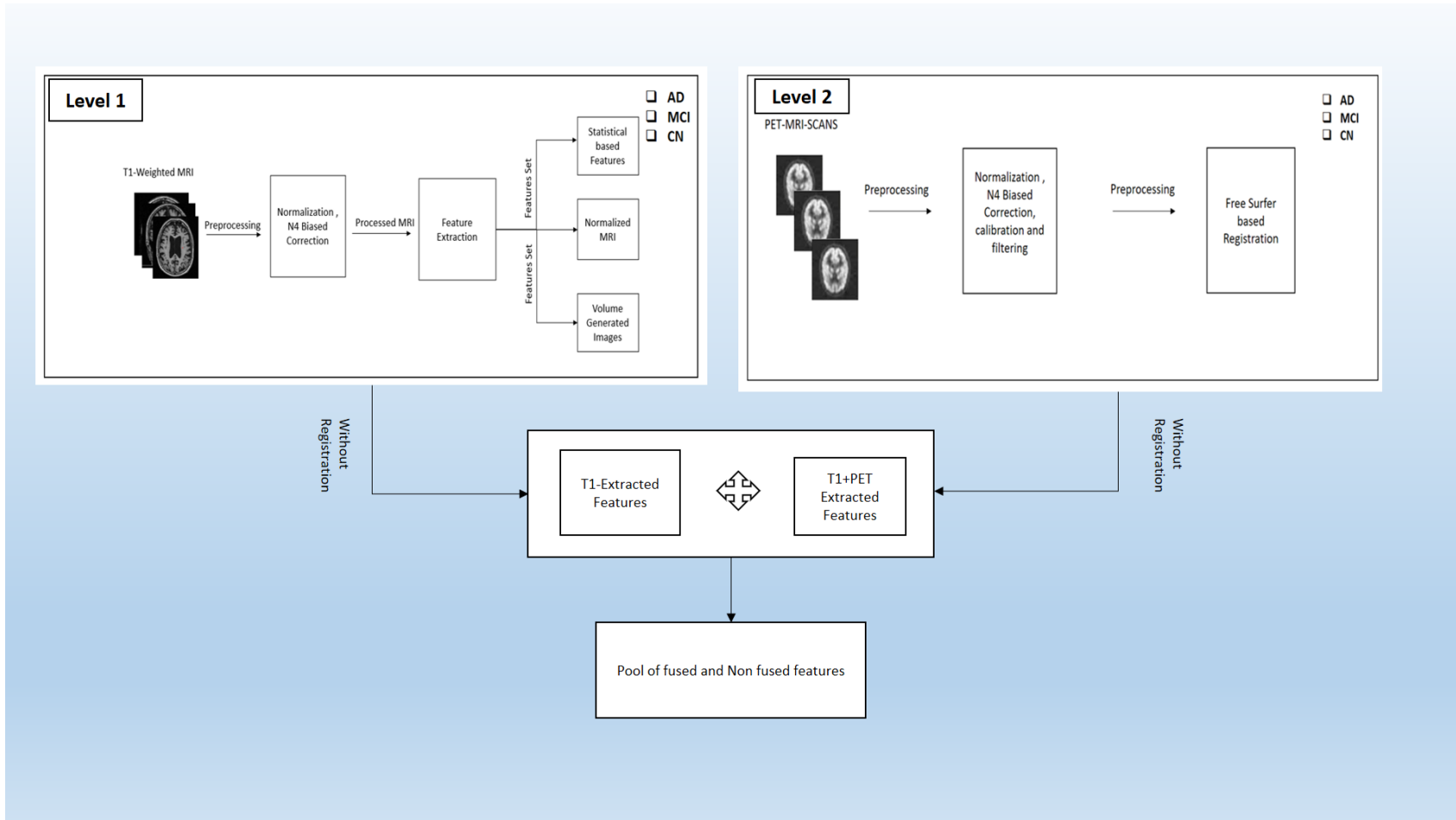
Figure 4.6: Feature Level Fusion of PET MRI Scans of AD, MCI, CN.

4.5 Ensemble Learning Methods

ML techniques are becoming increasingly popular for distinguishing between different stages of AD. However, the use of the ensemble technique to validate the results of these ML methods has not yet been explored. Our study combined the latest ML approach with an approach to classifying AD,MCI, and CN individuals. We used a feature fusion approach to obtain a pool of fused and nonfused features, such as area, maximum, mean, number of vertices, number of voxels, standard deviation, and volume from the fused PET and MRI scans. Additionally, we considered the segmented volume, mean, and area from the segmented region of the nonfused scans. These features were then passed through the ML and EL approaches for further AD, MCI and CN classification (see Figure 4.7).
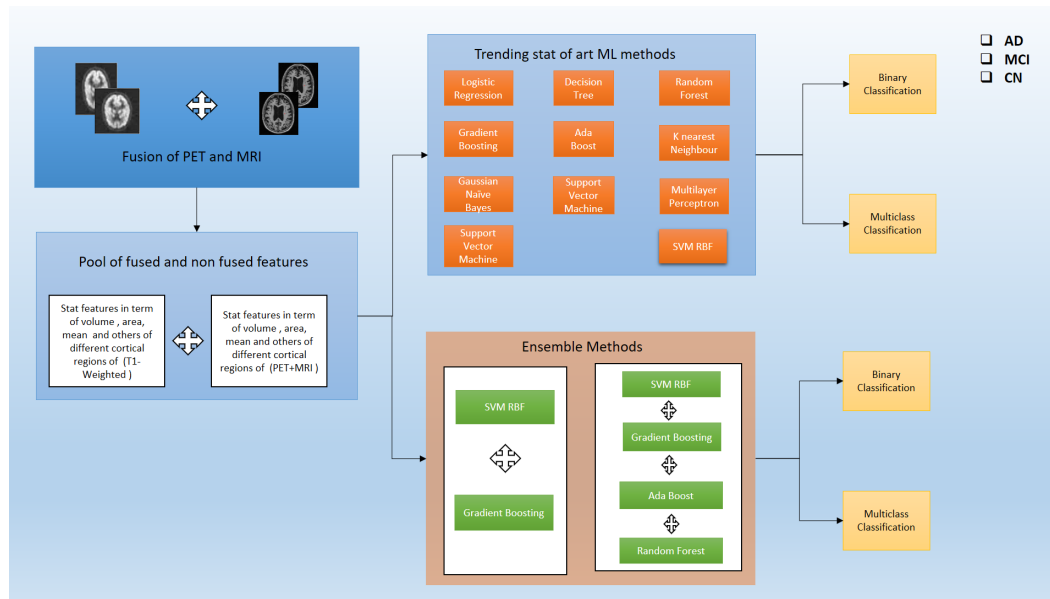
Figure 4.7: Statistical based feature selection using ensemble and traditional ML model.

4.6   Cross Validation

Cross Validation is a vital statistical method used to assess the performance of ML models. It involves partitioning the data into subsets, training the model on a subset, and then validating the model on the remaining data. The objective is to limit problems like overfitting, give an idea of how the model will generalize to an independent dataset, and ensure that every data point gets to be in a validation set exactly once. In our case, we perform cross-validation on the features extracted from the medical imaging data. This enables us to evaluate how well our feature extraction and subsequent classification methods are likely to perform on unseen data, providing a more robust estimate of model performance. We use three and four-fold cross-validation based on the requirements and nature of our data. In 3-fold cross-validation, the data are split into three parts. The model is trained in two parts, and the remaining part is used for validation. This process is repeated three times, each part serving as the validation set once. 4-fold cross-validation works in a similar way, but the data is divided into four parts instead. Each part is used as a validation set once in four iterations.

4.7   Result and Analysis

In this section, we perform a three-fold analysis to detect AD and its subtypes. The first analysis utilizes Ensemble and ML techniques to evaluate the single-modulality approach. Following that, the Dual-Modality approach is analyzed through a Fusion Approach, again employing ML and EL Techniques. Lastly, we perform a subcortical analysis to detect AD and its various subtypes.

   After fusion of the features extracted from the fused PET and T1 weighted

modalities and the non-fused modalities, the high intensity and noise-integrated features are in the generated stat file. These features required regress preprocessing prior to feature selection. The different feature normalization, scaling, and feature dropout techniques are applied to detect AD and the stages. First, this study uses the correlation approach to filter out relevant data whose impact is more significant than 0.9. This procedure already normalized these remaining features. The feature selection method ANOVA F value and RF technique have been used for the feature selection. Hence, the selected features are obtained. This set of features contains information on the different forms of statistical calculation of the other cortical regions of the brain. Hence, after the selection of features, this set of characteristics passed through various trending learning techniques to classify AD and its stages in Figure 4.8.

Figure 4.8: Feature Level Fusion of PET MRI Scans of AD, MCI, CN.

4.7.1 Fused (PET and sMRI) and Non Fused (sMRI) Multi modality Analysis

In Experiment 1 involved the performing binary class classification on three classes from the AD Data Set (AD, MCI, and CN). The results of the binary class applying these standalone learning and EL methods are described in Table 4.2 and in Figure 4.9.

Table 4.2: Describes the results achieved from the different trending methods and perform the Binary class (MCI vs. CN)

S. No	Model	A_{cc}	P_{rec}	R_{rec}	$F1_{score}$
1	LR	98%	98%	98%	98%
2	DT	98%	98%	98%	98%
3	SVM	99%	99%	99%	99%
4	RF	98%	99%	99%	99%
5	GB	97%	99%	99%	99%
6	AB	96%	99%	99%	99%
7	KNN	74%	79%	73%	72%
8	GNB	81%	81%	81%	81%
9	MLP	75%	84%	75%	74%
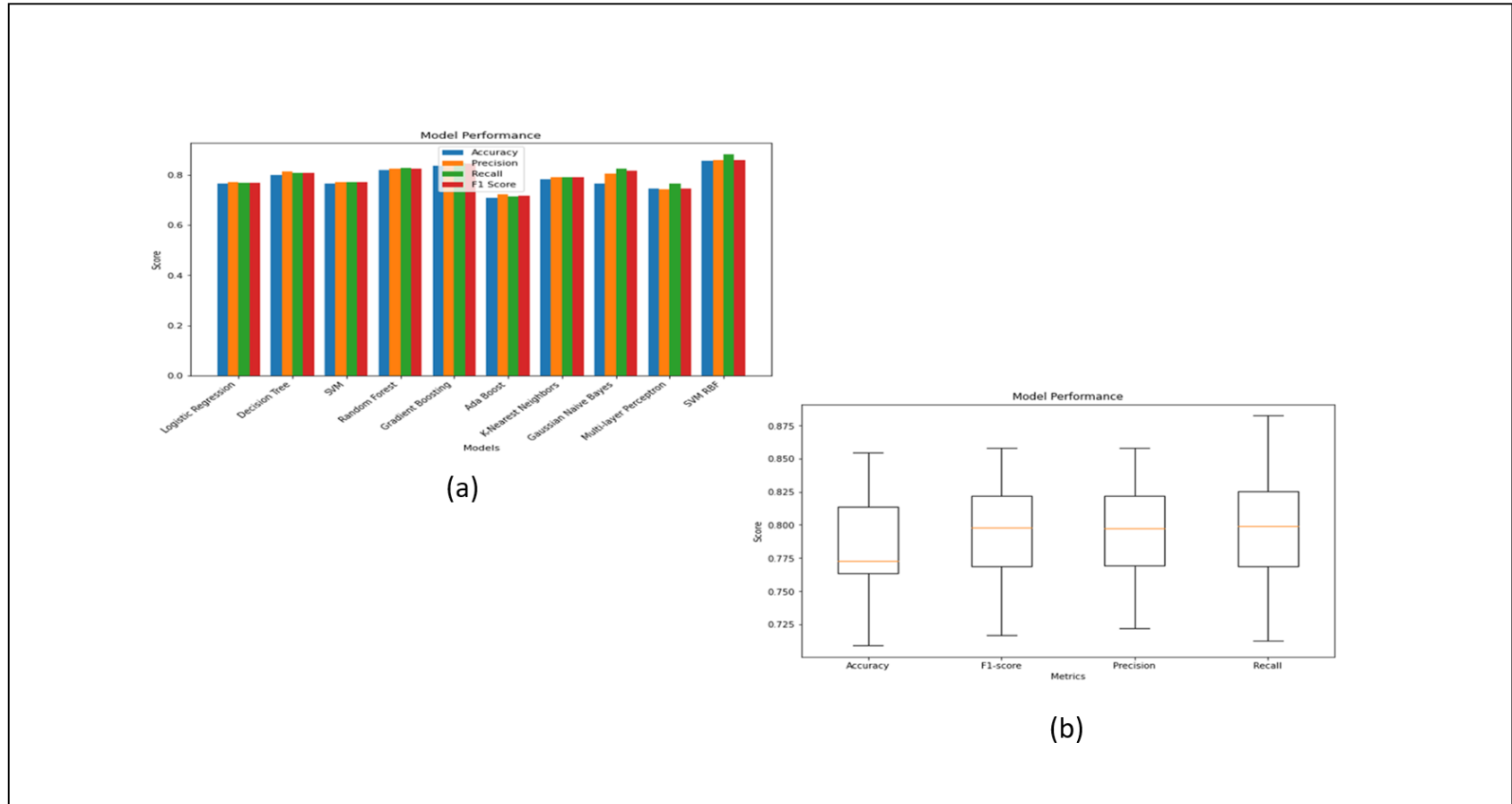
Figure 4.9: Performance Metrics and Model Performance of the Binary Class (MCI vs. CN): (a) Model comparison on the evaluation parameters. (b) Performance metrics values variation in (MCI vs. CN)

Among these models, SVM has the highest A_{cc} (98), P_{rec} (99), R_{rec} 99% , and $F1_{score}$ 99% , indicating that it performs the best overall. The other models also perform relatively well, with high Acc, P_{rec}, R_{rec} and $F1_{score}$, ranging from 98% to 99% . However, the KNN and MLP models have a relatively lower performance score. In the classification of MCI vs. CN we have not used the ensemble method, the adequate A_{cc} has been achieved through stand alone ML methods. Performance analysis through the graph and the box plot of all the models for these classifications is described in the figure 4.10. The model breakdown on the basis of the performances parameters for (MCI vs. CN). The roc curve and confusion matrix of the model with high and low A_{cc} are shown in figure 4.5.
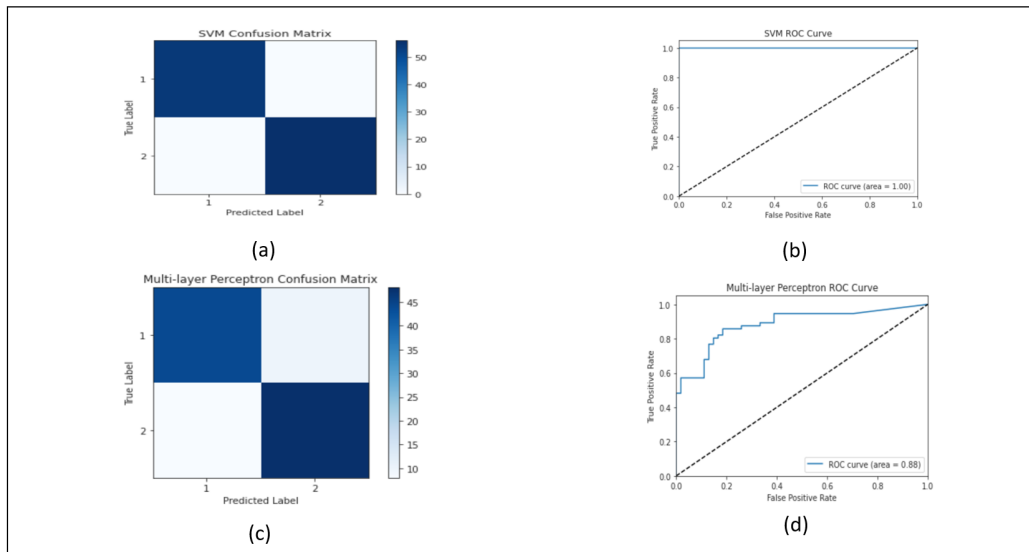
Figure 4.10: Confusion Matrix (a) SVM (c) Multilayer Perceptron and ROC curve (b) SVM roc curve (d) Multilayer perceptron of models for classification of Binary Class (MCI vs. CN).

Again we performed the other classes for the classification like AD vs. MCI. The conversion of MCI to AD is always a challenge in the classification. These challenges raise due to the similarity in there of some of the features, where the classification

model cannot find the difference in comparison. Here in this classification, we have used the stand alone methods and ensemble methods. The Table 3.1 below 4.3 describes the detail results that are obtained after applying all these models as shown in table 3.1.

Table 4.3: Describes the results achieved by the different ML models for the Binary Class (AD vs. MCI)

S. No	Model	A_{cc}	P_{rec}	R_{rec}	$F1_{score}$
1	LR	72.97%	74.55%	72.97%	72.89%
2	DT	81.08%	81.25%	81.08%	81.11%
3	SVM	72.97%	73.48%	72.97%	73.01%
4	RF	86.49%	86.65%	86.49%	86.51%
5	GB	89.19%	89.19%	89.19%	89.19%
6	AB	89.19%	89.57%	89.19%	89.11%
7	KNN	89.19%	89.74%	89.19%	89.21%
8	GB	54.05%	77.03%	54.05%	44.73%
9	MLP	54.05%	29.22%	54.05%	37.93%
10	SVM RBF	86.49%	86.53%	86.49%	86.45%
11	(SVM_RBF+AB+GB+RF)	91.89%	91.98%	91.89%	91.87%

Among these models, SVM has the highest A_{cc} (98), P_{rec} 99% , R_{rec} 99% , and $F1_{score}$ 99% , indicating that it performs the best overall. The other models also perform relatively well, with high A_{cc},P_{rec}, R_{rec} and $F1_{score}$ scores, ranging from 98 to 99. However, the KNN and MLP models have a relatively lower performance score. In the classification of MCI vs. CN we have not used the ensemble method, the adequate A_{cc} has been achieved through stand alone ML methods. Performance analysis through the graph and the box plot of all the models for these classifications is described in the figure 4.11.
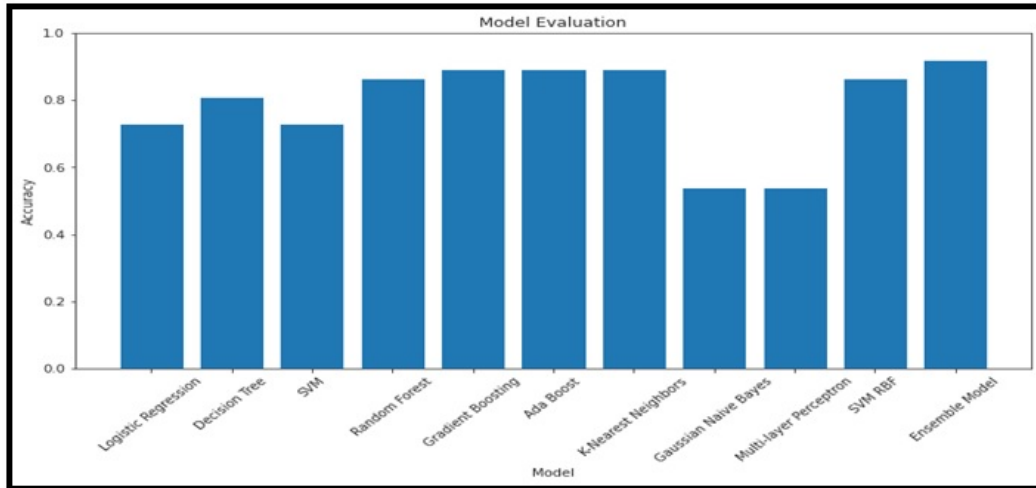
Figure 4.11: Performance comparison of different models for the binary class evaluation.

The Ensemble Method (SVM_RBF+AB+GB+RF) has the highest A_{cc} of 91.89% , P_{rec} of 91.98% , R_{rec} of 91.89% , and $F1_{score}$ $F1_{score}$ of 91.87% , indicating superior performance compared to other models. Models such as AB, GB, and KNN display good performance, with an A_{cc} of 89.19% and P_{rec}, R_{rec}, and $F1_{score}$ values close to 89% . In contrast, models such as LR, DT, SVM, GB, and MLP exhibit relatively lower performance across all metrics. Ensemble and RF, GB, and AB models show acceptable A_{cc}, while other models such as LR, DT, SVM, GB, and MLP struggle to adequately model the progression of MCI to AD. The model performance is assessed based on these metrics for the classification of AD versus MCI.The roc curve and confusion matrix of the model with high and low A_{cc} (AD vs. MCI) in figure 4.12.
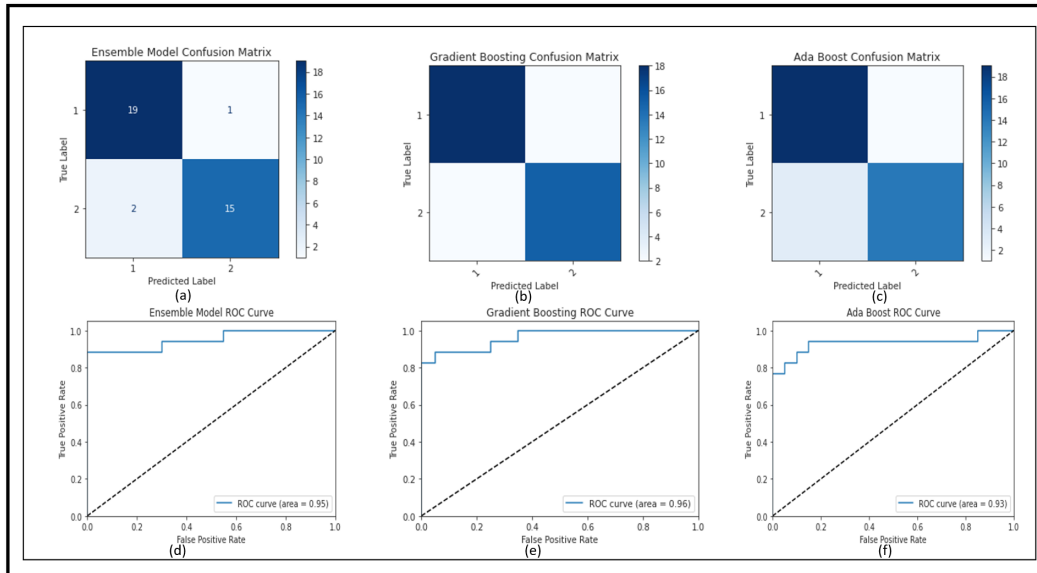
Figure 4.12: Confusion matrix of the different model for binary class :(a) Ensemble model,(b) Gradient Boosting, (c) Ada Boost. Roc curve for binary clas : (d) Ensemble model,(e) Gradient Boosting, (f) Ada Boost

In the previous classification we have observed that the conversion of AD vs. MCI is not providing the greater A_{cc} as compared to the CN vs. MCI. Adequate A_{cc} is achieved through the Ensemble Model of 91% . Now again we perform the classification of the pure AD class vs. the CN class. The performance of these different models is achieved and the results are described in the Table 4.4. The SVM model has the highest A_{cc} (99), P_{rec} (99), R_{rec} 99% , and $F1_{score}$ 99% , indicating that it performs the best overall. The RF and AB models also have high A_{cc} , P_{rec}, R_{rec} and $F1_{score}$ with a score of 99% and 98% , respectively. The LR, DT, GB, KNN, GNB, and MLP models have lower performance metrics in comparison to the other models. The performance analysis through the graph and the box plot of all the models for these classification has been described in the figure4.13.

Table 4.4: Describes the results achieved by the different ML models for the (BC) (AD vs. CN)

S. No	Model	A_{cc}	P_{rec}	R_{rec}	$F1_{score}$
1	LR	98%	98%	98%	98%
2	DT	97%	97%	97%	97%
3	SVM	99%	99%	99%	99%
4	RF	99%	98%	98%	99%
5	GB	97%	97%	98%	96%
6	AB	98%	98%	98%	98%
7	KNN	78%	78%	78%	78%
8	GNB	72%	74%	72%	71%
9	MLP	77%	79%	78%	77%
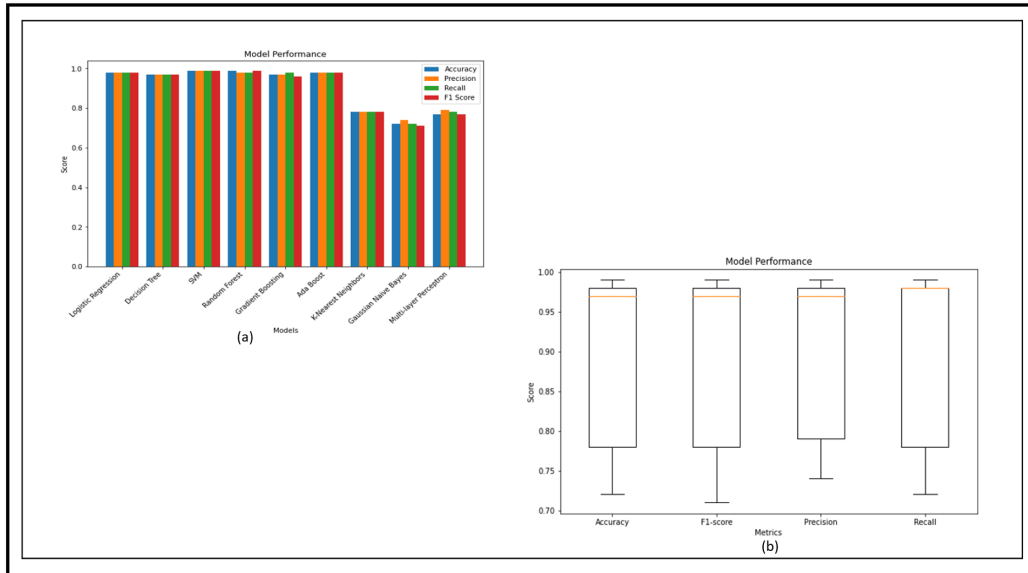
Figure 4.13: Performance Metrics and Model Performance of the Binary Class (AD vs. CN): (a) Model comparison on the evaluation parameters. (b) Performance metrics values variation in AD vs CN

The model is break down on the basis of the performances parameter for the classification of (AD vs. CN). The roc curve and confusion matrix of the highest

A_{cc} and lower A_{cc} achieved by the model for the classification in figure 4.14.
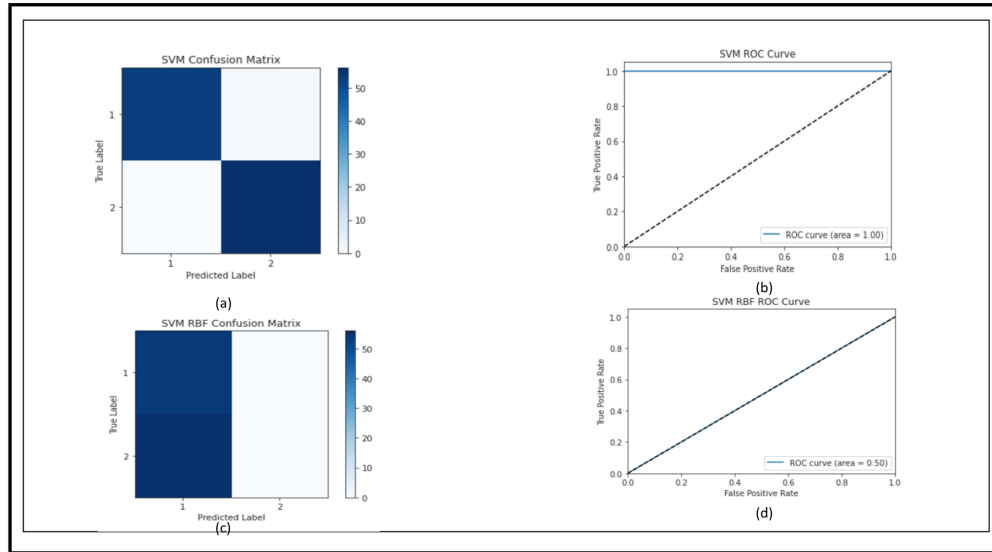
Figure 4.14: Confusion matrix (a) SVM (c) SVM_RBF and roc curve (b) SVM (d) SVM_rbf of models for classification of Binary Class (AD vs. CN).

Hence after seeing the performance in the classification of all the classes AD, MCI and CN. Binary class detection has the maximum A_{cc} of 99% using the SVM model. AD vs MCI classification also shows the sustainable A_{cc} as compared to the precious research trends. After the binary class we perform the multi class for the Detection of AD and there different stages.

Since the Binary class classification has been performed and the adequate A_{cc} is achieved using the classification models. Now we again apply this models for the (MC) and see the performance of these model in this scenario. The below Table 4.5 describe the detail results which are obtained after applying all these model (AD vs. MCI vs. CN).

Based on the results, it is apparent that the ensemble model possesses considerable potential for the multiclass classification of AD and its subtypes. A sustainable

114

Table 4.5: Describes the results achieved by the different ML models for the (BC) (AD vs. MCI vs. CN)

S. No	Model	A_{cc}	P_{rec}	R_{rec}	$F1_{score}$
1	LR	58.18%	61.41%	58.18%	57.27%
2	DT	82.73%	83.10%	82.73%	82.88%
3	SVM	59.09%	65.12%	59.09%	54.34%
4	RF	86.36%	87.57%	86.36%	86.51%
5	GB	93.64%	93.71%	93.64%	93.66%
6	AB	71.82%	73.45%	71.82%	72.24%
7	KNN	86.36%	89.78%	86.36%	86.45%
8	GNB	65.45%	69.16%	65.45%	65.25%
9	MLP	61.82%	65.23%	61.82%	60.71%
10	SVM_RBF	91.82%	93.00%	91.82%	91.90%
11	GB+SVM+RBF	96.36%	97.42%	96.36%	96.36%

A_{cc} is achieved in the multiclass through the ensemble model as compared to standalone learning methods. The ensemble model (GB_SVM_RBF) has the highest A_{cc}, with 96.36% A_{cc} and an $F1_{score}$ of 96.36% . In contrast, the Logistic Regression model has the second-lowest performance in both A_{cc} (58.18%) and $F1_{score}$ (57.27%). Other models like RF, Gradient Boosting (GB), and SVM with a radial basis function kernel (SVM_RBF) also demonstrate strong performance, while models like Gaussian Naive Bayes (GNB) and Multi-Layer Perception (MLP) are less accurate and have lower $F1_{score}$. The performance analysis through the graph and the box plot of all the models for these classifications is depicted in Figure 4.15.
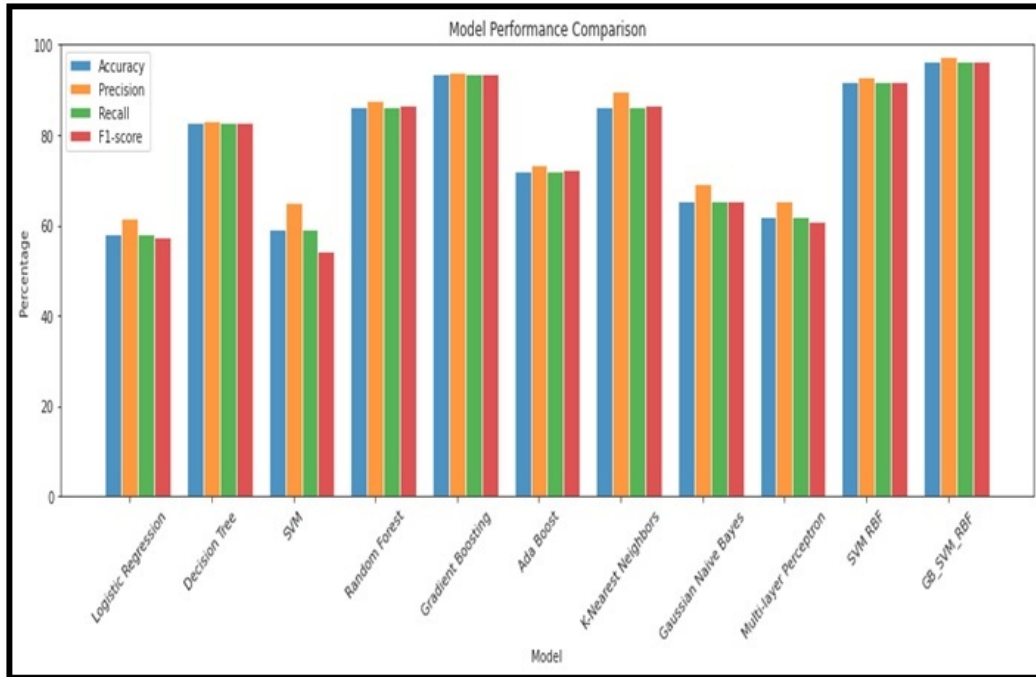
Figure 4.15: Performance Metrics and Model Performance of the Multi Class (AD vs. MCI vs. CN)

Following the evaluation of performance metrics and model performance for all models, we also examined the Confusion Matrix and ROC curve for each model in relation to the results obtained for (BC) (AD vs. MCI vs. CN) figure 4.16.
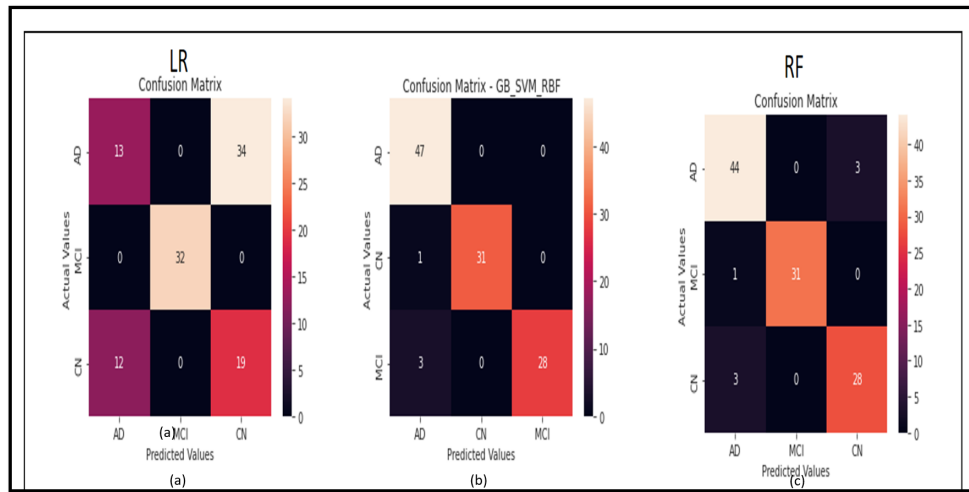
Figure 4.16: Confusion Matrix (a) LR (b) GB_SVM_RBF (C) RF for Multi Class (AD vs. MCI vs. CN).

To further validate our study, we employed various feature selection (Random Forest and KBest) and classification techniques and observed the differing results upon applying these models. In conducting an ablation study concerning feature selection methods and classification models, the ensemble model consistently demonstrated superior A_{cc} compared to the other models utilized in Table 4.6.

Table 4.6: Describes the ablation study of the different ML and Ensemble models for the multiclass (AD vs. MCI vs. CN)

S. No	Model	A_{cc}
1	RF + LR	72.73%
2	RF+ DT	87.27%
3	RF + SVM	80.00%
4	RF + GNB	70.91%
5	RF + KNN	86.36%
6	RF + MLP	86.36%
7	RF + RF	88.18%
8	RF+ GB	90.91%
9	RF+ AB	77.27%
10	KBest + LR	72.73%
11	KBest + DT	77.27%
12	KBest + SVM	82.73%
13	KBest + GNB	78.18%
14	KBest + KNN	80.00%
15	KBest + MLP	80.00%
16	KBest + RF	80.00%
17	KBest + GB	80.00%
18	KBest + AV	71.82%
19	GB_SVM_RBF	96.00%

The Table 3.4 presents the A_{cc} of various combinations of feature selection methods and classification models. The ensemble model, 'RF + GB', achieves the highest A_{cc}(90.91%) among the non-ensemble models. The original ensemble model, 'GB_SVM_RBF', outperforms all the other models, with an A_{cc} of 96% . Comparing the feature selection methods, models using 'RF' generally achieve higher A_{cc} than those using 'KBest'. Among the classifiers, 'DT', 'KNN', and 'MLP' consistently yield relatively high A_{cc} scores when combined with different feature selection methods. The 'GNB' and 'AB' classifiers result in lower A_{cc} scores in most cases, indicating they may not be the most suitable classifiers for this dataset. The ensemble model 'GB_SVM_RBF' demonstrates the best performance,

and utilizing the 'RF' feature selection method yields superior results to the 'KBest' method.

Regarding the fusion of the features and images, the result has effectively shown progress in detecting AD and its stages. The fusion approach has significantly outperformed other non-fusion methods. Demonstration of the different performance metrics of the various models for the binary and the multi-class classification of the AD. Acceptable A_{cc} is achieved in the binary class classification. Many ML and ensemble models have outperformed and shown sustain-able A_{cc}. But for Multi-class, even though the A_{cc} is also acceptable. But while comparing with the binary, there is still room for improvement. The results achieved in the article are compared and validated with the recent research made in AD detection in Table 4.7.1.

S. No	Author	Data Base	Method	Binary Class	Multi Class
1	[43]	ADNI	3D-CNN	AD vs CN 91.5%	NA
2	[80]	ADNI	Soft Max Classifier	CN vs. MCI 87.50%	NA
3	[4]	ADNI	BiLSTM	NA	AD vs. CN vs. MCI 84.95%
4	[208]	ADNI	Feature Fusion	AD vs. CN 90%	NA
5	[160]	ADNI	Graph Fusion	AD vs. CN 93%	NA
6	Proposed	ADNI	Image Fusion+ Feature Level Fusion + Ensemble method	AD vs. CN 99% , MCI vs. CN 99% , AD vs. MCI 91%	AD vs. MCI vs. CN 96%

119

The study proposed in the Table 4.7.1 utilized a combination of image fusion, feature level fusion, and ensemble methods for classification. For the binary classification of AD versus CN, an A_{cc} of 99% was achieved, which is higher than the A_{cc} obtained in the other studies. In the binary type of MCI vs. CN, an A_{cc} of 99% was obtained. When the binary classification of AD vs. MCI, an A_{cc} of 91% was achieved. For the multiclass category of AD vs. MCI vs. CN, an A_{cc} of 96 was obtained. The author reported that this result outperforms the multiclass classification A_{cc} of 84. 95%. Therefore, from the Table 4.7.1 above the proposed model shows effective A_{cc}.

Once we've applied a multimodal method to detect, we acknowledge the difficulties in assessing the influence of various brain regions in identifying AD and its subtypes.In the subsequent chapter 5, we delve into an analysis of different cortical and subcortical brain areas. The combination of these structures, including the accumbens, amygdala, caudate, hippocampus, pallidum, putamen, thalamus, and ventral DC, etc is essential for the diagnosis of AD . There fore We identify these regions and evaluate which ones exert the most significant influence on the identification of AD and its subtypes.

CHAPTER 5

CORTICAL AND SUBCORTICAL STRUCTURE ANALYSIS USING SINGLE MODALITY AND MULTIMODALITY

5.1   Introduction

AD is a neurological disorder that causes the brain to deteriorate, leading to a decline in cognitive abilities, behavior, and daily activities. This degeneration is caused by the accumulation of beta-amyloid plaques and tau protein, which eventually leads to brain death. sMRI scans are used to diagnose AD by detecting structural changes in the brain. Scientists have studied these changes in the cortical and subcortical regions associated with AD [118], to identify patterns that can be used for a reliable diagnosis. The unique design of subcortical structures has drawn attention. The combination of these structures, including the accumbens, amygdala, caudate, hippocampus, pallidum, putamen, thalamus, and ventral DC, is essential for the diagnosis of AD. [22]. These components are necessary for a variety of bodily functions and any deficiency can cause serious damage. For example, abnormalities in the left accumbens and amygdala, which are involved in memory processing, learning, and emotional reactions, may be indicative of early-onset Alzheimer's symptoms. Early

detection of these areas can lead to a proactive approach to treatment, resulting in better outcomes for those with AD [83]. The onset of AD is marked by early degenerative changes in regions such as the hippocampus and entorhinal cortex. Analysis of these changes can detect pathogenic modifications before the onset of clinical symptoms. Biomarkers, such as the volume and morphometry of subcortical structures, can be used to differentiate between AD and other neurodegenerative disorders, as well as to monitor the progression of the disease[157]. The study of patterns in subcortical atrophy can provide valuable information on disruptions within neural circuits and the spread of disease throughout the brain and can help explain the connection between structural variations and cognitive decline [214]. Combining different modalities can also be a useful approach to detect subcortical structures and analyze these regions [176]. Automated pipelines for automatic interpretation of subcortical regions are of relatively high use compared to other techniques. Artificial intelligence-based image classification models can quickly and accurately distinguish infected patients from healthy populations [207]. A computerized method like the Computational Anatomy Toolbox (CAT) analyzes brain structure, including segmentation, estimation of cortical thickness, and surface-based morphometry [68]. Vol Brain is an online platform for automatic brain segmentation by MRI and volumetric analysis. A multiatlas segmentation approach involves registering multiple atlases to the input image, combining the labels, and refining the segmentation using ML techniques [181]. Self-attained neural network that is a PSO-guided self-tuning convolution neural network (PSTCNN). This enhancement enables the model to automatically adjust its hyperparameters, significantly improving its ability to detect AD [206]. Different transfer learning approaches also accommodate the significant P_{rec} in the detection of AD in 2D modalities structures [175]. Brain Suite combines atlas- and surface-based segmentation techniques to identify different regions of the brain, including subcortical structures. Free Surfer is one of these approaches that performs both types of segmentation. Free Surfer uses Atlas-based segmentation, an essential step in the subcortical region segmentation process. It involves using a predefined probabilis-

tic atlas to identify and label different brain structures. The atlas is created from a large set of manually labeled MRI scans. It contains information on spatial location, intensity distribution, and statistical calculation of different brain structures, including subcortical regions [148]. The Hierarchical Image Processing System (HIPS) is well suited for basic image processing tasks, such as filtering, transformation, and segmentation, although it is not commonly used for neuroimaging data [78][178]. Pinpointing subcortical structures for AD detection has numerous obstacles, including individual structural variations, image clarity and P_{rec}, overlapping intensity outlines, disease diversity, distinguishing it from other neurodegenerative diseases, and conducting longitudinal studies. Influences such as age, sex, genetic heritage, and disease progression contribute to the variability of these structures. The intricate nature of subcortical regions makes them vulnerable to partial-volume effects and image aberrations. Adequately outlining arrangements with similar intensity profiles onsMRI requires sophisticated segmentation methods. The diversity within AD cases and its similarity to other neurodegenerative diseases complicate the identification process of consistent biomarkers, vital for the establishment of definitive diagnostic parameters. Lastly, there is the issue of longitudinal investigation, which can provide significant information on disease progression and the efficacy of treatments. These approaches enable different problems associated with variations in scanning equipment used over time and image registration issues. Furthermore, there is a pressing need for foolproof automated systems that can effectively identify minor changes. Therefore, in this article, we have used the two different modalities to understand the various regional effects on the brain using the registration approach. To understand the importance of these subcortical regions in identifying AD, we fused the two modalities (PET and T1) to better visualize the areas. Identifying subcortical structures for AD detection presents several challenges, including image quality and resolution, structural variability between individuals, overlapping intensity profiles, disease heterogeneity, differentiation from other neurodegenerative disorders, and longitudinal analysis. Therefore, the following contributions address these challenges and understand

Table 5.1: Data set for multimodality

S. No	Stages	Modality	Age	Gender	Quantity
1	AD	T1-Weighted MRI	80-85	M/F	200
2	CN	T1-Weighted MRI	82-85	M/F	200
3	MCI	T1-Weighted MRI	74-87	M/F	200
4	AD	PET	85-86	M/F	200
5	CN	PET	70-84	M/F	200
6	MCI	PET	85-89	M/F	200

the importance of subcortical structures for the identification of AD and its subtypes.

- Combination of two modalities (PET and T1) and a registration method to study the effect of diverse brain regions on AD.

- Segmentation of different subcortical regions using atlas-based registration methods to understand the impact on AD and its subtypes.

- Significance rating and evaluation of different subcortical areas using EM and ML methods. We discuss the associations and implications of these subcortical areas on multiple variants of AD.

- Multiclass classification based on the subcortical parameters of AD-affected brains and their subtypes.

5.2 Data Set

The data used in Table 5.1 was obtained from the Alzheimer's Disease Neuroimaging Initiative (ADNI) and consists of raw images that have not been preprocessed. The database link can be found at https://adni.loni.usc.edu/data-samples/access-data/. The Laboratory of Neuro Imaging at the University of Southern California in Los Angeles conducted the study. The data set encompasses medical images of individuals at varying stages of AD:

AD, MCI, and CN. Features two types of imaging: T1-weighted MRI and PET scans. There are differences in age among the groups. For T1-weighted sMRI, AD patients range between 80-85 years, CN participants range between 82-85 years, and MCI participants range between 74-87 years. Within the PET scan group, AD ages are 85-86 years, CN ages range from 70-84, and MCI is 85-89. Both male and female participants are included, with 200 samples for each combination of modality stages, as shown in Figure 5.1.(a) shows the relationship between the three classes. (b) Shows the relation between stage, modality, gender, and quantity.
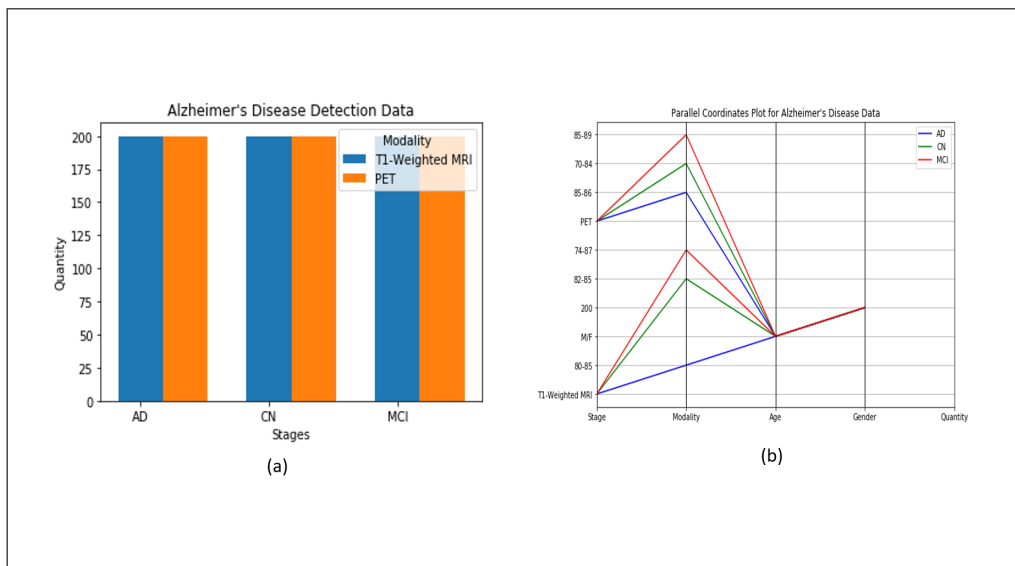
Figure 5.1: (a) Represent the analysis of the different classes. (b) Shows the relationship between the stages, modality, gender, quantity

5.3 Methods

Multimodal image fusion is crucial in identifying AD by merging data from multiple imaging techniques, such as T1-weighted MRI and PET, to gain deeper insights into brain structure and function. When MRI images are evaluated, it is vital to consider biased fields that may

cause intensity fluctuations due to magnetic fields, negatively affecting image quality and subsequent analysis. Fortunately, the N4 bias correction algorithm can address this issue by minimizing a cost function and estimating and rectifying these intensity fluctuations. After correcting the bias field, it is necessary to standardize the intensity to ensure consistent input image intensity values. This results in a more even intensity distribution, essential for precise segmentation and fusion. The fusion procedure entails several critical pre-processing steps, including bias field correction, intensity normalization, and registration. These steps are vital in detecting AD-related brain changes. Precise registration is essential to integrate information from various sources and observe AD-related changes efficiently. This is especially important when combining images of different modalities with varying intensity scales. Intensity normalization helps ensure that the corresponding tissues have consistent intensities in the input images, making the fusion process easier and allowing the detection of AD biomarkers. The next step, image registration, involves aligning input images spatially to match the corresponding anatomical structures. Depending on the nature of the input images and the desired A_{cc} level, image registration techniques can range from rigid and affine to deformable registration. Once the pre-processing and registration are complete, the fusion process can begin. A suitable fusion method combines complementary information from the input images to improve the detection of AD-related changes in the brain. Several fusion methods, such as pixel-based, region-based, and transform-based techniques, are chosen on the basis of the specific application and desired outcome. Here, in our approach, we have used the pixel-based method for the fusion process. To better understand AD, we preprocessed T1-weighted MRI and PET data using N4 bias correction, intensity normalization, and registration, as shown in Figure5.2.

126
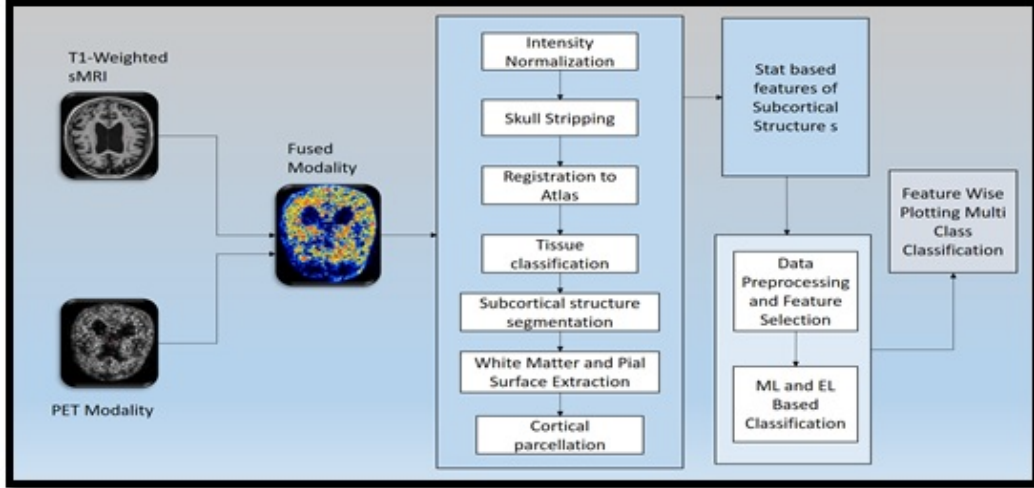
Figure 5.2: Entire work flow for the sub cortical structure analysis for the Detection of AD and there sub types

5.3.1   Intensity Normalization

MRI data fused together can sometimes have varying intensities because of magnetic field in homogeneity's, making it difficult to segment. To address this issue, the Free Surfer method utilizes N3 (non parametric non-uniform intensity normalization) to correct for variations. This process helps ensure that the intensities of different tissue types are uniform throughout the image in equation 5.1.

$$T(z) = \frac{(H_I^{-1}(H_T(z)))^{\gamma} - b}{1 - b} \qquad (5.1)$$

where $T(z)$ is the intensity value in the output normalized image, $H_I(z)$ is the CDF of the input histogram, $H_T(z)$ is the CDF of the target histogram, γ is the gamma parameter, and b is the bias parameter.

5.3.2 Skull Stripping

When an MRI image is taken, it includes brain tissues along with non-brain tissues like the skull, scalp, and meninges. To process the image effectively, removing these non-brain tissues is essential. This is called skull stripping, and Free Surfer uses a hybrid watershed algorithm involving morphological operations and deformable surface models. The resulting brain mask is used to remove non-brain tissue from the MRI image in equation 5.2.

$$B(x, y, z) = \prod_{i=1}^{N} P_i(I(x, y, z)) \tag{5.2}$$

where $B(x, y, z)$ is the probability of a voxel at position (x, y, z) being part of the brain mask, $P_i(I(x, y, z))$ is the probability of the voxel intensity value $I(x, y, z)$ belonging to the i-th tissue class (white matter, gray matter, or cerebrospinal fluid), and N is the number of tissue classes.

5.3.3 Registration To Atlas

Free Surfer uses linear (affine) and nonlinear (LTA) registration techniques to ensure precise alignment. Once the image is preprocessed, it is aligned to a common atlas space, like the Talairach or MNI305 atlas. This guarantees that the input image matches a template brain image that considers individual brain size and shape differences.The registration process involves computing a non-linear transformation that maps the individual brain image to the atlas space.The formula for the non-linear transformation used in FreeSurfer registration in equation 5.3.

$$v' = R \circ T(v) + \epsilon(v) \tag{5.3}$$

where v' is the position of a point in the atlas space, v is the corresponding position in the individual brain image, R is the rotation matrix that aligns the orientation of the two images, $T(v)$ is the translation vector that aligns the centers of mass of the two images, and $\epsilon(v)$

is the non-linear deformation field that captures local shape differences between the two images.

5.3.4 Tissue Classification

The segmentation process used by Free Surfer categorizes voxels in the image into various types of tissue, including gray matter (GM), white matter (WM), and cerebrospinal fluid (CSF). This categorization is determined through voxel intensity values, spatial information, and atlas-based priors. The process uses an algorithm called the Expectation-Maximization (EM) model, which estimates the most probable tissue type for each voxel based on observed intensities and prior information.Intensity probability distributions (Gaussian Mixture Model) as in equation 5.4.

$$P(I|T) = \sum P(I|\mu_t, \sigma_t) * P(T = t) \tag{5.4}$$

where I = intensity value of the voxel, T = tissue class, t = specific tissue class (e.g., white matter, gray matter, or cerebrospinal fluid), μ_t = mean intensity of tissue class t, σ_t = standard deviation of tissue class t, $P(I|\mu_t, \sigma_t)$ = Gaussian probability density function (pdf) for the intensity I given tissue class t's mean (μ_t) and standard deviation (σ_t), $P(T = t)$ = prior probability of tissue class t.Markov Random Fields (MRF) for spatial regularization in equation 5.5.

$$P(T|N) = \exp(-\beta * E(T, N)) \tag{5.5}$$

Where T is the tissue class, N is the collection of neighbouring voxels, β is the smoothing parameter, and $E(T, N)$ is the energy function that evaluates the degree of mismatch between the tissue class T and its neighbors N.

5.3.5 Subcortical Structure Segmentation

FreeSurfer helps to segment subcortical structures such as the thalamus, hippocampus, and caudate nucleus using a combination of atlas-based information and intensity-based approaches. The process involves registering the input image to an atlas that provides probabilistic information about the location and shape of these structures. The program then assigns voxel labels based on the atlas and observed intensities.The segmentation is then refined using the Expectation-Maximization (EM) algorithm to better fit the subject's MRI data.

5.3.6 White Matter Pial Section

FreeSurfer uses a deformable surface model to extract the white matter (WM) surface by detecting the boundary between gray and white matter. This process involves refining the position of an initial surface to match the WM/GM boundary precisely. A similar technique extracts the pial surface, identifying the boundary between gray matter and cerebrospinal fluid.This method iteratively refines a mesh representing the white matter or pial surface to minimize an energy function that balances the intensity information from the MRI data and the smoothness constraints imposed on the surface in equation 5.6.

$$E(S) = E_{\text{data}}(S) + \lambda * E_{\text{smooth}}(S) \tag{5.6}$$

where S = surface (white matter or pial), $E_{\text{data}}(S)$ = data term that measures the agreement between the surface S and the MRI data, λ = weighting parameter that controls the trade-off between data fidelity and smoothness, $E_{\text{smooth}}(S)$ = smoothness term that penalizes irregularities in the surface S.

5.3.7 Cortical Parcellation

The cortical surface is divided into different anatomical regions using a predefined atlas, such as the Desikan-Killiany or Destrieux atlas. This process involves registering the extracted surface to a template surface and labeling each vertex based on the atlas. Surface registration: In this step, the subject's cortical surface is registered to a template or atlas with predefined labels for different cortical regions. The registration process involves minimizing a cost function that measures the difference between the subject's cortical surface and the template in equation 5.7. Cost function:

$$C(R, S) = D(R(S), T) \tag{5.7}$$

where C = cost function, R = spatial transformation (e.g., rotation, translation, scaling), S = subject's cortical surface, T = template or atlas surface, D = distance metric that measures the dissimilarity between the registered subject's surface $R(S)$ and the template surface T.

5.3.8 Surface Feature Extraction

In order to improve the registration A_{cc}, various features of the cortical surface, such as curvature and sulcal depth, are extracted and used to guide the registration process. Curvature in equation 5.8:

$$K(x) = \frac{eG - 2fF + gE}{2 * \sqrt{EG - F^2}} \tag{5.8}$$

where x = a point on the cortical surface, E, F, G = coefficients of the first fundamental form of the surface. As a result, statistical features are generated by combining PET and T1 modalities for AD, MCI, and CN subtypes. These features include data from subcortical regions such as the right and left accumbens, amygdala, pallidum, putamen, thalamus, ventral DC, cudate, and hippocampus. The characteristics for these subcortical regions include SegId, Nvoxels, Volume_mm3, Mean, StdDev, Min, Max, and Range. These

features are then processed using Expectation Maximization and ML techniques to classify AD, MCI, and CN. The following section will discuss the importance of subcortical regions in detecting AD and its types.

5.4   Result Analysis

In this step, we preprocess, visualize, and reduce the dimensionality of a brain imaging dataset related to AD, MCI, and CN subjects. We import necessary libraries such as pandas, numpy, seaborn, matplotlib, and scikit-learn models and functions. We then read the data from a CSV file, remove duplicates and missing values, and reset the index. We visualize the data using a pair plot, which displays relationships between feature pairs in a matrix of scatter plots. We save the plot as a high-resolution image. We standardize the data using the StandardScaler function to bring all features to the same scale, and apply Principal Component Analysis (PCA) to reduce dimensionality. We select the top 2 principal components and use them to create a new DataFrame. We create a scatter plot of these components and save it as a high-resolution image. In conclusion, we have preprocessed, visualized, and applied PCA to a brain imaging dataset for AD, MCI, and CN subjects for all the subcortical regions. As an example, we have taken the pairplot of the Hippocampus in Figure 1. 5.3
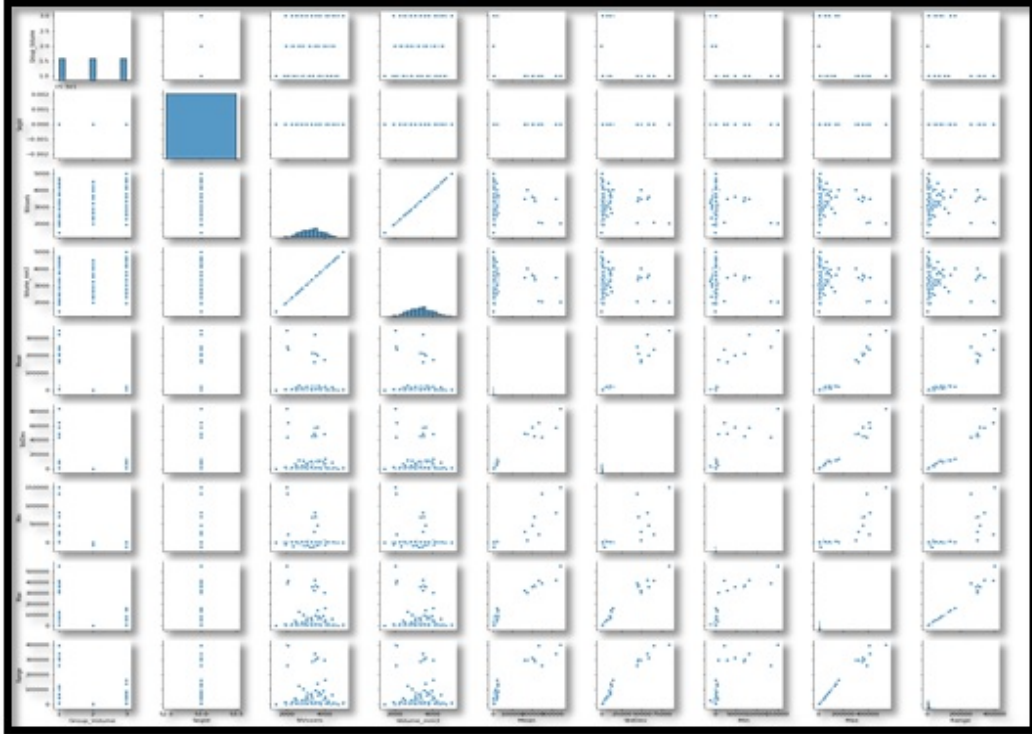
Figure 5.3: The pair plot of the Sub cortical region of Hippocampus region

In the context of the hippocampus region and features such as *SegId*, *Nvoxels*, *Volume_mm3*, *Mean*, *StdDev*, *Min*, *Max*, and *Range*, the pair plot can aid in identifying patterns, correlations, and outliers among these features. By examining the pair plot, insights can be obtained regarding the relationships between the features and their individual distributions. This information proves to be valuable for informing the selection, engineering, or transformation steps of the features, thus improving the quality of the data set for further analysis or modeling

. After pre-processing, principal component analysis (PCA) was utilized to standardize the data and the two most significant components (PC1 and PC2) were chosen to capture the majority of the variance in the dataset. These two components were then used as input features for five ML models: Logistic regression (LR), K-Nearest Neighbors (KNN), SVM, DT and RF. The two best models were then used to detect AD, MCI, and CN from the target

column. The data was divided into training and validation sets, and the models were trained and evaluated on these sets. The results of the multiclass classification for the different cortical regions were then obtained.

5.4.1 Left-Right Accumbens

The Left-Right Accumbens is a key cortical region that can be used to explain the various types of patients with AD. The multiclass classification results for the left-right seats have been obtained and are presented in Figure 5.4.. This Figure 5.4.shows the confusion matrix for the left and right accumbens, with class 0 representing AD, class 1 representing MCI, and class 2 representing CN. The Receiver Operating Characteristic (ROC) curve for the AD, MCI, and CN classes is 0.80, 0.64, and 0.66 for the right accumbens and 0.66, 0.64, and 0.66 for the left accumbens. Classes were trained and validated using 400 training set size features in the left and right accumbens in Figure 5.4.
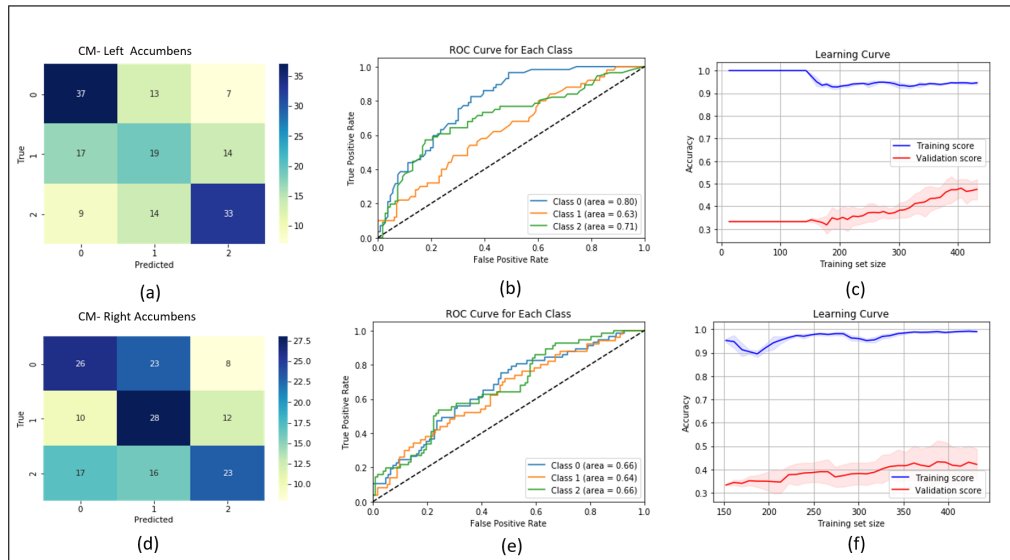
Figure 5.4: (a) Represent the confusion matrix for right accumbens. (b) Roc curve achieved for each class for right accumbens. (c) Training and validation curve for each for right accumbens. (d) Represent the confusion matrix for left accumbens. (e) Roc curve achieved for each class for left accumbens. (f) Training and validation curve for each left accumbens.

Table 5.2 presents the performance metrics of six models LR, KNN, SVC, DT, RF, and EM to predict the target variable in two regions: Right and left ascendents. Performance metrics include A_{cc}, P_{rec}, R_{rec}, and $F1_{score}$. In the right accumbens, the EM has the best performance, with an A_{cc} of 0.55 and an $F1_{score}$ of 0.54. KNN and RF models also perform similarly well, with A_{cc} of 0.54 each. The LR and SVC models have the lowest A_{cc} at 0.39 and 0.42, respectively, as represented in tab5.2.

Table 5.2: Performance metrics of different models for Left and Right Accumbens

Region	Model	A_{cc}	P_{rec}	R_{rec}	$F1_{score}$
Right Accumbens	LR	0.39%	0.43%	0.39%	0.38%
	KNN	0.54%	0.54%	0.54%	0.53%
	SVC	0.42%	0.50%	0.42%	0.39%
	DT	0.49%	0.49%	0.49%	0.49%
	RF	0.54%	0.53%	0.54%	0.53%
	EM	0.55%	0.54%	0.55%	0.54%
Left Accumbens	LR	0.42%	0.45%	0.42%	0.43%
	KNN	0.42%	0.43%	0.42%	0.41%
	SVC	0.40%	0.52%	0.40%	0.36%
	DT	0.41%	0.42%	0.41%	0.41%
	RF	0.44%	0.45%	0.44%	0.43%
	EM	0.47%	0.48%	0.47%	0.47%

For the Left-Accumbens-area, the EM again performs best, with an A_{cc} of 0.47 and an $F1_{score}$ of 0.47% . The RF model follows closely with an A_{cc} of 0.44% . The other models LR, KNN, SVC, and DT have comparable performances, with A_{cc} ranging between 0.40% and 0.42% . In summary, the EM demonstrates the best performance for both regions, followed by the RF model.

5.4.2 Left-Right Amygdala

The left and right amygdala are cortical regions in the left hemisphere that are involved in emotional processing, fear, and memory. To assess the differences between AD, MCI, and CN patients, a multiclass classification was performed on the left and right amygdala regions. Figure 5.55 shows the confusion matrix, roc curve, and training and validation curves for the different classes in these regions. The roc curve for AD, MCI, and CN was 0.88% , 0.71% , and 0.72% for the left amygdala and 0.85% , 0.78% , and 0.78% for the right amygdala. The training and validation curves had 400 training set sizes in the left and right amygdala for the different classes in Figure 5.5.

Figure 5.5: (a) Represent the confusion matrix for Left Amygdala. (b) Roc curve achieved for each class for left amygdala. (c) Training and validation curve for each left amygdala. (d) Represent the confusion matrix for right amygdala. (e) Roc curve achieved for each class for right amygdala. (f) Training and validation curve for each right amygdala

Table5.3 presents the performance metrics of six models (LR, KNN, SVC, DT, RF, and EM) for predicting the target variable in two regions: Left Amygdala and right Amygdala. Performance metrics include A_{cc}, P_{rec}, R_{rec}, and $F1_{score}$. In the left amygdala, EM performs

the best, with an A_{cc} of 0.62% and an $F1_{score}$ of 0.61% .

Table 5.3: Performance metrics of different models for Left and Right Amygdala

Region	Model	A_{cc}	P_{rec}	R_{rec}	$F1_{score}$
Left Amygdala	LR	0.52%	0.52%	0.52%	0.52%
	KNN	0.52%	0.52%	0.52%	0.51%
	SVC	0.58%	0.62%	0.58%	0.56%
	DT	0.55%	0.57%	0.55%	0.55%
	RF	0.59%	0.60%	0.59%	0.58%
	EM	0.62%	0.63%	0.62%	0.61%
Right Amygdala	LR	0.47%	0.48%	0.47%	0.47%
	KNN	0.54%	0.53%	0.54%	0.54%
	SVC	0.55%	0.59%	0.55%	0.50%
	DT	0.55%	0.55%	0.55%	0.55%
	RF	0.64%	0.65%	0.64%	0.64%
	EM	0.66%	0.67%	0.66%	0.66%

The RF model follows closely with an A_{cc} of 0.59% . The SVC and DT models have similar performance, with A_{cc} of 0.58% and 0.55% , respectively. LR and KNN models have the lowest A_{cc} at 0.52% each. For the right amygdala, EM again performs best, with an A_{cc} of 0.66% and an $F1_{score}$ of 0.66% . The RF model follows closely, with an A_{cc} of 0.64% . The other models (SVC, DT, KNN, and LR) have lower A_{cc} ranging between 0.47% and 0.55% .

5.4.3 Left-Right-Pallidum

The left-right-pallidum, a structure located in the left basal ganglia, is involved in motor control and the regulation of voluntary movement. This cortical region is particularly

important for the classification of different types of AD patients. Figure 5.6 illustrates the confusion matrix, roc curve, and training and validation curves for the left and right pallidum. The data set is divided into three classes: 0 for AD, 1 for MCI, and 2 for CN. The roc curve for AD, MCI, and CN is 0.70% , 0.62% , and 0.65% for the left pallidum, and 0.74% , 0.75% , and 0.73% for the right pallidum. The training and validation curves for the left and right pallidum have 400 training set sizes for the different classes in Figure 5.6.

Figure 5.6: (a) represent the confusion matrix for Left Pallidum. (b) roc curve achieved for each class for left pallidum. (c) training and validation curve for each left pallidum. (d) represent the confusion matrix for right pallidum. (e) roc curve achieved for each class for right pallidum. (f) training and validation curve for each right pallidum

The Table 5.4 presents the performance metrics of six models (LR, KNN, SVC, DT, RF, and EM) for predicting the target variable in two regions: Left palm and right palm. Performance metrics include A_{cc}, P_{rec}, R_{rec}, and $F1_{score}$. In the Left-Pallidum region, the EM performs the best, with an A_{cc} of 0.52 and an $F1_{score}$ of 0.51.

Table 5.4: Performance metrics of different models for Left and Right Pallidum

Region	Model	A_{cc}	P_{rec}	R_{rec}	$F1_{score}$
Left Pallidum	LR	0.32%	0.36%	0.32%	0.28%
	KNN	0.47%	0.47%	0.47%	0.46%
	SVC	0.35%	0.40%	0.35%	0.31%
	DT	0.44%	0.44%	0.44%	0.44%
	RF	0.49%	0.49%	0.49%	0.49%
	EM	0.52%	0.52%	0.52%	0.51%
Right Pallidum	LR	0.34%	0.42%	0.34%	0.33%
	KNN	0.40%	0.40%	0.40%	0.37%
	SVC	0.40%	0.43%	0.40%	0.36%
	DT	0.51%	0.52%	0.51%	0.51%
	RF	0.52%	0.53%	0.52%	0.52%
	EM	0.51%	0.52%	0.51%	0.51%

5.4.4   Left-Right-Putamen

The left basal ganglia, which is involved in motor control, learning, and reinforcement, is one of the important cortical regions for different types of patients with AD. Figure 5.7shows the confusion matrix, the roc curve and the training and validation curves for the left and right putamens. The data set is divided into three classes: 0 for AD, 1 for MCI, and 2 for CN. The roc curve for AD, MCI, and CN is 0.73, 0.68, and 0.58 for the left putamen, and 0.75, 0.61, and 0.71 for the right putamen. The training and validation curves have 400 training set sizes for each of the left and right putamen classes in Figure 5.7.
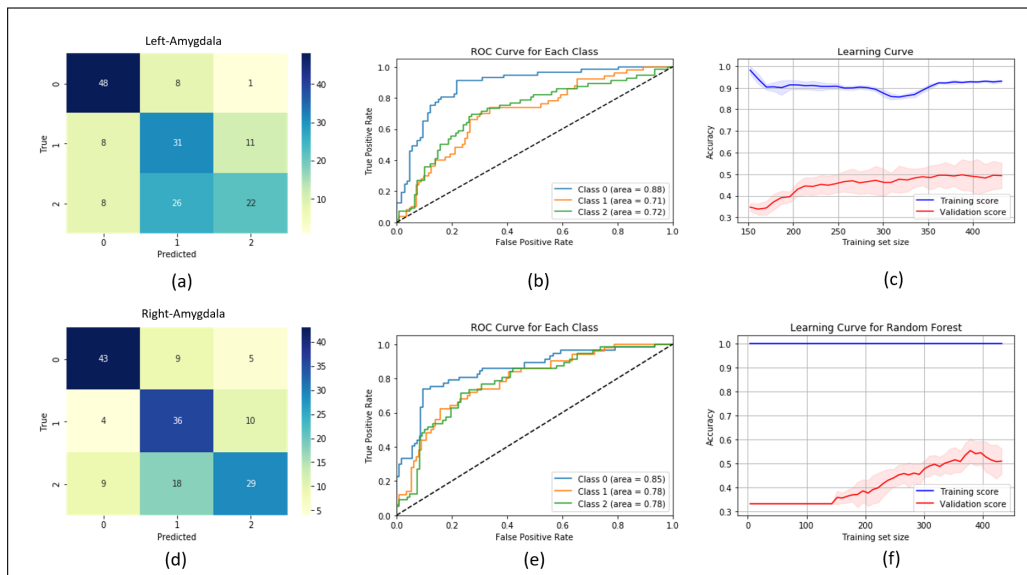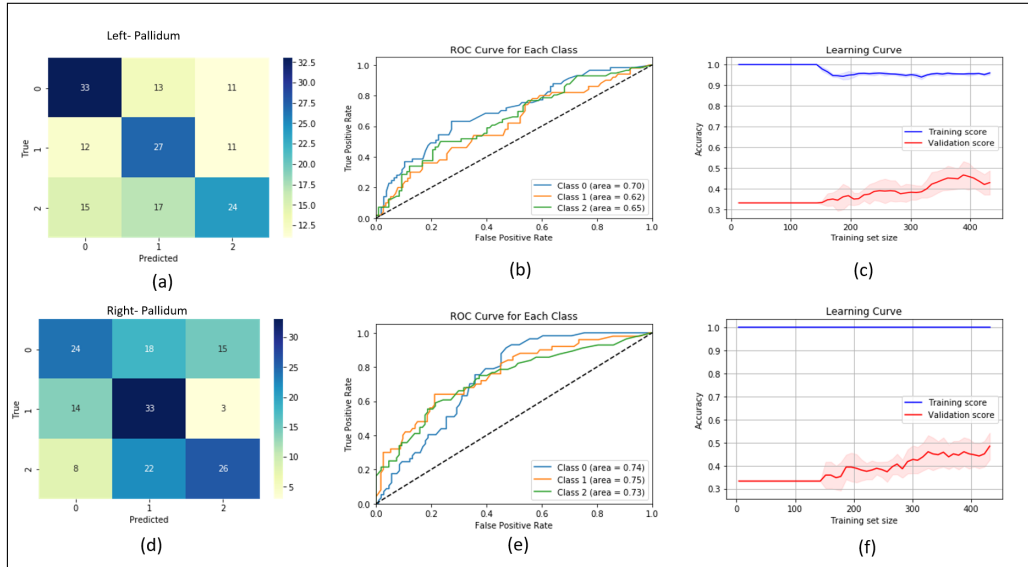
Figure 5.7: (a) represents the confusion matrix for left putamen. (b) roc curve achieved for each class for left putamen. (c) training and validation curve for each left putamen. (d) represents the confusion matrix for the right putamen. (e) roc curve achieved for each class for right putamen. (f) training and validation curve for each right putamen

The Table 5.5 presents the performance metrics of six models (LR, KNN, SVC, DT, RF, and EM) for predicting the target variable in two regions: Left-Putamen and Right-Putamen. Performance metrics include A_{cc}, P_{rec}, R_{rec}, and $F1_{score}$. In the Left-Putamen region, the EM performs best, with an A_{cc} of 0.47 and an $F1_{score}$ of 0.46. The RF and KNN models follow closely, both with A_{cc} of 0.44.

Table 5.5: Analysis of different subcortical regions using the different ML models and EM in Left-Right-Putamen.

Region	Model	A_{cc}	P_{rec}	R_{rec}	$F1_{score}$
Left Putamen	LR	0.37%	0.38%	0.37%	0.36%
	KNN	0.44%	0.42%	0.44%	0.42%
	SVC	0.40%	0.38%	0.40%	0.31%
	DT	0.40%	0.40%	0.40%	0.39%
	RF	0.44%	0.44%	0.44%	0.43%
	EM	0.47%	0.47%	0.47%	0.46%
Right Putamen	LR	0.36%	0.41%	0.36%	0.34%
	KNN	0.47%	0.48%	0.47%	0.46%
	SVC	0.39%	0.42%	0.39%	0.37%
	DT	0.47%	0.47%	0.47%	0.47%
	RF	0.55%	0.55%	0.55%	0.55%
	EM	0.47%	0.47%	0.47%	0.47%

The other models (LR, SVC, and DT) have lower A_{cc} ranging between 0.37% and 0.40% . For the right-patamen region, the RF model has the highest A_{cc} at 0.55% and an $F1_{score}$ of 0.55% . The EM, KNN, and DT models all have similar A_{cc} of 0.47% . The other models (LR and SVC) have lower A_{cc} at 0.36% and 0.39% , respectively.

5.4.5   Left-Right-Thalmus

The left hemisphere of the brain acts as a hub for sensory and motor information. The Left-Right Thalamus is a significant cortical region that may explain the various types of AD patients. Figure 5.8 illustrates the confusion matrix, the roc curve and the training and validation curves for the three classes (AD, MCI, and CN) in the Left-Right Thalamus. The

roc curve for AD, MCI, and CN is 0.80% , 0.77% , and 0.78% for the left thalamus and 0.68% , 0.69% , and 0.74% for the right thalamus. The training and validation curves feature 400 training set sizes in the left and right thalamus for these classes in Figure 5.8.
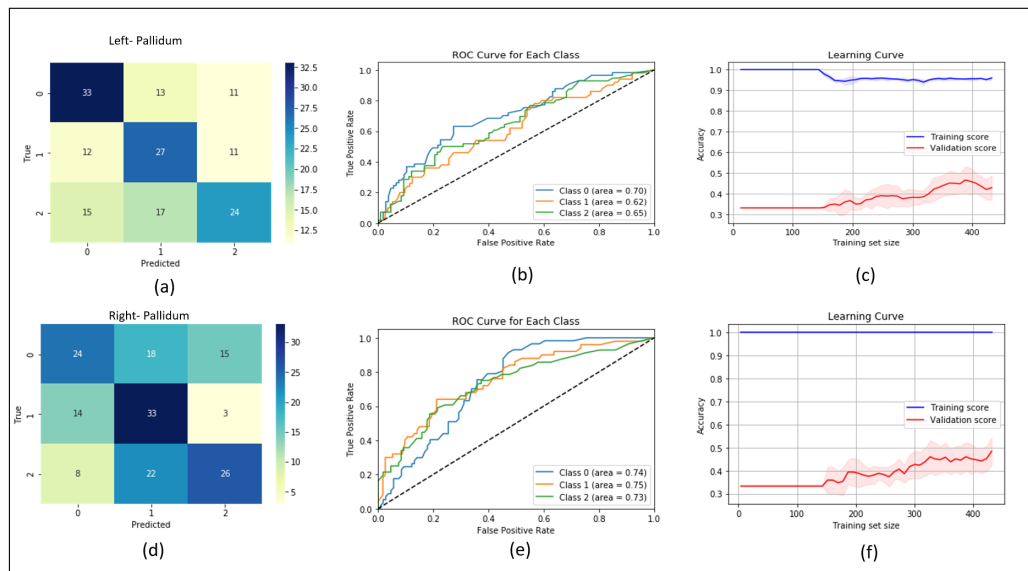

Figure 5.8: (a) represents the confusion matrix for left thalmus. (b) roc curve achieved for each class for the left thalmus. (c) training and validation curve for each left thalmus. (d) represents the confusion matrix for the right thalmus. (e) roc curve achieved for each class for right thalmus. (f) training and validation curve for each right thalmus

The Table 5.6 presents the performance metrics of six models (LR, KNN, SVC, DT, RF, and EM) for predicting the target variable in two regions: Left thamus and right thamus. Performance metrics include A_{cc}, P_{rec}, R_{rec}, and $F1_{score}$. In the Left-Thalamus region, the RF model performs best, with an A_{cc} of 0.55% and an $F1_{score}$ of 0.55% .

Table 5.6: Analysis of different subcortical regions using the different ML models and EM in Left-Right-Thalamus.

Region	Model	A_{cc}	P_{rec}	R_{rec}	$F1_{score}$
Left Thalamus	LR	0.36	0.41	0.36	0.34
	KNN	0.47%	0.48%	0.47%	0.46%
	SVC	0.39%	0.42%	0.39%	0.37%
	DT	0.47%	0.47%	0.47%	0.47%
	RF	0.55%	0.55%	0.55%	0.55%
	EM	0.47%	0.47%	0.47%	0.47%
Right Thalamus	LR	0.41%	0.45%	0.41%	0.40%
	KNN	0.44%	0.48%	0.44%	0.45%
	SVC	0.42%	0.56%	0.42%	0.40%
	DT	0.49%	0.49%	0.49%	0.49%
	RF	0.51%	0.52%	0.51%	0.51%
	EM	0.49%	0.49%	0.49%	0.49%

The DT, EM, and KNN models have similar A_{cc} of 0.47% . The other models (LR and SVC) have lower A_{cc} at 0.36% and 0.39% , respectively. For the Right-Thalamus region, the RF model has the highest A_{cc} at 0.51% and an $F1_{score}$ of 0.51% . The DT and EM follow closely, both with A_{cc} of 0.49% . The other models (LR, KNN, and SVC) have lower A_{cc} ranging between 0.41% and 0.44% .

5.4.6 Left-Right- VentralDC

The left-right ventral DC is part of the left basal ganglia, which is involved in motor control and reward-based learning. It is also an important cortical region that is responsible for the different types of AD patients. Figure 5.9 shows the confusion matrix, the roc curve, and

143

the training and validation curve for the calculation of the different classes in these regions. The data set is properly distributed for class 0 representing AD, class 1 representing MCI, and class 2 representing CN. The roc curve for the AD MCI and CN is 0.82% , 0.72% and 0.78% for the left VentralDC and 0.82% , 0.68% and 0.73% for the right VentralDC. The training and validation curve have features for 400 training set sizes in the left and right VentralDC for these classes Figure 5.9.
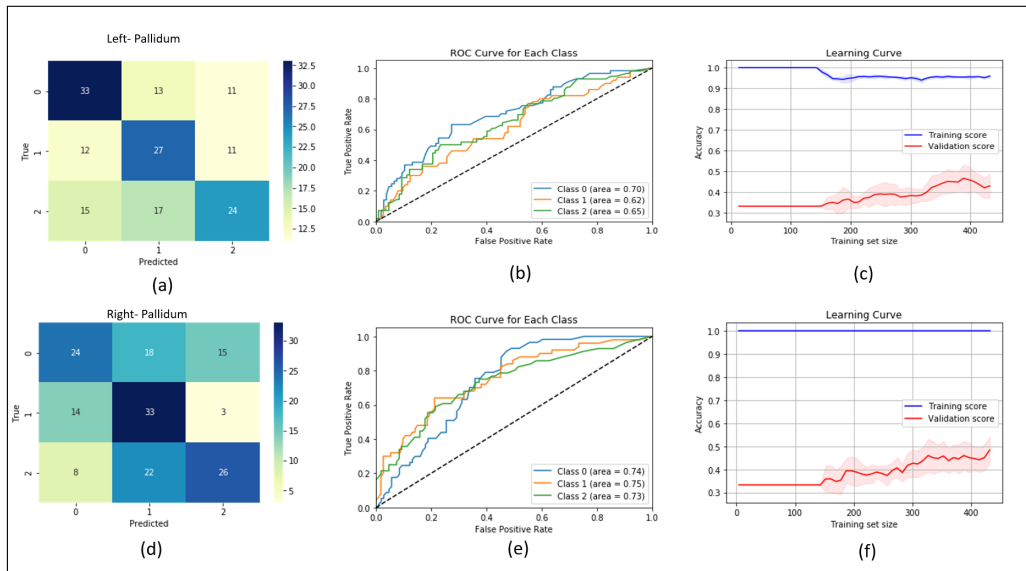

Figure 5.9: (a) represents the confusion matrix for left ventraldc. (b) roc curve achieved for each class for left ventraldc. (c) training and validation curve for each left ventraldc. (d) represent the confusion matrix for right ventraldc. (e) roc curve achieved for each class for right ventraldc. (f) training and validation curve for each right ventraldc

The Table 5.7 presents the performance metrics of six models (LR, KNN, SVC, DT, RF, and EM) for predicting the target variable in two regions: Left-VentralDC and Right-VentralDC. The performance metrics include A_{cc}, P_{rec}, R_{rec}, and $F1_{score}$. In the Left-VentralDC region, the RF model performs best, with an A_{cc} of 0.61% and an $F1_{score}$ of 0.61% . The DT and EM follow closely, both with A_{cc} of 0.57% . The KNN model has an A_{cc} of 0.53% , while the LR and SVC models have lower A_{cc} at 0.44% and 0.45% , respectively.

144

Table 5.7: Analysis of different subcortical regions using the different ML models and EM in Left-Right-VentralDC.

Region	Model	A_{cc}	P_{rec}	R_{rec}	$F1_{score}$
Left Ventral DC	LR	0.44%	0.46%	0.44%	0.44%
	KNN	0.53%	0.54%	0.53%	0.53%
	SVC	0.45%	0.59%	0.45%	0.42%
	DT	0.57%	0.60%	0.57%	0.58%
	RF	0.61%	0.62%	0.61%	0.61%
	EM	0.57%	0.60%	0.57%	0.58%
Right VentralDC	LR	0.48%	0.50%	0.48%	0.49%
	KNN	0.44%	0.45%	0.44%	0.44%
	SVC	0.43%	0.59%	0.43%	0.37%
	DT	0.61%	0.62%	0.61%	0.61%
	RF	0.60%	0.61%	0.60%	0.60%
	EM	0.61%	0.62%	0.61%	0.61%

For the Right-VentralDC region, the EM and DT models have the highest A_{cc} at 0.61% , with $F1_{score}$ of 0.61% and 0.61% , respectively. The RF model follows closely with an A_{cc} of 0.60% . The other models (LR, KNN, and SVC) have lower A_{cc} ranging between 0.43 and 0.48%.

5.4.7   Left-Right-Caudate

The Left-Right-Caudate is a structure in the left basal ganglia that is involved in motor control, learning, and memory. It is also an important cortical region that holds the reasons for the different types of AD patients. The results of the multiclass classification for the Left-Right-Caudate are shown in Figure 5.10. This figure displays the confusion matrix

for the left and right caudate. The data set is properly distributed for class 0 (AD), class 1 (MCI), and class 2 (CN). The roc curve for the AD, MCI, and CN is 0.71% , 0.68% , and 0.74% for the left caudate and 0.75% , 0.69% , and 0.75% for the right caudate. The training and validation curves have features for 400 training set sizes in the left and right caudate in these classes in Figure 5.10.
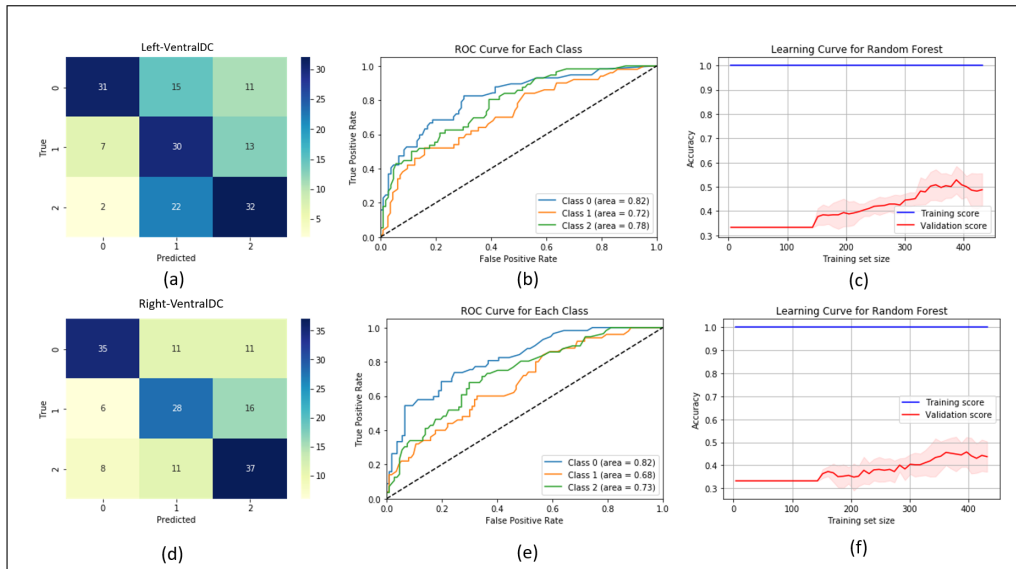

Figure 5.10: (a) represents the confusion matrix for left caduate. (b) roc curve achieved for each class for left caduate. (c) training and validation curve for each left caduate. (d) represent the confusion matrix for right caduate. (e) roc curve achieved for each class for right caduate. (f) training and validation curve for each right caduate

The Table 5.8 compares six ML models applied to Left-Caudate and Right-Caudate regions, with the following best-performing models and corresponding metric values: In the Left-Caudate region, the RF model achieves an A_{cc} of 0.51% , P_{rec} of 0.53% , R_{rec} of 0.51% , and an $F1_{score}$ of 0.51% in Table.

146

Table 5.8: Analysis of different subcortical regions using the different ML models and EM in left and right caudate.

Region	Model	A_{cc}	P_{rec}	R_{rec}	$F1_{score}$
Left Caudate	LR	0.37%	0.39%	0.37%	0.31%
	KNN	0.44%	0.46%	0.44%	0.43%
	SVC	0.36%	0.45%	0.36%	0.30%
	DT	0.48%	0.49%	0.48%	0.48%
	RF	0.51%	0.53%	0.51%	0.51%
	EM	0.48%	0.49%	0.48%	0.48%
Right Caudate	LR	0.40%	0.43%	0.40%	0.40%
	KNN	0.47%	0.48%	0.47%	0.47%
	SVC	0.40%	0.46%	0.40%	0.35%
	DT	0.56%	0.58%	0.56%	0.57%
	RF	0.53%	0.54%	0.53%	0.53%
	EM	0.56%	0.58%	0.56%	0.57%

In the Right-Caudate region, both the DT and EM have an A_{cc} of 0.56% , P_{rec} of 0.58% , R_{rec} of 0.56% , and an $F1_{score}$ of 0.57% . These values suggest that the RF model performs best in the Left-Caudate region, while the DT and EM excel in the Right-Caudate region.

5.4.8   Left-Right-Hippocampus

The left and right hippocampus are two cortical regions that are essential for learning and memory formation, particularly long-term memory. These regions are especially important for understanding the different types of AD patients. Figure 5.11 shows the confusion matrix, roc curve, and training and validation curve for the left and right hippocampus. The data set is divided into three classes: 0 for AD, 1 for MCI, and 2 for CN. The roc curve

for AD, MCI, and CN is 0.89% , 0.80% , and 0.82% for the left hippocampus and 0.90% , 0.77% , and 0.78 % for the right hippocampus. The training and validation curves feature 400 training set sizes in the left and right hippocampus for each of the three classes in Figure 5.11 .
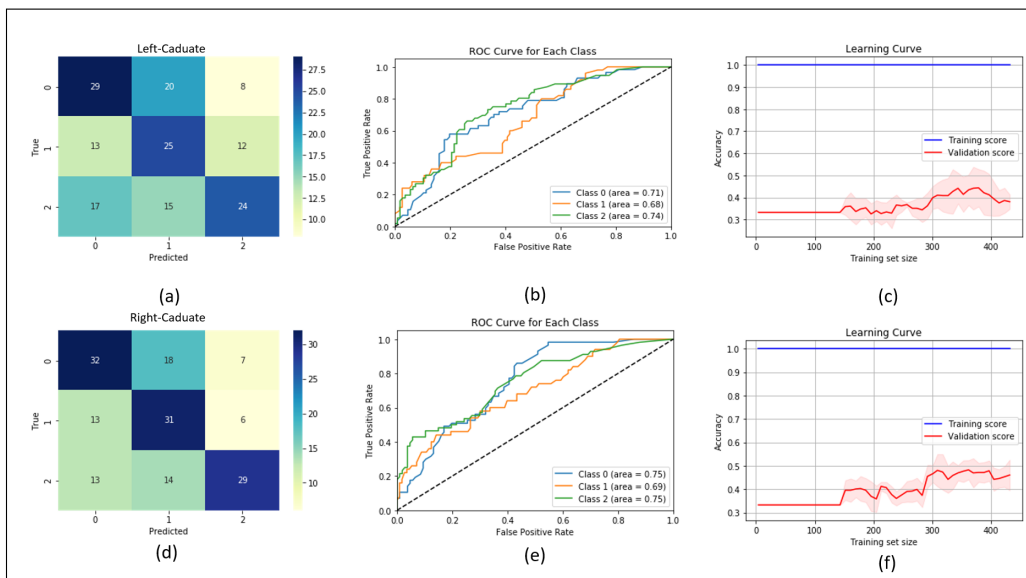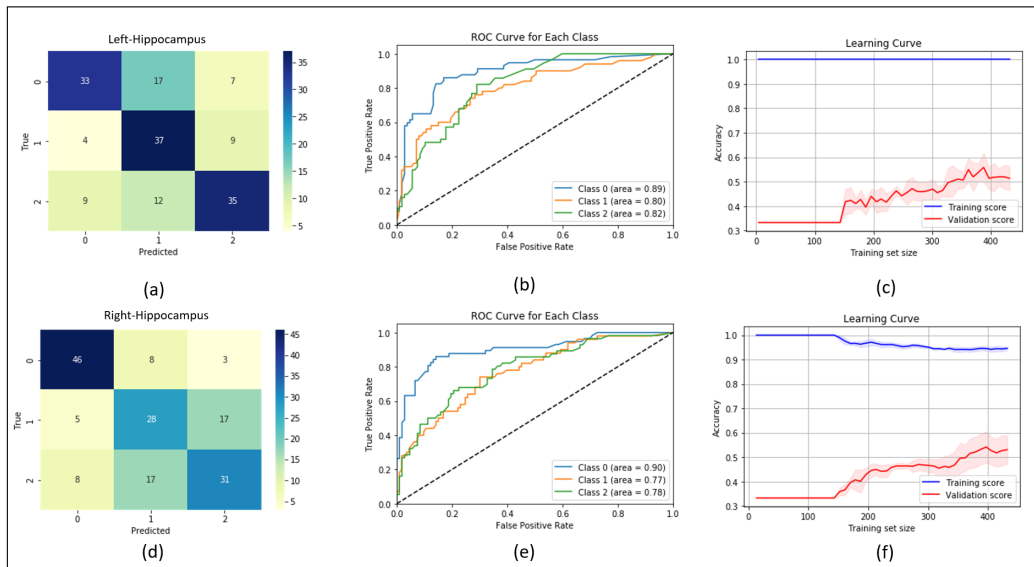

Figure 5.11: (a) represents the confusion matrix for left Hippocampus.(b) roc curve achieved for each class for left Hippocampus.(c) training and validation curve for each left Hippocampus.(d) represent the confusion matrix for right Hippocampus.(e) roc curve achieved for each class for right caduate.(f) training and validation curve for each right Hippocampus

The given Table 5.9 provides a comparison of various ML models based on their performance metrics (A_{cc}, P_{rec}, R_{rec} , and $F1_{score}$ for two regions: Left-Hippocampus and Right-Hippocampus. The models include LR, KNN, SVC, DT, RF, and EM.

Table 5.9: Analysis of different subcortical regions using the different ML and EM in left and right Hippocampus.

Region	Model	A_{cc}	P_{rec}	R_{rec}	$F1_{score}$
Left-Hippocampus	LR	0.52%	0.50%	0.52%	0.51%
	KNN	0.58%	0.57%	0.58%	0.56%
	SVC	0.53%	0.49%	0.53%	0.46%
	DT	0.64%	0.66%	0.64%	0.64%
	RF	0.68%	0.69%	0.68%	0.68%
	EM	0.64%	0.66%	0.64%	0.64%
Right-Hippocampus	LR	0.52%	0.50%	0.52%	0.51%
	KNN	0.58%	0.57%	0.58%	0.56%
	SVC	0.53%	0.49%	0.53%	0.46%
	DT	0.64%	0.66%	0.64%	0.64%
	RF	0.68%	0.69%	0.68%	0.68%
	EM	0.64%	0.66%	0.64%	0.64%

In both regions, the RF model achieves the highest A_{cc}, P_{rec}, R_{rec}, and $F1_{score}$, making it the best performing model among the ones tested. The DT and EM also perform well, with similar scores across the board. LR, KNN, and SVC models have lower performance metrics in comparison to the other models.

5.5 Cumulative Analysis

The cumulative data from the various cortical regions was analyzed in all three sets. We analyzed the left and right subcortical structures, and last, we did the combined analysis of the left and right subcortical structures, i.e., "Accumbens,' Amygdala,' Pallidum,' Putamen,'Thalamus,' VentralDC,' Caudate, and Hippocampus. The objective is to represent the

performance of several ML models on specific relevant brain areas and to see the impact of these regions on which region is more impactful for the identification of AD.

5.5.1 Left-Subcortical Structure

The evaluation of the six models is depicted in the plots, with the y-axis representing the performance metric. Each brain area is represented by a separate line plot, making it easy to distinguish between them. The horizontal axis denotes the ML models. The visual representation of the plots allows for a comparative analysis of the effectiveness of these models in various brain areas, as measured by the four metrics: A_{cc}, P_{rec}, R_{rec} , and $F1_{score}$. The EM has a higher A_{cc} rate of 0.47% in the left accumbens compared to the RF model, which has an A_{cc} of 0.43% . The EM also has a higher P_{rec} of 0.48% compared to the RF's P_{rec} of 0.44% . Both models have almost the same R_{rec} and $F1_{score}$, ranging from 0.43% to 0.47% . The EM marginally outperforms the RF model in this regard. In the left amygdala, the EM has a higher A_{cc} rate of 0.61% compared to the RF model's A_{cc} rate of 0.58% . The EM also has a greater A_{cc} of 0.63. Both models have similar R_{rec} metrics. However, the EM marginally outperforms the RF model in terms of $F1_{score}$, achieving a value of 0.610782% compared to 0.584635 for the RF model in Figure 5.12.

Figure 5.12: represent the left subcortical structure analysis plot with respect to the performance parameters that is A_{cc}, P_{rec}, R_{rec} and $F1_{score}$

Accumbens and left amygdala, but they often rank second or third place in other locations. The efficacy of EM techniques in this context highlights the fundamental concept that combining predictions from different models often results in enhanced performance. The performance of Logistic Regression on this dataset is notably challenging, particularly in locations such as the left pallidum, where it exhibits the lowest A_{cc} and $F1_{score}$. This observation suggests that the data exhibit a lack of linear correlation in several brain areas, diminishing the efficacy of linear models such as Logistic Regression.

5.5.2   Right-Subcortical Structure

The RF and EM models show similar performance in the right amygdala, right ventral DC and right caudate, with closely aligned A_{cc} rates and other measures. This implies that the EM incorporates the beneficial characteristics of RF in its components. However, the RF model outperforms the EM in certain areas, such as the right hippocampus, with an A_{cc} of 68%, compared to the EM's 64.4%. This could be due to the RF's ability to capture patterns

in complex or multifaceted data distributions. However, the EM has a slight advantage over the RF in the right-umbens area and right-pallidum, suggesting that the collective decision-making process used by the EM may sometimes produce better results. Generally, the superiority of one model over the other may depend on the location. EM techniques often improve overall predictive performance by combining different model predictions. The Logistic Regression model, however, is consistently inferior, particularly in the Right-Pallidum and Right-Putamen areas. This implies that the data in these regions may not follow a linear pattern and that the simplicity of this model may not be enough to account for the complexities of the data set in Figure 5.13.
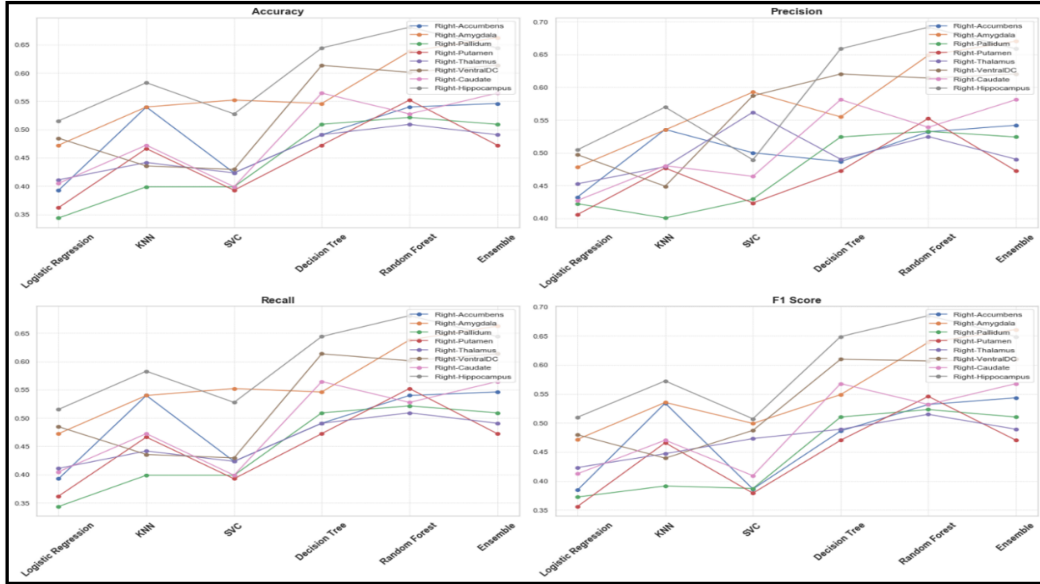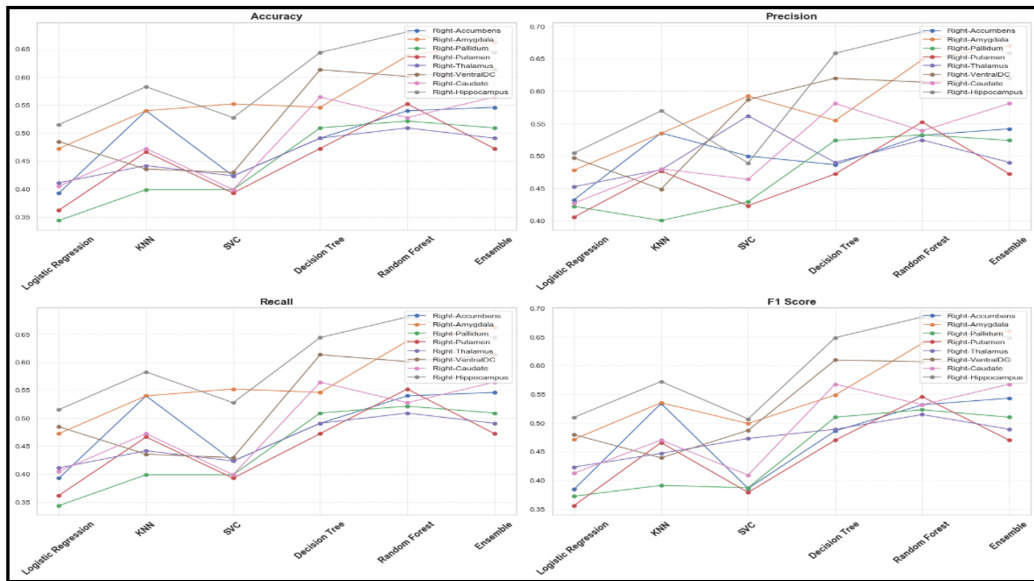

Figure 5.13: represent the right subcortical structure analysis plot with respect to the performance parameters that is A_{cc}, P_{rec}, R_{rec} and $F1_{score}$

5.5.3 Combined analysis of the left and right subcortical structures

A comparison of several ML models across distinct brain regions was conducted. The RF and Expectation Maximization (EM) procedures often showed superior performance in

terms of A_{cc} compared to other methods. In the case of specific areas, such as the right amygdala, the RF algorithm had an A_{cc} of 0.638% , while the EM had a slightly higher A_{cc} of 0.662% . Similarly, in the right hippocampus, the RF model had an Acc of 0.680% , which was comparable to the A_{cc} of 0.644% achieved by the EM. It is important to note that although EM are designed to incorporate multiple algorithms to enhance outcomes, they do not always guarantee a clear advantage over RF in the context of this dataset. Additionally, the SVM model often had a notable level of A_{cc}, indicating a valid positive rate. However, its $F1_{score}$ indicated a compromised R_{rec} in some regions, such as the Left-Accumbens-area. On the other hand, Logistic Regression usually had inferior performance metrics in most areas in Figure 5.14. When selecting a model for deployment in a practical application, it is essential to consider A_{cc}, P_{rec}, R_{rec} , and $F1_{score}$ to ascertain the model's dependability across different circumstances in Figure 5.14.
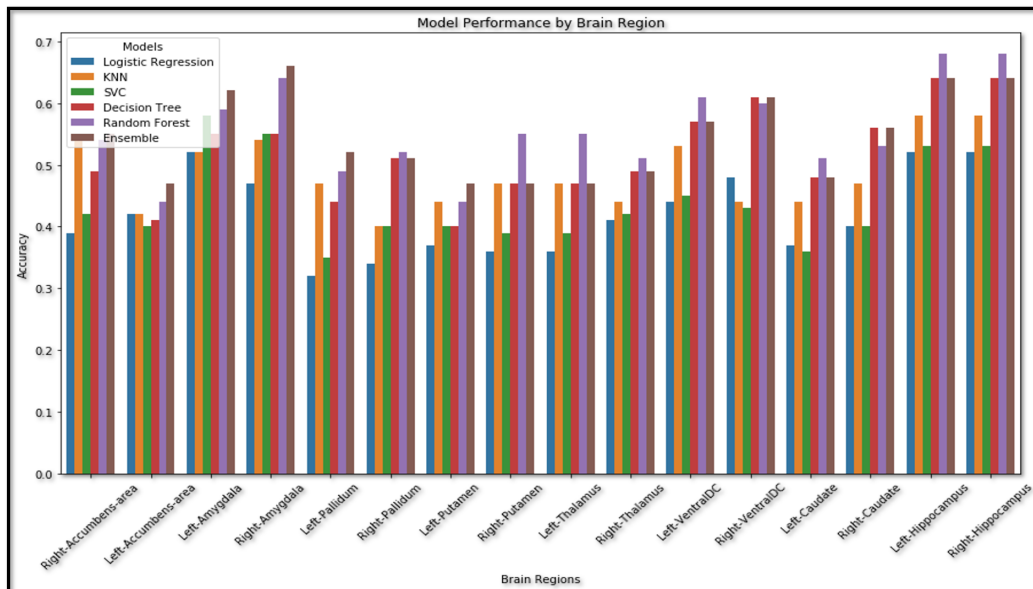
Figure 5.14: Performance Metrics of all the models to evaluate different subcortical regions.

The EM model was found to be the most effective across all subcortical regions, with A_{cc} scores ranging from 0.47% to 0.64% . The RF model also produced satisfactory results in certain regions, with A_{cc} scores ranging from 0.44% to 0.68% . Figure 5.14 showed

Table 5.10: Sub cortical structures Analysis

| Author	Model	Accum	Amyg.	Pall.	Put.	Thal.	V.DC	Caud.	Hipp.	Consideration and Effectiveness
[82]	Lin. Reg.	X	X	X	✓	X	✓	✓	X	Putamen, Ventral and Caudate explored
[107]	Co-active	X	✓	X	✓	X	X	X	X	Amygdala and Putamen were effective
[166]	Mult. Log. Reg.	X	X	✓	X	✓	X	X	✓	Pallidum, Thalmus and Hippocampus considered
[197]	Morph. Class.	X	✓	X	✓	X	X	X	✓	Putamen, cerebellum, brain stem, hippocampus
[53]	Mult. Log. Reg.	X	X	✓	✓	✓	X	X	✓	Pallidum, putamen, thalamus, hippocampus
[5]	Mult. GLM	X	X	X	✓	X	X	X	✓	Putamen, hippocampus
[112]	RF	X	✓	X	X	X	X	X	X	Amygdala
[183]	RF	X	✓	X	X	X	X	X	✓	Amygdala, Hippocampus
[189]	Voxel-wise	X	X	X	X	✓	X	X	X	Thalamus
Proposed	-	✓	✓	✓	✓	✓	✓	✓	✓	Hippocampus, Amygdala

that the right hippocampus was the most effective region for distinguishing between AD, MCI, and CN. This finding is in line with previous research that has highlighted the role of the hippocampus in memory formation and its vulnerability to AD-related pathological changes. The results suggest that ML models, particularly EM and RF models, can effectively differentiate between people with AD, MCI, and CN based on measurements of the subcortical area. The superior performance of the EM compared to individual models may be attributed to several key factors. EM combines predictions generated by multiple base models, thus reducing individual errors and increasing A_{cc}. This combination reduces the risk of overfitting seen in complex models and addresses the issue of underfitting in simpler models. In addition, EM benefits from incorporating different predictions, thus improving its ability to capture a more comprehensive understanding of patterns in the data. By combining multiple perspectives, EM can provide a more comprehensive and robust solution. EM essentially incorporates the idea that the combined intelligence of several views usually surpasses the performance of individual perspectives. Therefore, the performance comparison of the proposed method with the state-of-the-art methods for the analysis of the subcortical structure of the parameters is presented in Table 5.10. By comparing the proposed work to the other approaches outlined in the Table 5.10, it is evident that the EM and RF-based strategy has a clear advantage. This approach provides a comprehensive investigation of all subcortical areas, with a particular focus on the hippocampus and amygdala, which are known to be effective in detecting AD and its various forms. This is in stark

contrast to other contemporary methods, which often concentrate on only a portion of the areas. For example, the linear regression model focuses mainly on Putamen, Ventral DC, and Caudate, while the RF process, as used [82], is specifically focused on the Amygdala. Even multivariate logistic regression, which is considered one of the most comprehensive approaches available, examines only half of the areas [107]. This could lead to the possible omission of essential areas that may be crucial to accurately detect AD. The proposed method, which combines EM and RF techniques, stands out due to its comprehensive approach and could potentially improve the A_{cc} and reliability of AD and its prediction of subtypes. The identification and assessment of AD is hampered by a number of limitations. A major challenge is to differentiate AD from other medical conditions based on biological indicators. This is more than just recognizing symptoms, as it requires the accurate identification of molecular markers that are specific to AD. The complexity of the task is further increased by the influence of genetic factors. Genetic analysis is essential to gain an understanding of an individual's susceptibility to AD, which could lead to a more accurate and earlier diagnosis. By gaining a comprehensive knowledge of the genetic markers and mutations associated with AD, researchers and physicians can create prediction models that can detect the condition before severe clinical symptoms appear. Looking to the future, a major obstacle in diagnosing AD is the incorporation of multimodality into diagnostic methods. This involves using multiple diagnostic procedures together to gain a complete understanding of the condition. In AD, this could involve combining tract analysis, which looks at neural pathways affected by the illness, with genetic investigations. An integrated approach has the potential to provide a more comprehensive understanding of the disease, allowing the development of more tailored therapies and interventions.

CHAPTER 6

CONCLUSION AND FUTURE DIRECTION

The diagnosis and distinction of AD have been enhanced through a comprehensive study. sMRI has been identified as a key Biomarker in the identification of AD, with additional support from complementary methods such as DTI, PET, and FLAIR. The combination of human and automatic feature extraction, particularly in analyzing larger datasets, has highlighted the importance of DL methods in distinguishing different phases of AD. The investigation of single-modality sMRI using Ensemble classifiers revealed that the Ensemble_LR_SVM model had improved performance in binary, multiclass, and regional analysis. This research provided more insights into the discernible differences across brain hemispheres concerning different forms of AD. By utilizing a multimodal approach, the fusion approach to AD detection combined PET and sMRI techniques, thus establishing a solid foundation for accurate feature extraction. As a result, the use of advanced ML algorithms, including ensemble methods like SVM_RBF+AB+GB+RF and GB+SVM_RBF, has been instrumental in establishing notable benchmarks in terms of A_{cc}. A comprehensive study using sMRI and PET has demonstrated the importance of subcortical regions, particularly the Right Hippocampus, in distinguishing AD. The study showed the potential of EM and RF models to extend research beyond subcortical areas and incorporate factors such as cortical thickness. The progress made in the detection and classification of AD, aided by ensemble classifiers, is evident in the dynamic landscape of this field. Nevertheless, to

156

effectively address the many challenges associated with diagnosing and distinguishing AD, it is essential to focus on ongoing innovation, adopt broader research perspectives, and use integrated techniques in future endeavors.

6.1 Future Challanges

- The necessity of having a large and varied dataset to apply DL methods is evident. It is essential to find a balance between having a comprehensive dataset and improving the A_{cc} of the model. The complexity of diagnosing AD requires the use of a wide range of biomarkers and imaging techniques such as MRI, DTI, PET, and FLAIR. However, this approach can lead to difficulties in combining and understanding the data.

- Although manual feature extraction approaches have shown potential, there is a distinct need to enhance and optimize this methodology. Similarly, it is worth delving more into ensemble approaches, namely the Ensemble_LR_SVM model, which has shown promise in binary classifications. This calls for more extensive investigation and refinement in many categorizations.

- Imaging techniques in many fields have become more prevalent in recent years. These techniques include a range of methodologies that enable the investigation of the fusion, and synergistic effects of several imaging modalities have the potential to enhance the P_{rec} of AD identification. This entails broadening the integration of diverse modalities beyond sMRI and PET and further investigating regions such as the right hippocampal, which has shown a substantial impact in distinguishing AD).

- Future research efforts must embrace a more comprehensive and encompassing perspective in light of the specific emphasis on particular regions, such as the subcortical areas. This involves including other crucial brain characteristics, such as the thick-

ness of the cortex and the connection of brain regions. In addition, using insights derived from certain areas of the brain can provide valuable guidance for subsequent research, leading to the discovery of more refined diagnostic procedures.

- With the increasing complexity of AD detection methods, it is essential to prioritize the accurate interpretation and practical use of the findings obtained within real-world clinical environments. This highlights the importance of improving the dependability and applicability of ML models in diagnosing AD, requiring strong collaboration between researchers and clinicians.

BIBLOGRAPHY

[1] (2010). Highly accurate inverse consistent registration: A robust approach. *NeuroImage*, 53(4):1181–1196.

[2] Abbas, S., Chi, L., and Chen, Y. (2023). Transformed domain convolutional neural network for alzheimer's disease diagnosis using structural mri. *Pattern Recognition*, 133:109031.

[3] Abdelaziz, M., Wang, T., and Elazab, A. (2021). Alzheimer's disease diagnosis framework from incomplete multimodal data using convolutional neural networks. *J. Biomed. Inform.*, 121:103863.

[4] Abuhmed, T., El-Sappagh, S., and Alonso, J. (2021). Robust hybrid deep learning models for alzheimer's progression detection. *Knowledge-Based Systems*, 213:106688.

[5] Addiego, F. M., Zajur, K., Knack, S., Jamieson, J., Rayhan, R. U., and Baraniuk, J. N. (2021). Subcortical brain segment volumes in gulf war illness and myalgic encephalomyelitis/chronic fatigue syndrome. *Life Sciences*, 282:119749.

[6] Aderghal, K., Boissenin, M., Benois-Pineau, J., Catheline, G., and Afdel, K. (2016). Classification of smri for ad diagnosis with convolutional neuronal networks: A pilot 2-d+ study on adni. In *International Conference on Multimedia Modeling*, pages 690–701. Springer.

[7] Afzal, S. and Maqsood, M. (2021). Alzheimer disease detection techniques and methods: A review. *International Journal of Interactive Multimedia & Artificial Intelligence*, 6(7).

[8] Ahmed, O. B. and Mizotin, M. (2015). Alzheimer's disease diagnosis on structural mr images using circular harmonic functions descriptors on hippocampus and posterior cingulate cortex. *Computerized Medical Imaging and Graphics*, 44:13–25.

[9] Aishwarya, T. and Ravi Kumar, V. (2021). Machine learning and deep learning approaches to analyze and detect covid-19: a review. *SN computer science*, 2(3):226.

[10] Alam, S., Kwon, G., and Initiative, A. (2017). Alzheimer disease classification using kpca, lda, and multi-kernel learning svm. *International Journal of Imaging Systems and Technology*, 27(2):133–143.

[11] Albert, A. L. W. M. L. and Feldman, A. R. G. (1974). The 'subcortical dementia' of progressive supranuclear palsy. *J Neurol Neurosurg Psychiatry*, 37(2):121–130.

[12] Allioui, H., Sadgal, M., and Elfazziki, A. (2020). Utilization of a convolutional method for alzheimer disease diagnosis. *Machine Vision and Applications*, 31(4):25.

[13] Amin-Naji, M., Mahdavinataj, H., and Aghagolzadeh, A. (2019). Alzheimer's disease diagnosis from structural mri using siamese convolutional neural network. In *2019 4th international conference on pattern recognition and image analysis (IPRIA)*, pages 75–79. IEEE.

[14] Aprahamian, I., Stella, F., and Forlenza, O. V. (2013). New treatment strategies for alzheimer's disease: is there a hope? *The Indian journal of medical research*, 138(4):449.

[15] Arco, J. E., Ram'irez, J., G'orriz, J. M., Ruz, M., and Initiative, A. D. N. (2021). Data fusion based on searchlight analysis for the prediction of alzheimer's disease. *Expert Systems with Applications*, 185:115549.

[16] Arora, H., Ramesh, M., Rajasekhar, K., and Govindaraju, T. (2020). Molecular tools to detect alloforms of aβ and tau: Implications for multiplexing and multimodal diagnosis of alzheimer's disease. *Bull. Chem. Soc. Jpn.*, 93:507–546.

[17] Asgari, H. and Kaye, J. (2017). Predicting mild cognitive impairment from spontaneous spoken utterances. *Dementia Translational Research Amp*, 3:219–228.

[18] Ashraf, G., Nigel, H., Taqi, A., Iftekhar, H., Shams, T., Shazi, S., Ishfaq, A., Syed, K., Mohammad, A., and Nasimu-deen, R. (2014). Protein misfolding and aggregation in alzheimer's disease and type 2 diabetes mellitus. *CNS Neurol. Disord.-Drug Targets (Former. Curr. Drug Targets-CNS Neurol. Disord.)*, 13:1280–1293.

[19] Association, A. (2023). Home page. Accessed: May 24, 2023.

[20] Basaia, S. and Agosta, F. (2019). Automated classification of alzheimer's disease and mild cognitive impairment using a single mri and deep neural networks. *NeuroImage: Clinical*, 21:101645.

[21] Battineni, G., Hossain, M., Chintalapudi, N., Traini, E., Dhulipalla, V., Ramasamy, M., and Amenta, F. (2021). Improved alzheimer's disease detection by mri using multimodal machine learning algorithms. *Diagnostics*, 11:2103.

[22] Bauer, S., Wiest, R., Nolte, L.-P., and Reyes, M. (2013). A survey of mri-based medical image analysis for brain tumor studies. *Physics in Medicine & Biology*, 58(13):R97.

[23] Beckett, L. A. and Harvey, D. J. (2010). The alzheimer's disease neuroimaging initiative: Annual change in biomarkers and clinical outcomes. *Alzheimer's & Dementia*, 6(3):257–264.

[24] Beheshti, I. (2016). Feature-ranking-based alzheimer's disease classification from structural mri. *Magn Reson Imaging*, 34(3):252–263.

[25] Beheshti, I., Demirel, H., Farokhian, F., Yang, C., Matsuda, H., and Initiative, A. D. N. (2016). Structural mri-based detection of alzheimer's disease using feature ranking and classification error. *Computer methods and programs in biomedicine*, 137:177–193.

[26] Ben, b. O. A. (2017). Recognition of alzheimer's disease and mild cognitive impairment with multimodal image-derived biomarkers and multiple kernel learning. *Neurocomputing*, 220:98–110.

[27] Bhagwat, N., Pipitone, J., Voineskos, A., Chakravarty, M., and Initiative, A. (2019). An artificial neural network model for clinical score prediction in alzheimer disease using structural neuroimaging measures. *Journal of psychiatry neuroscience: JPN*, 44(4):246.

[28] Bhateja, V. and Moin, A. (2016). Multispectral medical image fusion in contourlet domain for computer based diagnosis of alzheimer's disease. *Review of Scientific Instruments*, 87(7):74303.

[29] Bi, X. and Wang, H. (2019). Early alzheimer's disease diagnosis based on eeg spectral images using deep learning. *Neural Networks*, 114:119–135.

[30] Bird, V., Premkumar, P., Kendall, T., Whittington, C., Mitchell, J., and Kuipers, E. (2010). Early intervention services, cognitive–behavioural therapy and family intervention in early psychosis: systematic review. *The British Journal of Psychiatry*, 197(5):350–356.

[31] Blennow, K. (2004). Cerebrospinal fluid protein biomarkers for alzheimer's disease. *NeuroRx*, 1(2):213–225.

[32] Bosni'c, Z., Brati'c, B., Ivanovi'c, M., Semnic, M., Oder, I., Kurbalija, V., Stankov, T. V., and Ignjatovi'c, V. B. (2021). Improving alzheimer's disease classification by performing data fusion with vascular dementia and stroke data. *Journal of Experimental Theoretical Artificial Intelligence*, 33(6):1015–1032.

162

[33] Bramati, d. R. I. (2020). Fractional anisotropy changes in parahippocampal cingulum due to alzheimer's disease. *Sci Rep*, 10(1):1–8.

[34] Böhle, M., Eitel, F., Weygandt, M., and Ritter, K. (2019). Layer-wise relevance propagation for explaining deep neural network decisions in mri-based alzheimer's disease classification. *Frontiers in aging neuroscience*, 11:194.

[35] Caine, D. (2004). Posterior cortical atrophy: A review of the literature. *Neurocase*, 10(5):382–385.

[36] Cataldo, A. M., Peterhoff, C. M., Troncoso, J. C., Gomez-Isla, T., Hyman, B. T., and Nixon, R. A. (2000). Endocytic pathway abnormalities precede amyloid β deposition in sporadic alzheimer's disease and down syndrome: differential effects of apoe genotype and presenilin mutations. *The American journal of pathology*, 157(1):277–286.

[37] Chaves, R., Ramírez, J., Górriz, J., López, M., Salas-Gonzalez, D., Alvarez, I., and Segovia, F. (2009). Svm-based computer-aided diagnosis of the alzheimer's disease using t-test nmse feature selection with feature correlation weighting. *Neuroscience letters*, 461(3):293–297.

[38] Chen, X. L. L. (2017). Prediction and classification of alzheimer disease based on quantification of mri deformation. *PLoS One*, 12(3):e0173372–e0173372.

[39] Chetelat, B. and Desgranges (2003). Mild cognitive impairment: can fdg-pet predict who is to rapidly convert to alzheimer's disease? *Neurology*, 60:1374–1377.

[40] Choi, B., Madusanka, N., Choi, H., So, J., Kim, C., Park, H., Bhatta-charjee, S., and Prakash, D. (2020). Convolutional neural network-based mr image analysis for alzheimer's disease classification. *Current Medical Imaging*, 16(1):27–35.

[41] Cotman, C. W., Poon, W. W., Rissman, R. A., and Blurton-Jones, M. (2005). The role of

caspase cleavage of tau in alzheimer disease neuropathology. *Journal of neuropathology & experimental neurology*, 64(2):104–112.

[42] Cox, R. (1996). Afni: software for analysis and visualization of functional magnetic resonance neuroimages. *Computers and Biomedical research*, 29(3):162–173.

[43] Cui, R., Liu, M., and Initiative, A. (2019). Rnn-based longitudinal analysis for diagnosis of alzheimer's disease. *Computerized Medical Imaging and Graphics*, 73:1–10.

[44] Cusack, R., Vicente-Grabovetsky, A., Mitchell, D., Wild, C., Auer, T., Linke, A., and Peelle, J. (2015). Automatic analysis (aa): efficient neuroimaging workflows and parallel processing using matlab and xml. *Frontiers in neuroinformatics*, 8:90.

[45] Dai, Z., Yan, C., Wang, Z., Wang, J., Xia, M., Li, K., and He, Y. (2012). Discriminative analysis of early alzheimer's disease using multi-modal imaging and multi-level characterization with multi-classifier (m3). *Neuroimage*, 59:2187–2195.

[46] Daianu, M., Jahanshad, N., Nir, T. M., Jack Jr, C. R., Weiner, M. W., Bernstein, M. A., Thompson, P. M., and Initiative, A. D. N. (2015). Rich club analysis in the alzheimer's disease connectome reveals a relatively undisturbed structural core network. *Human brain mapping*, 36(8):3087–3103.

[47] Daly, E. and Zaitchik, D. (2000). Predicting conversion to alzheimer disease using standardized clinical information. *Arch. Neurol.*, 57:675–680.

[48] Davatzikos, C., Resnick, S. M., Wu, X., Parmpi, P., and Clark, C. M. (2008). Individual patient diagnosis of ad and ftd via high-dimensional pattern classification of mri. *Neuroimage*, 41(4):1220–1227.

[49] De, A. and Chowdhury, A. S. (2021). Dti based alzheimer's disease classification with rank modulated fusion of cnns and random forest. *Expert Systems with Applications*, 169:114338.

[50] Devanand, D., Pradhaban, G., Liu, X., Khandji, A., Santi, S., Segal, S., Rusinek, H., Pelton, G., Honig, L., and Mayeux, R. (2007). Hippocampal and entorhinal atrophy in mild cognitive impairment: prediction of alzheimer disease. *Neurology*, 68(11):828–836.

[51] Dimitriadis, S. I., Liparas, D., Tsolaki, M. N., and Initiative, A. D. N. (2018). Random forest feature selection, fusion and ensemble strategy: Combining multiple morphological mri measures to discriminate among healthy elderly, mci, cmci and alzheimer's disease patients: From the alzheimer's disease neuroimaging initiative (adni) database. *Journal of neuroscience methods*, 302:14–23.

[52] Ding, Y., Sohn, J., Kawczynski, M., Trivedi, H., Harnish, R., Jenkins, N., Lituiev, D., Copeland, T., Aboian, M., and Aparici, C. (2019). A deep learning model to predict a diagnosis of alzheimer disease by using 18f-fdg pet of the brain. *Radiology*, 290(2):456–464.

[53] Dong, X., Xu, G., Wang, J., Yin, N., and Meng, N. (2022). Clinical and mri predictors of cognitive decline in patients with relapsing-remitting multiple sclerosis: A 2-year longitudinal study. *Multiple Sclerosis and Related Disorders*, 65:103838.

[54] Du, X., Wang, X., and Geng, M. (2018). Alzheimer's disease hypothesis and related therapies. *Translational neurodegeneration*, 7(1):1–7.

[55] Ebrahimi, A., Luo, S., Chiong, R., and Initiative, A. (2021). Deep sequence modelling for alzheimer's disease detection using mri. *Computers in Biology and Medicine*, page 104537.

[56] Ebrahimi-Ghahnavieh, A., Luo, S., and Chiong, R. (2019). Transfer learning for alzheimer's disease detection on mri images. pages 133–138.

[57] El, S. and Saleh, S. (2021). Alzheimer's disease progression detection model based on an early fusion of cost-effective multimodal data. *Future Gener. Comput. Syst.*, 115:680–699.

[58] Escott-Price, V., Shoai, M., Pither, R., Williams, J., and Hardy, J. (2017). Polygenic score prediction captures nearly all common genetic risk for alzheimer's disease. *Neurobiology of aging*, 49:214–e7.

[59] Esteban, O., Markiewicz, C., Blair, R., Moodie, C., Isik, A., Erramuzpe, A., Kent, J., Goncalves, M., DuPre, E., and Snyder, M. (2019). fmriprep: a robust preprocessing pipeline for functional mri. *Nature methods*, 16(1):111–116.

[60] Fadil, H., Borazanci, A., Haddou, E. A. B., Yahyaoui, M., Korniychuk, E., Jaffe, S. L., and Minagar, A. (2009). Early onset dementia. *International Review of Neurobiology*, 84:245–262.

[61] Fan, K. C. C. (2018). Combining polygenic hazard score with volumetric mri and cognitive measures improves prediction of progression from mild cognitive impairment to alzheimer's disease. *Front Neurosci*, 12:1–7.

[62] Farooq, A., Anwar, S., Awais, M., and Rehman, S. (2017). A deep cnn based multi-class classification of alzheimer's disease using mri. In *2017 IEEE International Conference on Imaging systems and techniques (IST)*, pages 1–6.

[63] Feng, C., Elazab, A., Yang, P., Wang, T., Zhou, F., Hu, H., Xiao, X., and Lei, B. (2019). Deep learning framework for alzheimer's disease diagnosis via 3d-cnn and fsbi-lstm. *IEEE Access*, 7:63605–63618.

[64] Filippi, M., Basaia, S., Canu, E., Imperiale, F., Magnani, G., Falautano, M., Comi, G., Falini, A., and Agosta, F. (2009). Changes in functional and structural brain connectome along the alzheimer's disease continuum. *Mol Psychiatry*, 25(1):29743 583–29743 583.

[65] Folego, G., Weiler, M., Casseb, R., Pires, R., and Rocha, A. (2020). Alzheimer's disease detection through whole-brain 3d-cnn mri. *Frontiers in Bioengineering and Biotechnology*, 8:534592.

[66] Galasko, D., Xiao, M., Xu, D., Smirnov, D., Salmon, D., Dewit, N., Vanbrabant, J., Jacobs, D., Vanderstichele, H., and Vanmechelen, E. (2019). Synaptic biomarkers in csf aid in diagnosis, correlate with cognition and predict progression in mci and alzheimer's disease. *Alzheimer's Dementia: Translational Research Clinical Interventions*, 5:871–882.

[67] Garyfallidis, E., Brett, M., Amirbekian, B., Rokem, A., Walt, S., Descoteaux, M., and Nimmo-Smith, I. (2014). Dipy, a library for the analysis of diffusion mri data. *Frontiers in neuroinformatics*, 8:8.

[68] Gaser, C., Dahnke, R., Thompson, P. M., Kurth, F., and Luders, E. (2022). Cat-a computational anatomy toolbox for the analysis of structural mri data. *BioRxiv*, pages 2022–06.

[69] Ge, C., Qu, Q., Gu, I., and Jakola, A. (2019). Multi-stream multi-scale deep convolutional networks for alzheimer's disease detection using mr images. *Neurocomputing*, 350:60–69.

[70] Goenka, S. T. N. (2021). Deep learning for alzheimer prediction using brain biomarkers. *Artif Intell Rev*, 54(7):4827–4871.

[71] Goenka, S. T. N. (2022). Alzvnet: A volumetric convolutional neural network for multiclass classification of alzheimer's disease through multiple neuroimaging computational approaches. *Biomed Signal Process Control*, 74:103500.

[72] Gorgolewski, K. et al. (2016). Nipype: a flexible, lightweight and extensible neuroimaging data processing framework in python.

[73] Graña, M., Termenon, M., Savio, A., Gonzalez-Pinto, A., Echeveste, J., Pérez, J., and Besga, A. (2011). Computer aided diagnosis system for alzheimer disease using brain diffusion tensor imaging features selected by pearson's correlation. *Neuroscience letters*, 502(3):225–229.

[74] Gulhare, K., Shukla, S., and Sharma, L. (2017). Deep neural network classification method to alzheimer's disease detection. *International Journals of Advanced Research in Computer Science and Software Engineering*, 7(6):1–4.

[75] Hake, A. M., Dacks, P. A., Arnerić, S. P., working group, C. I., et al. (2017). Concise informed consent to increase data and biospecimen access may accelerate innovative alzheimer's disease treatments. *Alzheimer's & Dementia: Translational Research & Clinical Interventions*, 3(4):536–541.

[76] Hallikainen, M. I. (2016). Alzheimer's disease neuroimaging initiative. rey's auditory verbal learning test scores can be predicted from whole brain mri in alzheimer's disease. *Neuroimage Clin*, 13:415–427.

[77] Hampel, H. and O'Bryant, S. E. (2018). Blood-based biomarkers for alzheimer disease: mapping the road to the clinic. *Nat Rev Neurol*, 14(11):639–652.

[78] Harrison, G. W. (2008). Neuroeconomics: A critical reconsideration. *Economics & Philosophy*, 24(3):303–344.

[79] Hsu, R. (2013). Alzheimer's disease risk assessment using large-scale machine learning methods. *PLoS ONE*, 8:77949.

[80] Hu, C., Ju, R., Shen, Y., Zhou, P., and Li, Q. (2016). Clinical decision support for alzheimer's disease based on deep learning and brain network. In *2016 IEEE International Conference on Communications (ICC)*, pages 1–6. IEEE.

[81] Hussain, E., Hasan, M., Hassan, S., Azmi, T., Rahman, M., and Parvez, M. (2020). Deep learning based binary classification for alzheimer's disease detection using brain mri images. In *2020 15th IEEE Conference on Industrial Electronics and Applications (ICIEA)*, pages 1115–1120.

[82] Hwang, I. S. and Hong, S. B. (2022). Association between body mass index and subcortical volume in pre-adolescent children with autism spectrum disorder: An exploratory study. *Autism Research*, 15(12):2238–2249.

[83] Indo, Y. (2014). Neurobiology of pain, interoception and emotional response: lessons from nerve growth factor-dependent neurons. *European Journal of Neuroscience*, 39(3):375–391.

[84] Initiative, A. D. N. (2021-2022). Accessed on: 2022.

[85] Islam, J. and Zhang, Y. (2017). A novel deep learning based multi-class classification method for alzheimer's disease detection using brain mri data. In *International conference on brain informatics*, pages 213–222.

[86] Jellinger, K. A., Janetzky, B., Attems, J., and Kienzl, E. (2008). Biomarkers for early diagnosis of alzheimer disease:'alzheimer associated gene'–a new blood biomarker? *Journal of cellular and molecular medicine*, 12(4):1094–1117.

[87] Jeong, J. (2002). Nonlinear dynamics of eeg in alzheimer's disease. *Drug development research*, 56(2):57–66.

[88] Jeong, J. (2004). Eeg dynamics in patients with alzheimer's disease. *Clinical neurophysiology*, 115(7):1490–1505.

[89] Jo, T., Nho, K., and Saykin, A. (2019). Deep learning in alzheimer's disease: diagnostic classification and prognostic prediction using neuroimaging data. *Frontiers in Aging Neuroscience*, 11:220.

[90] Johnson, P., Vandewater, L., Wilson, W., Maruff, P., Savage, G., Graham, P., Macaulay, L., Ellis, K., Szoeke, C., and Martins, R. (2014). Genetic algorithm with logistic regression for prediction of progression to alzheimer's disease. *BMC bioinformatics*, 15(16):1–14.

[91] Joshi, A., Choi, S., Chong, M., Sonkar, G., Gonzalez-Martinez, J., Nair, D., Wisnowski, J., Haldar, J., Shattuck, D., and Damasio, H. (2020). A hybrid high-resolution anatomical mri atlas with sub-parcellation of cortical gyri using resting fmri. *bioRxiv*.

[92] Jutten, R. J., Thompson, L., Sikkes, S. A., Maruff, P., Molinuevo, J. L., Zetterberg, H., Alber, J., Faust, D., Gauthier, S., Gold, M., et al. (2022). A neuropsychological perspective on defining cognitive impairment in the clinical study of alzheimer's disease: Towards a more continuous approach. *Journal of Alzheimer's Disease*, (Preprint):1–14.

[93] Khansari, S. S. M. (2017). Predicting brain network changes in alzheimer's disease with link prediction algorithms. *Mol Biosyst*, 13(4):725–735.

[94] Killiany, R. J., Gomez-Isla, T., Moss, M., Kikinis, R., Sandor, T., Jolesz, F., Tanzi, R., Jones, K., Hyman, B. T., and Albert, M. S. (2000). Use of structural magnetic resonance imaging to predict who will get alzheimer's disease. *Annals of Neurology: Official Journal of the American Neurological Association and the Child Neurology Society*, 47(4):430–439.

[95] Kim, D. and Kim, K. (2018). Detection of early stage alzheimer's disease using eeg relative power with deep neural network. In *2018 40th Annual International Conference of the IEEE Engineering in Medicine and Biology Society (EMBC)*, pages 352–355.

[96] Kim, D. K., Park, J., Han, D., Yang, J., Kim, A., Woo, J., Kim, Y., and Mook-Jung, I. (2018). Molecular and functional signatures in a novel alzheimer's disease mouse model assessed by quantitative proteomics. *Molecular neurodegeneration*, 13(1):1–19.

[97] Kiuchi, K., Morikawa, M., Taoka, T., Nagashima, T., Yamauchi, T., Makinodan, M., Norimoto, K., Hashimoto, K., Kosaka, J., Inoue, Y., et al. (2009). Abnormalities of the uncinate fasciculus and posterior cingulate fasciculus in mild cognitive impairment and early alzheimer's disease: a diffusion tensor tractography study. *Brain research*, 1287:184–191.

[98] Kruggel, F., Masaki, F., and Solodkin, A. (2017). Analysis of longitudinal diffusion-weighted images in healthy and pathological aging: An adni study. *Journal of Neuroscience Methods*, 278:101–115.

[99] Lancaster, M., Seidenberg, M., Smith, J., Nielson, K., Woodard, J., Durgerian, S., and Rao, S. (2016). Diffusion tensor imaging predictors of episodic memory decline in healthy elders at genetic risk for alzheimer's disease. *Journal of the International Neuropsychological Society*, 22(10):1005–1015.

[100] Lee, Y. G. K. H. (2019a). Early diagnosis of alzheimer's disease using combined features from voxel-based morphometry and cortical, subcortical, and hippocampus regions of mri t1 brain images. *PLoS One*, 14(10):222446.

[101] Lee, Y. G. K. H. (2019b). National research center for dementia; alzheimer's disease neuroimaging initiative. early diagnosis of alzheimer's disease using combined features from voxel-based morphometry and cortical, subcortical, and hippocampus regions of mri t1 brain images. *PLoS One*, 14(10):6777799.

[102] Lei, B., Chen, S., Ni, D., and Wang, T. (2016). Discriminative learning for alzheimer's disease diagnosis via canonical correlation analysis and multimodal fusion. *Frontiers in Aging Neuroscience*, 8:77.

[103] Leon, J. and Golomb (1993). The radiologic prediction of alzheimer disease: the atrophic hippocampal formation. *Am. J. Neuroradiol.*, 14:897–906.

[104] Li, R. W. C. (2016). Prediction of conversion from mild cognitive impairment to alzheimer's disease using mri and structural network features. *Front Aging Neurosci*, 8:1–11.

[105] Liu, M. and Zhang, D. (2014). Hierarchical fusion of features and classifier decisions for alzheimer's disease diagnosis. *Human Brain Mapping*, 35(3):1305–1319.

[106] Liu, S. and Liu, S. (2014). Multimodal neuroimaging feature learning for multi-class diagnosis of alzheimer's disease. *IEEE Transactions on Biomedical Engineering*, 62:1132–1140.

[107] Liu, T., Yan, Z., Han, Z., Zhang, J., Fang, B., and Yan, T. (2023). Cortico–subcortical spatiotemporal dynamics in parkinson's disease can be modulated by transcranial alternating current stimulation. *Brain Science Advances*, 9(2):114–135.

[108] Liu, Y., Li, Z., Ge, Q., Lin, N., and Xiong, M. (2019). Deep feature selection and causal analysis of alzheimer's disease. *Frontiers in Neuroscience*, 13:1–11.

[109] Lo, C.-Y., Wang, P.-N., Chou, K.-H., Wang, J., He, Y., and Lin, C.-P. (2010). Diffusion tensor tractography reveals abnormal topological organization in structural cortical networks in alzheimer's disease. *Journal of Neuroscience*, 30(50):16876–16885.

[110] Long, X., Chen, L., Jiang, C., Zhang, L., and Initiative, A. D. N. (2017). Prediction and classification of alzheimer disease based on quantification of mri deformation. *PloS one*, 12(3):e0173372.

[111] Lopes, S. (2016). Cerebral hypoperfusion and hypometabolism detected by arterial spin labeling mri and fdg-pet in early-onset alzheimer's disease. *J. Neuroimaging*, 26:207–212.

[112] Mabrouk, B., BenHamida, A., Drissi, N., Bouzidi, N., and Mhiri, C. (2023). Contribution of brain regions asymmetry scores combined with random forest classifier in the diagnosis of alzheimer's disease in his earlier stage. *Journal of Medical and Biological Engineering*, 43(1):74–82.

[113] Mahmood, R. and Ghimire, B. (2013). Automatic detection and classification of alzheimer's disease from mri scans using principal component analysis and artificial neural networks. In *2013 20th International Conference on Systems, Signals and Image Processing (IWSSIP)*, pages 133–137.

[114] Mahmoud, N., Fouad, H., Alsadon, O., and Soliman, A. (2020). Detecting dental problem related brain disease using intelligent bacterial optimized associative deep neural network. *Cluster Computing*, 23(3):1647–1657.

[115] Mamun, M., Shawkat, S., Ahammed, M., Uddin, M., Mahmud, M., and Islam, A. (2022). Deep learning based model for alzheimer's disease detection using brain mri images. In *2022 IEEE 13th Annual Ubiquitous Computing, Electronics Mobile Communication Conference (UEMCON)*, pages 0510–0516.

[116] Maqsood, M., Nazir, F., Khan, U., Aadil, F., Jamal, H., Mehmood, I., and Song, O. (2019). Transfer learning assisted classification and detection of alzheimer's disease stages using 3d mri scans. *Sensors*, 19(11):2645.

[117] Maringanti, H., Mishra, M., and Pradhan, S. (2023). Machine learning and deep learning models for early-stage detection of alzheimer's disease and its proliferation in human brain. In *Artificial Intelligence for Neurological Disorders*. Academic Press, Cambridge, MA, USA.

[118] Matej, R., Tesar, A., and Rusina, R. (2019). Alzheimer's disease and other neurodegenerative dementias in comorbidity: A clinical and neuropathological overview. *Clinical biochemistry*, 73:26–31.

[119] Mayo, C. D., Garcia-Barrera, M. A., Mazerolle, E. L., Ritchie, L. J., Fisk, J. D., Gawryluk, J. R., and Initiative, A. D. N. (2019). Relationship between dti metrics and cognitive function in alzheimer's disease. *Frontiers in aging neuroscience*, 10:436.

[120] McCarthy, C. S. and Ramprashad, A. (2015). A comparison of freesurfer-generated data with and without manual intervention. *Front Neurosci*, 9:379.

[121] McEvoy, L., Fennema-Notestine, C., Roddey, J., Hagler, D., Jr, Holland, D., Karow, D., Pung, C., Brewer, J., and Dale, A. (2009). Alzheimer disease: quantitative structural

neuroimaging for detection and prediction of clinical and structural changes in mild cognitive impairment. *Radiology*, 251:195–205.

[122] Mehmood, A., Maqsood, M., Bashir, M., and Shuyuan, Y. (2020). A deep siamese convolution neural network for multi-class classification of alzheimer disease. *Brain sciences*, 10(2):84.

[123] Mielke, M., Rosenberg, P., Tschanz, J., Cook, L., Corcoran, C., Hayden, K., Norton, M., Rabins, P., Green, R., and Welsh-Bohmer, K. (2007). Vascular factors predict rate of progression in alzheimer disease. *Neurology*, 69(19):1850–1858.

[124] Mito, R., Raffelt, D., Dhollander, T., Vaughan, D. N., Tournier, J.-D., Salvado, O., Brodtmann, A., Rowe, C. C., Villemagne, V. L., and Connelly, A. (2018). Fibre-specific white matter reductions in alzheimer's disease and mild cognitive impairment. *Brain*, 141(3):888–902.

[125] Monaco, N. A. A. (2017). Topological measurements of dwi tractography for alzheimer's disease detection. *Comput Math Methods Med*, 2017(Md):1–10.

[126] Montagne, C., Kodewitz, A., Vigneron, V., Giraud, V., and Lelandais, S. (2013). 3d local binary pattern for pet image classification by svm, application to early alzheimer disease diagnosis. In *6th International Conference on Bio-Inspired Systems and Signal Processing (BIOSIGNALS 2013)*, pages 145–150.

[127] Moon, W.-J., Kim, H.-J., Roh, H. G., Choi, J. W., and Han, S.-H. (2012). Fluid-attenuated inversion recovery hypointensity of the pulvinar nucleus of patients with alzheimer disease: its possible association with iron accumulation as evidenced by the t2* map. *Korean Journal of Radiology*, 13(6):674–683.

[128] Mueller, S. G. and Schuff, N. (2010). Hippocampal atrophy patterns in mild cognitive impairment and alzheimer's disease. *Hum Brain Mapp*, 31(9):1339–1347.

[129] Mueller, S. G., Weiner, M. W., Thal, L. J., Petersen, R. C., Jack, C. R., Jagust, W., Trojanowski, J. Q., Toga, A. W., and Beckett, L. (2005). Ways toward an early diagnosis in alzheimer's disease: the alzheimer's disease neuroimaging initiative (adni). *Alzheimer's & Dementia*, 1(1):55–66.

[130] Myers, S. (2012). Prediction of alzheimer's disease using individual structural connectivity networks. *Neurobiol. Aging*, 33:2756–2765.

[131] Müller, E., Edwin, T., Stokke, C., Navelsaker, S., Babovic, A., Bogdanovic, N., Knapskog, A., and Revheim, M. (2019). Amyloid-β pet—correlation with cerebrospinal fluid biomarkers and prediction of alzheimers´ disease diagnosis in a memory clinic. *PLoS One*, 14(8):e0221365.

[132] Nelson, A. P. and O'Connor, M. G. (2008). Mild cognitive impairment: a neuropsychological perspective. *CNS spectrums*, 13(1):56–64.

[133] Nir, P. T. M. (2013). Tractography density and network measures in alzheimer's disease. In *Proceedings - International Symposium on Biomedical Imaging*, pages 692–695.

[134] Noonan, K. A., Jefferies, E., Visser, M., and Lambon Ralph, M. A. (2013). Going beyond inferior prefrontal involvement in semantic control: evidence for the additional contribution of dorsal angular gyrus and posterior middle temporal cortex. *Journal of cognitive neuroscience*, 25(11):1824–1850.

[135] Nordberg, A., Rinne, J. O., Kadir, A., and Långström, B. (2010). The use of pet in alzheimer disease. *Nature Reviews Neurology*, 6(2):78–87.

[136] Nordstedt, C., Caporaso, G., Thyberg, J., Gandy, S., and Greengard, P. (1993). Identification of the alzheimer beta/a4 amyloid precursor protein in clathrin-coated vesicles purified from pc12 cells. *Journal of Biological Chemistry*, 268(1):608–612.

[137] Oishi, K., Mielke, M. M., Albert, M., Lyketsos, C. G., and Mori, S. (2011). Dti analyses and clinical applications in alzheimer's disease. *Journal of Alzheimer's Disease*, 26(s3):287–296.

[138] Olama, A., Wason, J., Tuladhar, A., van Leijsen, E., Koini, M., Hofer, E., Morris, R., Schmidt, R., de Leeuw, F., and Markus, H. (2020). Simple mri score aids prediction of dementia in cerebral small vessel disease. *Neurology*, 94(12):e1294–e1302.

[139] Orr, M. E., Reveles, K. R., Yeh, C.-K., Young, E. H., and Han, X. (2020). Can oral health and oral-derived biospecimens predict progression of dementia? *Oral diseases*, 26(2):249–258.

[Pagani et al.] Pagani, M., Giuliani, A., Öberg, J., Chincarini, A., Morbelli, S., Brugnoloº, A., Arnaldi, D., Picco, A., Bauckneht, M., Buschiazzo, A., et al. Predicting the transition from normal aging to alzheimer's disease: A ttes.

[141] Pal, A., Siotto, M., Prasad, R., and Squitti, R. (2015). Towards a unified vision of copper involvement in alzheimer's disease: a review connecting basic, experimental, and clinical research. *Journal of Alzheimer's Disease*, 44(2):343–354.

[142] Pan, D., Zeng, A., Jia, L., Huang, Y., Frizzell, T., and Song, X. (2020). Early detection of alzheimer's disease using magnetic resonance imaging: a novel approach combining convolutional neural networks and ensemble learning. *Frontiers in neuroscience*, 14:259.

[143] Park, C., Ha, J., and Park, S. (2020). Prediction of alzheimer's disease based on deep neural network by integrating gene expression and dna methylation dataset. *Expert Systems with Applications*, 140:112 873.

[144] Park, W. J. M. J. Y. (2016). A comparison of substantia nigra t1 hyperintensity in parkinson's disease dementia, alzheimer's disease and age-matched controls: Volumetric analysis of neuromelanin imaging. *Korean J Radiol*, 17(5):633–640.

[145] Paterson, R. W. and Wellington, H. (2018). Csf neurogranin or tau distinguish typical and atypical alzheimer disease. *Ann Clin Transl Neurol*, 5(2):162–171.

[146] Penny, W., Friston, K., Ashburner, J., Kiebel, S., and Nichols, T. (2011). *Statistical parametric mapping: the analysis of functional brain images*. Elsevier.

[147] Peña-Bautista, C., Durand, T., Oger, C., Baquero, M., Vento, M., and Cháfer-Pericás, C. (2019). Assessment of lipid peroxidation and artificial neural network models in early alzheimer disease diagnosis. *Clinical biochemistry*, 72:64–70.

[148] Pipitone, J., Park, M. T. M., Winterburn, J., Lett, T. A., Lerch, J. P., Pruessner, J. C., Lepage, M., Voineskos, A. N., Chakravarty, M. M., and Initiative, A. D. N. (2014). Multi-atlas segmentation of the whole hippocampus and subfields using multiple automatically generated templates. *Neuroimage*, 101:494–512.

[149] Platero, C. (2017). Combining a patch-based approach with a non-rigid registration-based label fusion method for the hippocampal segmentation in alzheimer's disease. *Neuroinformatics*, 15(2):165–183.

[150] Podcasy, J. L. and Epperson, C. N. (2022). Considering sex and gender in alzheimer disease and other dementias. *Dialogues in clinical neuroscience*.

[151] Preische, O., Schultz, S., Apel, A., Kuhle, J., Kaeser, S., Barro, C., Gräber, S., Kuder-Buletta, E., LaFougere, C., and Laske, C. (2019). Serum neurofilament dynamics predicts neurodegeneration and clinical progression in presymptomatic alzheimer's disease. *Nature medicine*, 25(2):277–283.

[152] Prestia, A. and Caroli, A. (2013). Prediction of dementia in mci patients based on core diagnostic markers for alzheimer disease. *Neurology*, 80:1048–1056.

[153] Protas, H. D., Chen, K., Langbaum, J. B., Fleisher, A. S., Alexander, G. E., Lee, W., Bandy, D., De Leon, M. J., Mosconi, L., Buckley, S., et al. (2013). Posterior cingulate

glucose metabolism, hippocampal glucose metabolism, and hippocampal volume in cognitively normal, late-middle-aged persons at 3 levels of genetic risk for alzheimer disease. *JAMA neurology*, 70(3):320–325.

[154] Punjabi, A. and Martersteck, A. (2019). Neuroimaging modality fusion in alzheimer's classification using convolutional neural networks. *PLoS ONE*, 14(9):e0225759.

[155] Rabeh, A., Benzarti, F., and Amiri, H. (2016). Diagnosis of alzheimer diseases in early step using svm (support vector machine). In *2016 13th International conference on computer graphics, imaging and visualization (CGiV)*, pages 364–367.

[156] Rajalingam, B., Priya, R., and Bhavani, R. (2019). Medical image fusion based on hybrid algorithms for neuro cysticercosis and neoplastic disease analysis. *Journal of Mechanics of Continua and Mathematical Sciences*, 14(4):171–187.

[157] Ramani, A., Jensen, J. H., and Helpern, J. A. (2006). Quantitative mr imaging in alzheimer disease. *Radiology*, 241(1):26–44.

[158] Ramírez, J. and Górriz, J. (2010). Computer aided diagnosis system for the alzheimer's disease based on partial least squares and random forest spect image classification. *Neuroscience Letters*, 472:99–103.

[159] Reitz, C., Tang, M., Schupf, N., Manly, J., Mayeux, R., and Luchsinger, J. (2010). A summary risk score for the prediction of alzheimer disease in elderly persons. *Archives of neurology*, 67(7):835–841.

[160] Rohanian, M., Hough, J., and Purver, M. (2021). Multi-modal fusion with gating using audio, lexical and disfluency features for alzheimer's dementia recognition from spontaneous speech. *arXiv preprint arXiv:2106.09668*.

[161] Roostaei, T., Nazeri, A., Felsky, D., De Jager, P. L., Schneider, J. A., Pollock, B. G., Bennett, D. A., and Voineskos, A. N. (2017). Genome-wide interaction study of

brain beta-amyloid burden and cognitive impairment in alzheimer's disease. *Molecular psychiatry*, 22(2):287–295.

[162] Røvang, M. S., Selnes, P., MacIntosh, B. J., Rasmus Groote, I., Pålhaugen, L., Sudre, C., Fladby, T., and Bjørnerud, A. (2023). Segmenting white matter hyperintensities on isotropic three-dimensional fluid attenuated inversion recovery magnetic resonance images: Assessing deep learning tools on a norwegian imaging database. *PloS one*, 18(8):e0285683.

[163] Ryoo, L. H. (2017). Morphological and microstructural changes of the hippocampus in early mci: A study utilizing the alzheimer's disease neuroimaging initiative database. *Journal of Clinical Neurology (Korea)*, 13(2):144–154.

[164] Sabbagh, M. N., Shi, J., Lee, M., Arnold, L., Al-Hasan, Y., Heim, J., and McGeer, P. (2018). Salivary beta amyloid protein levels are detectable and differentiate patients with alzheimer's disease dementia from normal controls: Preliminary findings. *BMC neurology*, 18(1):1–4.

[165] Salehi, A., Baglat, P., Sharma, B., Gupta, G., and Upadhya, A. (2020). A cnn model: Earlier diagnosis and classification of alzheimer disease using mri. In *2020 International Conference on Smart Electronics and Communication (ICOSEC)*, pages 156–161.

[166] Sandry, J. and Dobryakova, E. (2021). Global hippocampal and selective thalamic nuclei atrophy differentiate chronic tbi from non-tbi. *Cortex*, 145:37–56.

[167] Sarraf, S. and Tofighi, G. (2016). Classification of alzheimer's disease structural mri data by deep learning convolutional neural networks. *arXiv preprint arXiv:1607.06583*.

[168] Scheltens, P., Fox, N., Barkhof, F., and De Carli, C. (2002). Structural magnetic resonance imaging in the practical assessment of dementia: beyond exclusion. *The Lancet Neurology*, 1(1):13–21.

179

[169] Schouten, C. v. S. M. d. R. J. v. d. G. S. A. R. B. R. d. V. T. M. (2016). Combining multiple anatomical mri measures improves alzheimer's disease classification. *Hum Brain Mapp*, 37(5):1920–1929.

[170] Sciancalepore, F. (2021). Neuroimaging and neuropsychological differences between early-onset alzheimer and late-onset alzheimer. alzheimer's disease and treatment. *Med-Docs Publishers*, 3:31–36.

[171] Scott, J., Tosun, D., Braskie, M., Maillard, P., Thompson, P., Weiner, M., DeCarli, C., and Carmichael, O. (2017). Independent value added by diffusion mri for prediction of cognitive function in older adults. *NeuroImage: Clinical*, 14:166–173.

[172] Shan, P. C. X. (2017). Sparse shared structure based multi-task learning for mri based cognitive performance prediction of alzheimer's disease. *Pattern Recognit*, 72:219–235.

[173] Shi, M. and Caudle, W. (2009). Biomarker discovery in neurodegenerative diseases: a proteomic approach. *Neurobiology of Disease*, 35:157–164.

[174] Shukla, A., Tiwari, R., and Tiwari, S. (2023a). Alz-convnets for classification of alzheimer disease using transfer learning approach. *SN Computer Science*, 4(4):404.

[175] Shukla, A., Tiwari, R., and Tiwari, S. (2023b). Alz-convnets for classification of alzheimer disease using transfer learning approach. *SN Computer Science*, 4(4):404.

[176] Shukla, A., Tiwari, R., and Tiwari, S. (2023c). Alzheimer's disease detection from fused pet and mri modalities using an ensemble classifier. *Machine Learning and Knowledge Extraction*, 5(2):512–538.

[177] Shukla, A., Tiwari, R., and Tiwari, S. (2023d). Review on alzheimer disease detection methods: Automatic pipelines and machine learning techniques. *Sci*, 5(1):13.

[178] Shukla, A., Tiwari, R., and Tiwari, S. (2023e). Review on alzheimer disease detection methods: Automatic pipelines and machine learning techniques. *Sci*, 5(1):13.

[179] Siu, H. G. W. (2017). Mri assessment of whole-brain structural changes in aging. *Clin Interv Aging*, 12:1251–1270.

[180] Soares, W. and Potter, Z. (2012). Plasma biomarkers associated with the apolipoprotein e genotype and alzheimer disease. *Arch Neurol*, 69(10):1310–1317.

[181] Sohail, N. and Anwar, S. M. (2022). A modified u-net based framework for automated segmentation of hippocampus region in brain mri. *IEEE Access*, 10:31201–31209.

[182] Somasundaram, K. and Kalaiselvi, T. (2011). Automatic brain extraction methods for t1 magnetic resonance images using region labeling and morphological operations. *Computers in Biology and Medicine*, 41(8):716–725.

[183] Song, M., Jung, H., Lee, S., Kim, D., and Ahn, M. (2021). Diagnostic classification and biomarker identification of alzheimer's disease with random forest algorithm. *Brain Sciences*, 11(4):453.

[184] Stern, Y. and Tang, M. (1997). Predicting time to nursing home care and death in individuals with alzheimer disease. *JAMA*, 277:806–812.

[185] Suk, H., Lee, S., Shen, D., and Initiative, A. D. N. (2014). Hierarchical feature representation and multimodal fusion with deep learning for ad/mci diagnosis. *NeuroImage*, 101:569–582.

[186] Suk, H. and Shen, D. (2013). Deep learning-based feature representation for ad/mci classification. In *International Conference on Medical Image Computing and Computer-Assisted Intervention*, pages 583–590.

[187] Sun, B.-L., Li, W.-W., Zhu, C., Jin, W.-S., Zeng, F., Liu, Y.-H., Bu, X.-L., Zhu, J., Yao, X.-Q., and Wang, Y.-J. (2018). Clinical research on alzheimer's disease: progress and perspectives. *Neuroscience bulletin*, 34:1111–1118.

[188] Tabert, M., Manly, J., Liu, X., Pelton, G., Rosenblum, S., Jacobs, M., Zamora, D., Goodkind, M., Bell, K., and Stern, Y. (2006). Neuropsychological prediction of conversion to alzheimer disease in patients with mild cognitive impairment. *Archives of general psychiatry*, 63(8):916–924.

[189] Takahashi, R., Ishii, K., Sousa, K., Marumoto, K., Kashibayashi, T., Fujita, J., and Yokoyama, K. (2021). Distinctive regional asymmetry in dopaminergic and serotoninergic dysfunction in degenerative parkinsonisms. *Journal of the Neurological Sciences*, 423:117363.

[190] Talo, M., Yildirim, O., Baloglu, U., Aydin, G., and Acharya, U. (2019). Convolutional neural networks for multi-class brain disease detection using mri images. *Computerized Medical Imaging and Graphics*, 78:101673.

[191] Tan, X., Liu, Y., Li, Y., Wang, P., Zeng, X., Yan, F., and Li, X. (2018). Localized instance fusion of mri data of alzheimer's disease for classification based on instance transfer ensemble learning. *Biomedical Engineering Online*, 17(1):1–17.

[192] Taoka, T., Masutani, Y., Kawai, H., Nakane, T., Matsuoka, K., Yasuno, F., Kishimoto, T., and Naganawa, S. (2017). Evaluation of glymphatic system activity with the diffusion mr technique: diffusion tensor image analysis along the perivascular space (dti-alps) in alzheimer's disease cases. *Japanese Journal of Radiology*, 35(4):172–178.

[193] Tarawneh, R. and Holtzman, D. M. (2012). The clinical problem of symptomatic alzheimer disease and mild cognitive impairment. *Cold Spring Harbor perspectives in medicine*, 2(5):a006148.

[194] Termenon, M. (2012). A two stage sequential ensemble applied to the classification of alzheimer's disease based on mri features. *Neural Processing Letters*, 35:1–12.

[195] Teunissen, C., De Vente, J., Steinbusch, H., and De Bruijn, C. (2002). Biochemical

markers related to alzheimer's dementia in serum and cerebrospinal fluid. *Neurobiology of aging*, 23(4):485–508.

[196] Tierney, M. C., Szalai, J. P., Snow, W. G., and Fisher, R. H. (1996). The prediction of alzheimer disease: the role of patient and informant perceptions of cognitive deficits. *Archives of Neurology*, 53(5):423–427.

[197] Tomasi, D., Wiers, C. E., Manza, P., Shokri-Kojori, E., Michele-Vera, Y., Zhang, R., others, and Volkow, N. D. (2021). Accelerated aging of the amygdala in alcohol use disorders: Relevance to the dark side of addiction. *Cerebral Cortex*, 31(7):3254–3265.

[198] Tong, T. and Gray, K. (2017). Multi-modal classification of alzheimer's disease using nonlinear graph fusion. *Pattern Recognition*, 63:171–181.

[199] Toniolo, S., Sen, A., and Husain, M. (2020). Modulation of brain hyperexcitability: Potential new therapeutic approaches in alzheimer's disease. *International Journal of Molecular Sciences*, 21(23):9318–9318.

[200] Tran, F. (2015). A robust deep model for improved classification of ad/mci patients. *IEEE Journal of Biomedical and Health Informatics*, 19:1610–1616.

[201] Tustison, N. et al. (2017). The ants longitudinal cortical thickness pipeline. *bioRxiv*, page 170209.

[202] Utermohlen, W., Green, J., Montpetit, M. A., Diaz, J., Kooken, W., Kerr, N., Kerr, J. M., Criley, M., Cook, K., and Hudson, W. (2015). Pursuing the ephemeral, painting the enduring: Alzheimer's and the artwork of william utermohlen.

[203] Van Cauwenberghe, C., Van Broeckhoven, C., and Sleegers, K. (2016). The genetic landscape of alzheimer disease: clinical implications and perspectives. *Genetics in Medicine*, 18(5):421–430.

[204] Villatoro-Tello, E., Dubagunta, S. P., Fritsch, J., Ram'irez-de-la Rosa, G., Motlicek, P., and Magimai-Doss, M. (2021). Late fusion of the available lexicon and raw waveform-based acoustic modeling for depression and dementia recognition. pages 1927–1931.

[205] Wang, K. and Liang, M. (2007). Altered functional connectivity in early alzheimer's disease: A resting-state fmri study. *Human Brain Mapping*, 28:967–978.

[206] Wang, W., Pei, Y., Wang, S. H., Gorrz, J. m., and Zhang, Y. D. (2023). Pstcnn: Explainable covid-19 diagnosis using pso-guided self-tuning cnn. *Biocell: official journal of the Sociedades Latinoamericanas de Microscopia Electronica... et. al*, 47(2):373.

[207] Wang, W., Zhang, X., Wang, S. H., and Zhang, Y. D. (2022). Covid-19 diagnosis by we-saj. *Systems science & control engineering*, 10(1):325–335.

[208] Wang, Y., Liu, X., and Yu, C. (2021). Assisted diagnosis of alzheimer's disease based on deep learning and multi-modal feature fusion. *Complexity*, 2021:1–10.

[209] Wang, Y., Xu, C., Park, J.-H., Lee, S., Stern, Y., Yoo, S., Kim, J. H., Kim, H. S., and Cha, J. (2018). Diagnosis and prognosis using machine learning trained on brain morphometry and white matter connectomes. *bioRxiv*, page 255141.

[210] Williams, O., Zeestraten, E., Benjamin, P., Lambert, C., Lawrence, A., Mackinnon, A., Morris, R., Markus, H., Barrick, T., and Charlton, R. (2019). Predicting dementia in cerebral small vessel disease using an automatic diffusion tensor image segmentation technique. *Stroke*, 50(10):2775–2782.

[211] Woolrich, M., Jbabdi, S., Patenaude, B., Chappell, M., Makni, S., Behrens, T., Beckmann, C., Jenkinson, M., and Smith, S. (2009). Bayesian analysis of neuroimaging data in fsl. *Neuroimage*, 45(1):173–186.

[212] Xie, S., Xiao, J., Wang, Y., Wu, H., Gong, G., and Jiang, X. (2005). Evaluation of

bilateral cingulum with tractography in patients with alzheimer's disease. *NeuroReport*, 16(12):1275–1278.

[213] Yanyan, H. and Shen (2019). Ensemble of 3d densely connected convolutional network for diagnosis of mild cognitive impairment and alzheimer's disease. *Neurocomputing*, 333:145–156.

[214] Yi, L., Wang, J., Jia, L., Zhao, Z., Lu, J., Li, K., Jia, J., He, Y., Jiang, C., and Han, Y. (2012). Structural and functional changes in subcortical vascular mild cognitive impairment: a combined voxel-based morphometry and resting-state fmri study. page e44758.

[215] Yu, J. and Lee, T. (2019). Verbal memory and hippocampal volume predict subsequent fornix microstructure in those at risk for alzheimer's disease. *Brain Imaging and Behavior*.

[216] YİĞİT, A. and Işik, Z. (2020). Applying deep learning models to structural mri for stage prediction of alzheimer's disease. *Turkish Journal of Electrical Engineering and Computer Sciences*, 28(1):196–210.

[217] Zhan, L., Zhou, J., Wang, Y., Jin, Y., Jahanshad, N., Prasad, G., Nir, T. M., Leonardo, C. D., Ye, J., Thompson, P. M., et al. (2015). Comparison of nine tractography algorithms for detecting abnormal structural brain networks in alzheimer's disease. *Frontiers in aging neuroscience*, 7:48.

[218] Zhang, A. R. A. K. Y. (2012). Linking white matter integrity loss to associated cortical regions using structural connectivity information in alzheimer's disease and frontotemporal dementia: The loss in connectivity (loco) score. *Neuroimage*, 61(4):1311–1323.

[219] Zhang, X. C. H. (2017). Extraction of dynamic functional connectivity from brain grey matter and white matter for mci classification. *Hum Brain Mapp*, 38(10):5019–5034.

185

[220] Zhang, Y., Teng, Q., Liu, Y., Liu, Y., and He, X. (2022). Diagnosis of alzheimer's disease based on regional attention with smri gray matter slices. *Journal of neuroscience methods*, 365:109376.

[221] Zhang, Y. and Wang, S. (2021). Alzheimer's disease multiclass diagnosis via multimodal neuroimaging embedding feature selection and fusion. *Inf. Fusion*, 66:170–183.

[222] Zhang, Y., Zhang, Y., Hou, X., Chen, H., and Wang, S. (2018). Seven-layer deep neural network based on sparse autoencoder for voxelwise detection of cerebral microbleed. *Multimedia Tools and Applications*, 77(9):10 521–10 538.

[223] Zhang, Z., Xi, X., Luo, X., Jiang, Y., Dong, J., and Wu, X. (2021). Multimodal image fusion based on global-regional-local rule in nsst domain. *Multimedia Tools and Applications*, 80:2847–2873.

[224] Zhimin, Y. and Long (2020). Dihydroartemisinin ameliorates learning and memory in alzheimer's disease through promoting autophagosome-lysosome fusion and autolysosomal degradation for a clearance. *Frontiers in Aging Neuroscience*, 12:47.

[225] Zhu, X., Suk, H.-I., and Shen, D. (2014). A novel matrix-similarity based loss function for joint regression and classification in ad diagnosis. *NeuroImage*, 100:91–105.

Dissemination of Work

Publications

1. Shukla, A., Tiwari, R., Tiwari, S. Structural biomarker-based Alzheimer's disease detection via ensemble learning techniques. International Journal of Imaging Systems and Technology.

2. Shukla, A., Tiwari, R., Tiwari, S. (2024). Analyzing subcortical structures in Alzheimer's disease using ensemble learning. Biomedical Signal Processing and Control, 87, 105407. https://doi.org/10.1016/j.bspc.2023.105407.

3. Shukla, A., Tiwari, R., Tiwari, S. (2023). Alzheimer's Disease Detection from Fused PET and MRI Modalities Using an Ensemble Classifier. Machine Learning and Knowledge Extraction, 5(2), 512-538.

4. Shukla, A., Tiwari, R., Tiwari, S. (2023). Alz-ConvNets for Classification of Alzheimer Disease Using Transfer Learning Approach. SN Computer Science, 4(4), 404.

5. Shukla, A., Tiwari, R., Tiwari, S. (2023). Review on alzheimer disease detection methods: Automatic pipelines and machine learning techniques. Sci, 5(1), 13.

6. Shukla, A., Tiwari, R., Tiwari, S. (2022, October). Automated Pipeline Preprocessing Techniques for Alzhiemer Disease Detection. In 2022 10th International Conference on Reliability, Infocom Technologies and Optimization (Trends and Future Directions)(ICRITO) (pp. 1-7). IEEE.

Thesis_Final